A GENERAL METHODOLOGY FOR THE ASSESSMENT OF THE IMPACT OF CLIMATE CHANGE – EVALUATION OF SNOW LOADS

Dissertation

submitted to and approved by the

Faculty of Architecture, Civil Engineering and Environmental Sciences
University of Braunschweig – Institute of Technology

and the

Department of Civil and Environmental Engineering
University of Florence

in candidacy for the degree of a
Doktor-Ingenieur (Dr.-Ing.) /
Dottore di Ricerca in Civil and Environmental Engineering[*)]

by
Filippo Landi
born 26/02/1989
from Pisa, Italy

Submitted on	11 February, 2019
Oral examination on	06 May, 2019
Professorial advisors	Prof. Hermann G. Matthies Prof. Pietro Croce, Dr. Paolo Formichi

2019

*) Either the German or the Italian form of the title may be used.

ABSTRACT

Structural design of buildings and infrastructures is significantly influenced by the definition of climatic actions (snow, wind and thermal loads) that the structure shall withstand during its life, which could be significantly greater than the design service life, assumed period for which the structure is to be used with anticipated maintenance but without major repair.
Therefore, the impact of climate change on climatic actions could significantly affect, in the mid-term future, the design of new structures as well as the reliability of existing ones designed in accordance to the provisions of present and past codes. Indeed, the definition of climatic actions on structures is currently based on extreme value analysis applied to past observations of the natural phenomena, under the assumption of stationary climate conditions, in this way stationary return level and no changes in the frequency of extremes are usually assumed.
In this work, a general methodology to derive future trends of snow load on structures is presented aiming to study the influence of climate change at European scale in view of definition of updated snow maps for the new generation of structural Eurocodes.
First, a general algorithm based, on Monte Carlo simulations, is defined to estimate ground snow loads maxima considering daily outputs of the climate models, in terms of maximum and minimum air temperatures and precipitation, supplemented by local information of snowfall and snow melting conditions derived from the elaboration of real measurements of actual meteorological events. Once validated the procedure, reproducing observed data series of annual maximum ground snow loads, trends in characteristic values of the load are investigated according different climate models and scenarios. Analysing different climate models and scenarios, the relevant issue of uncertainty assessment of climate projections is deeply investigated. In particular, the three main sources of uncertainty affecting climate projections: model uncertainty, scenarios uncertainty and internal variability, are assessed also implementing an innovative ad hoc developed weather generator, able to generate future weather series directly from climate model outputs.
In this context, the outcome obtained using the weather generator can be also supplemented with a Bayesian technique for snow map refinement. Thus, a

dynamic, sequential model updating procedure can be set up as soon as new model data and in particular, new measurements become available. Spatial variation of the extreme value process is also investigated and a Bayesian hierarchical model for extreme ground snow load is presented, in which the standard extreme value representation at each site is combined with a latent process thus considering the parameter's variation over homogeneous climatic regions.
In order to take into account the non-stationarity of climate conditions, moving time windows of forty years are considered in the analysis for the historical and future period. In this way, factor of change confidence maps are finally derived combining all the presented results and providing guidance for potential amendments of the current version of snow load maps given in technical standards.

ZUSAMMENFASSUNG

Die Tragwerksplanung von Bauwerken und Infrastrukturen wird maßgeblich durch die Definition klimatischer Ereignisse (Schnee-, Wind- und Wärmelasten) beeinflusst, denen das Bauwerk während seiner Lebensdauer standhalten soll, die deutlich größer sein können als die geplante Nutzungsdauer.
Daher können die Auswirkungen des Klimawandels auf das Wetter in der mittelfristig die Gestaltung neuer Strukturen sowie die Zuverlässigkeit bestehender Strukturen, die nach den Bestimmungen aktueller und alter Richtlinien basierend auf der Annahme stationäre Klimabedingungen entworfen wurden, erheblich beeinflussen.
In dieser Arbeit wird eine allgemeine Methodik zur Herleitung zukünftiger Trends der Schneelast auf Bauwerken vorgestellt, die den Einfluss des Klimawandels auf europäischer Ebene im Hinblick auf die Definition aktualisierter Schneekarten für die neue Generation von strukturellen Eurocodes untersuchen soll. Zunächst wird ein allgemeiner Algorithmus definiert, der auf Monte-Carlo-Simulationen basiert, um Maxima an Bodenschneelasten unter Berücksichtigung der täglichen Ergebnisse der Klimamodelle in Bezug auf maximale und minimale Lufttemperaturen und Niederschläge zu schätzen, ergänzt durch lokale Informationen über Schneefall und Schneeschmelzbedingungen, die aus der Ausarbeitung von realen Messungen tatsächlicher meteorologischer Ereignisse abgeleitet wurden. Nach der Validierung des Verfahrens, bei der die beobachteten Datenreihen der jährlichen maximalen Bodenschneelasten reproduziert werden, werden die Trends der charakteristischen Werte der Last anhand verschiedener Klimamodelle und Szenarien untersucht.
Durch die Analyse verschiedener Klimamodelle und Szenarien wird die relevante Frage der Unsicherheitsbewertung von Klimasimulationen eingehend untersucht. Insbesondere werden die drei Hauptquellen der Unsicherheit, die die Klimaprojektionen beeinflussen: Modellunsicherheit, Szenarienunsicherheit und interne Variabilität, bewertet und ein innovativer, ad hoc entwickelter Wettergenerator implementiert, der in der Lage ist, zukünftige Wetterreihen direkt aus den Ergebnissen der Klimamodelle zu generieren. In diesem Zusammenhang kann das mit dem Wettergenerator erzielte Ergebnis auch durch eine Bayes'sche Technik zur Schneekartenverfeinerung ergänzt werden, die die räumliche Variation des Extremwertprozesses berücksichtigen kann. So

kann ein dynamisches, sequentielles Modellaktualisierungsverfahren entwickelt werden, sobald neue Modelldaten und insbesondere neue Messungen verfügbar werden.
A Confidence Map für die Änderungsfaktoren wird schließlich abgeleitet, indem alle präsentierten Ergebnisse kombiniert werden und als Orientierungshilfe für mögliche Änderungen der aktuellen Version der Schneelastkarten in strukturellen Codes dienen.

SOMMARIO

La progettazione strutturale risulta essere fortemente influenzata dalla valutazione delle azioni climatiche (neve, vento e azioni termiche) che la struttura deve essere in grado di sostenere durante la sua vita, a maggior ragione se si pensa che questa può risultare significatamente più lunga della vita nominale per la quale viene progettata.
In quest'ottica, gli effetti del riscaldamento globale possono significatamene influenzare, in un medio lungo periodo, sia la progettazione di nuove costruzioni che l'affidabilità degli edifici esistenti progettati in conformità con le attuali, o precedenti, normative strutturali. Difatti, l'attuale definizione delle azioni climatiche agenti sulle strutture si basa su un analisi dei valori estremi, applicata alle osservazioni del fenomeno naturale, ipotizzando un condizione di stazionarietà per il clima. In questo modo, valori del carico costanti risultano associati a determinati periodi di ritorno e cambi nella frequenza dei valori estremi non sono così considerati.
Nel presente lavoro viene proposta una metodologia generale per la valutazione dei futuri andamenti del carico neve, con l'obiettivo di studiare l'influenza del cambiamento climatico su scala europea in vista della definizione delle mappe aggiornate del carico per la nuova generazione di Eurocodici strutturali.
In primo luogo, è stato definito un algoritmo, basato su simulazioni Monte Carlo, per la stima del carico neve al suolo sulla base di quelli che sono i principali output dei modelli climatici, ovvero temperature e precipitazioni giornaliere. L'algoritmo che simula il processo di formazione del manto nevoso è quindi supportato da informazioni locali sulle condizioni di precipitazione nevosa e scioglimento, derivate dalla elaborazione di osservazioni puntali degli eventi meteorologici. Una volta validata la procedura, riproducendo serie osservate di massimi annuali di carico neve al suolo, l'andamento futuro viene valutato analizzando attraverso l'algoritmo le proiezioni climatiche ottenute da diversi modelli climatici e considerando differenti scenari futuri di emissione di gas serra. Esaminando differenti modelli climatici e scenari, il tema della quantificazione dell'incertezza associata alle proiezioni climatiche è stato quindi debitamente affrontato. In particolare, le tre principali cause di incertezza, legate ai modelli climatici, agli scenari di emissione e alla variabilità interna del clima, sono state studiate anche attraverso un generatore di clima, sviluppato

nell'ambito della presente tesi, che permette di generare potenziali future serie climatiche direttamente a partire dagli output dei modelli climatici.
In questo contesto, il risultato ottenuto attraverso l'analisi delle serie di proiezioni climatiche può essere supportato da una tecnica di aggiornamento Bayesiano per un affinamento delle mappe del carico. Così facendo, una procedura di aggiornamento dinamico e sequenziale può essere messa a punto man mano che nuove osservazioni diventano disponibili. L'approccio Bayesiano ci consente inoltre di valutare le relazioni spaziali che caratterizzano il processo stocastico dei valori estremi. A tal proposito, è stato definito un modello gerarchico per gli estremi del carico neve al suolo, in cui la classica rappresentazione puntuale viene combinata con un processo spaziale latente, considerando così la variazione dei parametri della distribuzione dei valori estremi in una omogenea regione climatica.
Per tener conto della non stazionarietà del clima, successive finestre temporali di quaranta anni sono state considerate nelle analisi dei valori estremi per le serie climatiche osservate e future. In questo modo, sono state infine derivate mappe per i fattori di cambiamento del carico con i relativi intervalli di confidenza ad essi associati. Tali mappe possono costituire una guida per le possibili modifiche da applicare alle attuali mappe dei carichi climatici presenti nelle normative strutturali.

To my parents

Acknowledgements

First and foremost, I would like to express my gratitude to my Italian advisors Prof. Dr. Ing. Pietro Croce and Dr. Ing. Paolo Formichi, for introducing me to the subject of structural safety and code development, for the inspiration underlying this research work and for many constructive discussions.
I would like also to thank my German advisor Prof. Dr. Hermann Matthies for hosting me at the Institute of Scientific Computing of the University of Braunschweig, and for the fruitful and inspiring discussions.
A big thank goes to Dr. Ing. Noemi Friedman of the Institute of Scientific Computing, for helping me with the topics of uncertainty quantification, inverse problems and Bayesian analysis.
My gratefulness goes also to all current and former colleagues in Braunschweig, and especially to Dr. Elmar Zander, Dr. Ing. Bojana Rosic and Dr. Thilo Moshagen, as well as those at the University of Pisa, and especially to Dr. Ing. Francesca Marsili for having welcomed me at the beginning of PhD and for her constant advices.
Last, but not least, I am grateful to my parents, who highly supported me during these years.

Filippo Landi

Pisa, Italy, February 2019

Thesis outline

The thesis is subdivided in the following way: Chapter 1 defines the general framework and the objectives of this work; Chapter 2, 3 and 4 review the state of the art respectively in the definition of climatic actions on structures, in the assessment of climate change effects, and in the definition of snow load on structures. Chapter 5 investigates the status of harmonization of European snow load maps and Chapter 6 describes the potential implications of climate change on snowfall extremes. The following Chapter 7 to 11 illustrate new ideas and applications developed by the author, and thus they represent the most original part of the work. Chapter 12 draws the conclusions and the further steps of the research. In particular:

Chapter 1 identifies the motivation behind the research and the scope of the thesis. The main objectives of the thesis are thus presented and discussed also presenting the practical applications that have been developed;

In **Chapter 2** current methods for the definition of climatic actions in structural codes, based on extreme value theory and on the assumption of stationary climate are reviewed. Climate is always changing but the marked changes emphasized by recent studies make the stationary assumption more questionable and draw the attention on the necessity to set-up new models for extremes relying not only on past observations but incorporating also climate model projections. Then, methods for the analysis of extremes in a changing climate are introduced focusing on their suitability for structural design;

In **Chapter 3** the topic of climate change is introduced, considering observed changes in the climate system and presenting the most recent climate models and scenarios for the evaluation of future changes. The relevant issue of uncertainty in climate projections is assessed and calibration strategies for the analysis of climate model simulations are introduced. Finally, potential implications on structural design are discussed;

Chapter 4 reviews the state of art about the definition of ground snow loads for structural design. The European Snow Load Research Project is presented together with its results that lead to the Eurocode EN1991-1-3:2003. The current version of the European Ground Snow Load map is also drawn analysing the provisions given by National Annexes;

In **Chapter 5** the snow load maps given in the informative Annex C of EN1991-1-3 are compared with those given in National Annexes. The comparison shows that higher characteristic values of snow load are obtained according National Annexes than in Annex C for large part of the populated European territory denoting an hidden safety factor in snow load definition. Moreover, characteristic values of ground snow loads across borders of neighbouring Countries are evaluated, to investigate the status of harmonization, in view of the elaboration of the second generation of the Eurocodes to be published in 2020-2023. The results still show the lack of a full consistency of characteristic values across administrative borders between Countries, enlightening the need of a further work to enhance the harmonization of the European snow load map;

In **Chapter 6** the review and analysis of the state of art is completed by recent research studies about implications of climate change on snowfall extremes. It is shown how although a decrease in mean snowfall is expected in most regions due to the decrease of snowfall frequency, a contrasting response may be experienced for snowfall extremes due to the increase of precipitation rate with temperature. The recent failures of roofs in Europe caused mainly by heavy snow load and discussed in the last paragraph, confirm the relevance of the problem and call for an estimation of the expected snow load on structures taking into account the implications of the climate change;

In **Chapter 7**, a procedure for the assessment of future trends of climatic actions, starting from regional climate model output, is presented. In particular, a new simple weather generator is developed to investigate the internal variability of climate models. Analysing the climate series generated according different climate models, factors of change for extreme statistics are derived together with their uncertainty range.
An application of the proposed technique is shown to evaluate future trends in 50 year return period of maximum and minimum daily temperature and precipitation, for an Italian climatic region. The results, presented in terms of prediction interval maps for the investigated region, show how this technique is very promising and can provide guidance for the assessment of the impacts of

climate change on climate extremes, allowing also to evaluate the uncertainty in the prediction. Significant changes in extreme temperatures, maximum and minimum, are found for the study region, even more evident than the expected changes for mean temperature. A robust change in precipitation extremes is also detected for the study region, confirming the increase of heavy rainfall expected in a warming climate;

In **Chapter 8**, a general procedure to evaluate future trends of snow loads on structures is illustrated combining available outputs of climate models in terms of maximum and minimum temperatures and water precipitation, with local information of snowfall and snow melting conditions. The methodology, which is based on Monte Carlo simulations, is presented together with the results obtained for some Italian and German weather stations. Factors of change maps are thus shown for characteristic ground snow loads in an Italian and German climatic region;

Chapter 9 presents a stochastic technique for bias correction and downscaling of climate projections together with an application for the local assessment of future trends of snow loads;

In **Chapter 10**, a technique for snow load map refinement is proposed. Ground snow loads derived starting from gridded climate data as those provided by climate models, are combined with observed point measurements and then suitably updated following the Bayesian approach;

In **Chapter 11**, a Bayesian hierarchical model for extreme snow loads is set-up in order to take into account the variation of the extreme value process over the region. The main features and the potentialities of the proposed method are highlighted referring to a relevant case study, concerning the updating of snow load maps obtained according an ensemble of Regional Climate Models. Factors of change maps are then shown for characteristic ground snow loads in an Italian climatic region having considered in the estimation of future trends: the influence of inherent uncertainty of the outcomes of climate models, the spatial variation of the extreme value process and the dependence on future emission scenarios;

Finally, in **Chapter 12** the main conclusions of the work are drawn discussing the results and giving some suggestions and indications for future research.

Contents

List of Abbreviations

AOGCM	Atmosphere–Ocean General Circulation Models
CDF	Cumulative Distribution Function
CEN	European Committee for Standardization
CMIP	Climate Model Intercomparison Project
CORDEX	COordinated regional climate Downscaling EXperiment
DEM	Digital Elevation Model
DMI	Danish Meteorological Institute
DSL	Design Service Life
ESLRP	European Snow Load Research Project
FC	Factor of Change
GCM	Global Climate Model
GEV	Generalized Extreme Value
GIS	Geographic Information System
GP	Generalized Pareto
IPCC	Intergovernmental Panel on Climate Change
IPSL	Institute Pierre Simon Laplace
KL	Karhunen Loeve (expansion)
KNMI	Royal Netherlands Meteorological Institute
LSM	Least Square Method
MCMC	Markov Chain Monte Carlo

MLM	Method of Maximum Likelihood
MOM	Method of Moments
MPI	Max Planck Institute
NA	National Annex
NDP	Nationally Determined Parameter
NSB	National Standard Body
PDF	Probability Density Function
POT	Peak Over Threshold
RCM	Regional Climate Model
RCPs	Representative Concentration Pathways
SLS	Serviceability Limit State
SWE	Snow Water Equivalent
ULS	Ultimate Limit State
WCRP	World Climate Research Programme

Chapter 1

General Overview

In this chapter an introduction to the topic of climate change and its implications on new and existing structures is given. The main objectives of the thesis are thus presented and discussed.

Contents

1.1 Introduction

Warming of the climate system is unequivocal [67], according to many different kinds of evidence. Observations show increases in globally averaged air and ocean temperatures, as well as widespread diminishing of snow and ice, rising of averaged sea level and increasing of concentration of greenhouse gasses. Climate is always changing, however many of the observed changes are unprecedented over decades to millennia [67] and cannot be explained by the natural variability of the climate. Climate change potentially affects all regions of the world by alteration of natural processes, modification of precipitation patterns, melting of glaciers, rise of sea levels, etc.
Whatever the warming scenarios and the level of success of mitigation policies, in the coming decades the impact of climate change is generally expected to increase because of the delayed impacts of past and current greenhouse gas emissions[44]. Then, unavoidable climate change impacts need to be considered, taking into account its economic, environmental and social consequences in different fields. Adaptation strategies to enhance the capacity to withstand climate change effects are especially needed in key sectors such as infrastructures and buildings, which are vulnerable and characterized by long life span and high costs.
In this context, a central role is played by technical standards and by their evolution during the lifetime cycle of infrastructures and buildings [46], also considering that the real life span of most structures is much longer than their design working life.
Since structural design is often governed by climatic actions such as thermal, wind, snow and ice loads, alteration of them caused by climate change could significantly affect the design of new structures and infrastructures as well as the reliability of the existing ones designed in accordance to the provisions of current or past Codes.
Therefore, the assessment of climate change impact on design of new structures and on the reliability of existing ones becomes a key aspect in the future evolution of standards, as requested by the European Commission for the second generation of the structural Eurocodes [43] and all other standards relevant to transport infrastructures, energy infrastructures, and buildings/constructions [45].
In particular, the evaluation of the impact of climate change on climatic actions in relation to structural design issues is requested in order to prepare modified or additional clauses for climatic actions codes in the Eurocode 1

Figure 1.1: Eurocode I - Parts related to climatic actions.

suite (EN1991-1-3 [14], EN1991-1-4 [16], EN1991-1-5 [15] and the new EN 1991-1-9, see Figure 1.1). Potential amendments to current codes will be done with the primary focus to include, during this revision phase, possible climate change effects in the design rules, avoiding future expensive structural changes.

1.2 Objectives

The main objective of the present Ph.D. thesis is the definition of a suitable methodology to evaluate climatic actions on structures under changing climate conditions, combining information provided by past observations and climate projections. Indeed, observed data series upon which the current definition of climatic actions is based, generally consist of 40-50 years of measurements, which do not sufficiently extend over time to reflect the effects of the climate change. At present it is therefore necessary to rely on climate projections, resulting from appropriate Global or Regional Climate Models, which are the major source of knowledge about future climate.
The proposed general methodology allows to derive factors of change for

climatic actions, providing guidance for potential amendments of current definitions in technical standards to take into account the non-stationary of the climate. A special attention has been devoted to the assessment of climate change impact on ground snow loads.
A new procedure for the estimation of ground snow loads from available climate model output, supplemented by local information on snowfall and snow melting condition, has been developed and tested in different European weather stations. Analysing different climate models and scenarios, future trends of snow loads are assessed, considering the main sources of uncertainty affecting climate projections. In particular, an innovative ad hoc developed weather generator and an original stochastic downscaling technique have been set up to quantify uncertainties in future projections.
Finally, the definition of Bayesian hierarchical models is proposed to characterize the spatial variation of the extreme value process in homogeneous climatic region. Results in terms of factors of change confidence maps are thus presented for ground snow loads in Italy and Germany.

Chapter 2

Climatic actions and structural design

In this chapter, current methods for definition of climatic actions in structural codes, based on extreme value theory are reviewed and the analysis of extremes in a changing climate is introduced.

Contents

2.1 Definition of climatic actions on structures

The definition of climatic actions on structures in structural Codes is currently based on the statistical analysis applied to past observations of the underlying natural phenomenon. Annual maxima are extracted from data collected at weather stations and an extreme value analysis is carried out in order to estimate the cumulative distribution function (CDF) and the probability density function (PDF) of the investigated climate variable.
Then, the value of the load to be used for structural design is specified by structural Codes as a value that has some small probability of being exceeded in any given year. Rules for the definition of climatic actions, as well as for other design loads, are thus given in relevant standards such as the ASCE (American Society of Civil Engineers) Standard [1], where snow, wind, rain and icing loads are treated, and ISO Standards for snow (ISO 4355:2013 [70]), wind (ISO 4354:2009 [69]) and atmospehric icing (ISO 12494:2017 [71]).
In Europe, climatic loads for Structural design are defined in structural Eurocodes, especially EN1991-1-3 [14] for snow loads, EN1991-1-4 [16] for wind loads and EN1991-1-5 [15] for thermal loads, while the new part for icing loads EN1991-1-9 is scheduled for 2020 [17].
In the verification of the structural performance, characteristic values of the climatic actions are associated to a given probability of exceedance in a reference period. In EN1990 [13], it is specified that the characteristic value of climatic actions is based upon the probability of 0.02 of its time-varying part being exceeded for a reference period of one year, then a mean return period of 50 years is assumed. Characteristic values of climatic actions and their maps are typically considered country specific data, to be included in National Annex as Nationally Determined Parameters. Maps for characteristic ground snow loads s_k, basic wind velocity $v_{b,0}$, maximum and minimum shade air temperature $T_{\max}$ and $T_{\min}$, are then reported in National Annexes to EN1991-1-3 [14], EN1991-1-4 [16] and EN1991-1-5 [15].
Although different procedures for the analysis of extreme can be adopted by different countries, the current definition of characteristic values of climatic actions is based on the extreme value analysis of past observations of the natural phenomena, under the assumption of stationary climate conditions, and no potential effects of climate change are considered.

2.2 Analysis of climate extremes

2.2.1 Classical Extreme Value Theory

2.2.1.1 Extreme Value Modelling

Statistics of extremes have played an important role in engineering practice [79] and the extreme value theory provides a rigorous framework for the analysis of climate extremes and their return level [18]. The cornerstone of extreme values theory is the extremal types theorem [19] that guarantees the convergence of the distribution of maxima to one of the three limiting distributions usually referred as Gumbel or extreme value type I distribution, Fréchet or extreme value type II distribution and Weibull or extreme value type III distribution. The three extreme value distributions behave differently, but they can be synthesised into a single family of three parameters distribution called Generalized Extreme Value (GEV) distribution [19] having the cumulative distribution function, for the random variable X, of the form

$$F(x) = \exp\{-[1+\xi(\frac{x-\mu}{\sigma})]^{\frac{-1}{\xi}}\} \tag{2.1}$$

defined on the set $\{z : 1+\xi(\frac{x-\mu}{\sigma}) > 0\}$ where the location μ, scale σ and shape ξ parameters satisfy the inequalities $-\infty < \mu < \infty$, $\sigma > 0$, and $-\infty < \xi < \infty$. The type II (Fréchet) and type III (Weibull) classes of extreme value distributions correspond respectively to the cases $\xi > 0$ and $\xi < 0$ and the subset of the GEV family with $\xi = 0$ is interpreted as the limit of Equation 2.1 as $\xi \to 0$, corresponding to the type I (Gumbel) family with cumulative distribution function

$$F(x) = \exp\{-\exp[-(\frac{x-\mu}{\sigma})]\} \tag{2.2}$$

where the location parameter μ specifies the centre of the distribution and the scale parameter σ determines the size of deviations around the location parameter. The GEV distributions are presented in Figure 2.1. The type II distribution ($\xi > 0$) is said to be heavy tailed, because its probability density function decreases at a slow rate in its upper tail. Moments are even infinite for orders greater than $1/\xi$ (e.g. first moment, the mean, is infinite for $\xi \geq 1$ and

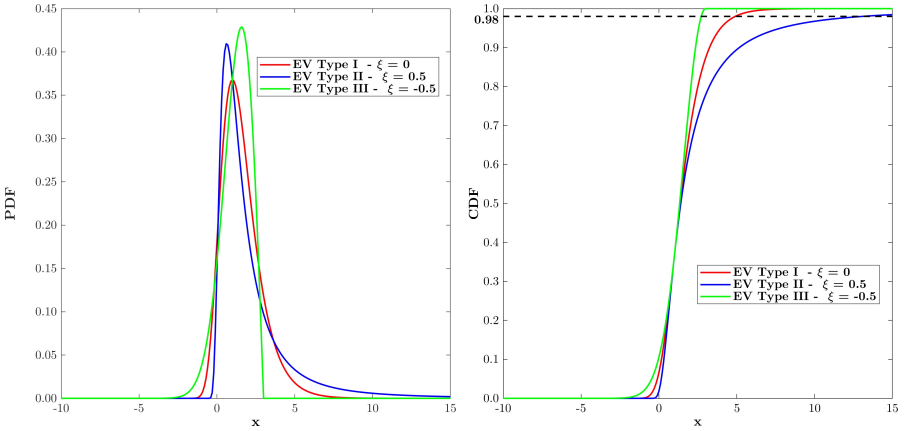

Figure 2.1: Generalized Extreme Value distribution, PDFs and CDFs for $\mu = 1$ and $\sigma = 1$.

second moment, the variance, is infinite for $\xi \geq \frac{1}{2}$). The type III distribution ($\xi < 0$) is instead characterized by a bounded upper tail, while the type I ($\xi = 0$) has an unbounded thin upper tail.

In order to model extremes of a series of independent observations, the so called "block maxima approach" is followed: data are blocked into sequences of observations generating a series of block maxima to which the GEV distribution can be fitted. Blocks are usually chosen to correspond to a time period of one year, and the block maxima are thus annual maxima. Estimates of extreme quantiles x_p of the annual maximum distribution are then obtained by inverting Equation 2.1 and 2.2

$$x_p = \begin{cases} \mu - \frac{\sigma}{\xi}\{1 - [-\log(1-p)]^{-\xi}\} & for \quad \xi \neq 0 \\ \mu - \sigma \log[-\log(1-p)] & for \quad \xi = 0 \end{cases} \tag{2.3}$$

where x_p is the return level associated with the return period $\frac{1}{p}$ since to a reasonable degree of accuracy, x_p is expected to be exceeded on average once every p years [19]. As mentioned in the previous paragraph, a return period of 50 years ($p = 0.02$) is commonly taken as reference period for the definition of climatic actions on structures. A different approach for extreme value modelling is based on the exceedance of an high threshold, the so called Peak Over Threshold (POT) approach. In this case, the generalized Pareto (GP) distribution is the limiting distribution associated to the extreme process. The

cumulative distribution function of the excess of a threshold u, $y = X - u$, is given by

$$F(y) = 1 - (1 + \frac{\xi y}{\hat{\sigma}})^{\frac{-1}{\xi}} \tag{2.4}$$

defined on the set $\{y : y > 0 \quad \text{and} \quad (1 + \frac{\xi y}{\hat{\sigma}})^{\frac{-1}{\xi}} > 0\}$, where the shape parameter ξ is equivalent to that of the GEV distribution while the scale parameter $\hat{\sigma}$ is obtained according the following equation

$$\hat{\sigma} = \sigma + \xi(u - \mu). \tag{2.5}$$

The peaks over threshold method and Pareto distribution are commonly used in hydrology and finance, but seldom applications can be found in the definition of climatic actions on structures. The reason can be explained with the heavy tail of the distribution that may lead to the definition of too conservative design loads.

2.2.1.2 Parameter Estimation and Return Levels

Many techniques have been proposed for parameter estimation in extreme value models [19]. Each of them has its pros and cons and there is no generally accepted fitting method. Parameter estimation methods include:

- Regression methods based on probability plot, which consists in a graph paper with non-linear scales on the probability and maxima axes chosen so that if the data came from the selected distribution then the cumulative distribution plot should be distorted to lie along a straight line. Assuming an extreme value type I distribution, a plot of x-value against the cumulative probability of non-exceedance (1-p) should give a straight line according to the following formula

  $$x_p = \mu + \sigma\{-\log[-\log(1-p)]\} \tag{2.6}$$

  where the parameters μ and σ merely represent the parameters of the linear relationship between x_p and the reduced variate $y = -\log[-\log(1-p)]$. Determining the expected probability of exceedance p is not a trivial

problem, since it requires the assignment of plotting positions to each event in the sample. This is commonly done by arranging maxima in descending order of magnitude and then assigning a probability p considering the position i of the considered observation in the ordered sample of n maxima. Different plotting positions formulas can be found in literature for extreme value analysis as described in [98], but the formula $p = i/(n+1)$ proposed by Weibull [154] is the most commonly used and it is the only one correct in estimating the return periods of extreme events [98]. The distribution is then fitted by putting a straight line through the plotted values, either by eye (graphical methods) or by least squares method (LSM) estimating parameters according the following formulas

$$\sigma = \frac{n\sum_{i=1}^{n} x_i y_i - \sum_{i=1}^{n} x_i \sum_{i=1}^{n} y_i}{n\sum_{i=1}^{n} y_i^2 - (\sum_{i=1}^{n} y_i)^2} \tag{2.7}$$

$$\mu = \frac{\sum_{i=1}^{n} x_i - \sigma \sum_{i=1}^{n} y_i}{n} \tag{2.8}$$

or by using the Gumbel fitting method [97]

$$\sigma = \frac{\sqrt{\sum_{i=1}^{n}(x_i - \bar{x})^2}}{\sqrt{\sum_{i=1}^{n}(y_i - \bar{y})^2}} \tag{2.9}$$

$$\mu = \bar{x} - \sigma\bar{y} \tag{2.10}$$

- The method of moments (MOM) is an analytic method based on the simple idea that, since the first two moments of the distribution (mean and variance) depend on the parameter values, estimates of these values can be obtained using estimates of the mean and variance from the data. In this way, μ and σ are estimated by the sample mean $\bar{x}$ and standard deviation S_x

$$\sigma = \frac{S_x\sqrt{6}}{\pi} \approx 0.7797 S_x \tag{2.11}$$

$$\mu = \bar{x} - \gamma\sigma \approx \bar{x} - 0.5772\sigma \tag{2.12}$$

where γ is the Euler constant equal to 0.5772.

- The method of maximum likelihood (MLM) which consists of finding the values for the distribution parameters, maximizing the likelihood or the log-likelihood that the observed maxima come from the assumed distribution. Assuming an extreme value type I distribution the log-likelihood function is

$$l(\mu,\sigma) = -n\log(\sigma) - \sum_{i=1}^{n}\frac{x_i-\mu}{\sigma} - \sum_{i=1}^{n}\exp[-(\frac{x_i-\mu}{\sigma})] \tag{2.13}$$

and the parameters μ and σ which maximize the log-likelihood function can be determined by numerically solving the following equations

$$\sigma = \bar{x} - \frac{\sum_{i=1}^{n} x_i \exp(\frac{-x_i}{\sigma})}{\sum_{i=1}^{n}\exp(\frac{-x_i}{\sigma})} \tag{2.14}$$

$$\mu = -\sigma\log(\frac{\sum_{i=1}^{n}\exp(\frac{-x_i}{\sigma})}{n}). \tag{2.15}$$

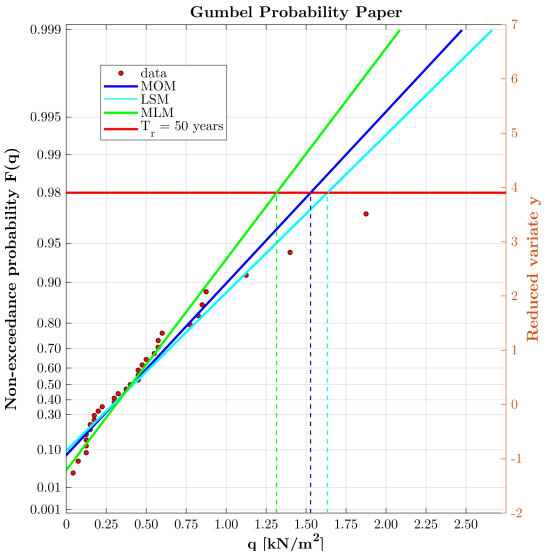

Method	q_k[kN/m^2]
MOM	1.53
LSM	1.63
MLM	1.32

Figure 2.2: Comparison of parameter estimation methods - Bologna (IT).

Once estimated the extreme value parameters return levels can be derived according Eq.2.6. In particular, characteristic values can be calculated for $p = 0.02$. Figure 2.2 and 2.3 show, as an example, a comparison of the results obtained according to the different methods for ground snow load maxima q

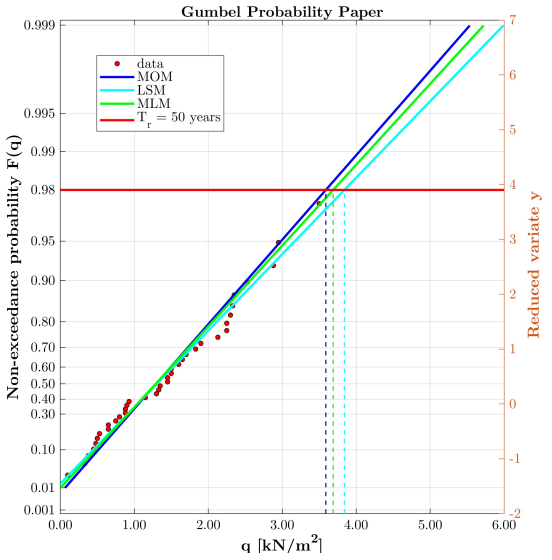

Method	q_k[kN/m^2]
MOM	3.59
LSM	3.84
MLM	3.69

Figure 2.3: Comparison of parameter estimation methods - Pavullo (IT).

at two Italian weather stations in a Gumbel probability paper. As expected different fitted distributions are obtained (blue solid lines represent the MOM fit, cyan lines the LSM fit and green solid lines the MLM fit). The LSM fit generally gives the highest values in terms of characteristic loads, as confirmed by both stations, and it was chosen in the European Snow Load Project [126].

2.2.2 Non stationary extremes

As mentioned before, in a changing climate the common assumption of stationary climate is becoming debatable. The frequency of extremes events is continuously evolving and the changes are likely to continue in the future. Therefore, the growing interest in this field is leading to the definition of non-stationary extreme value models where time dependency is taken into account defining a trend model for the parameters of the extreme value distributions. Time dependency of the parameters is usually modelled in climatology assuming the existence of a functional relationship between the distribution parameters and time. Although different models may be defined, simple linear

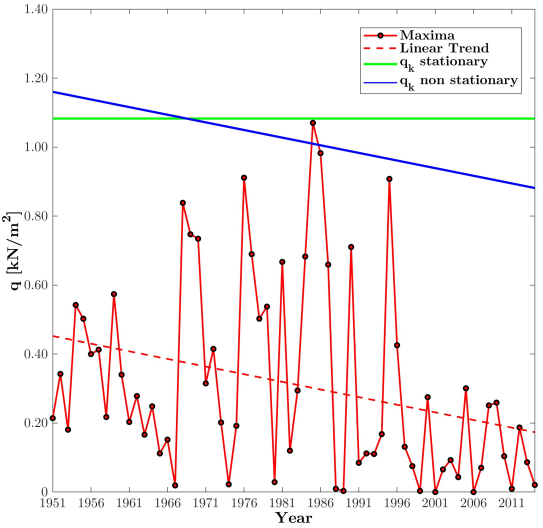

Figure 2.4: Annual maxima of ground snow loads based on observations - Stationary and non stationary characteristic loads.

or log-linear models are normally used [77]

$$\mu(t) = \mu_0 + \mu_1 t, \quad \log(\sigma(t)) = \sigma_0 + \sigma_1 t, \quad \xi(t) = \xi, \tag{2.16}$$

and most applications consider non-stationarity only for the location parameter, assuming the scale and the shape parameter nearly constant [18].
Nevertheless, significant uncertainties remain in the definition of the trend model, because the simple analysis of block maxima often is not sufficient to identify an univocal trend over a long time period. This consideration appears quite obvious looking to some practical example, such as the one illustrated in Figure 2.4, where the annual maxima ground snow loads are illustrated together with characteristic values q_k obtained for an Italian weather station under stationary (green solid line) or non-stationary conditions (blue solid line).

Although the trend is not univocal in the investigated period, the analysis of the entire population of data using the Mann-Kendall test [100][80], with significance level $\alpha = 0.05$ as suggested in [18], detects the presence of a decreasing linear trend in the extremes. This result may lead to the definition

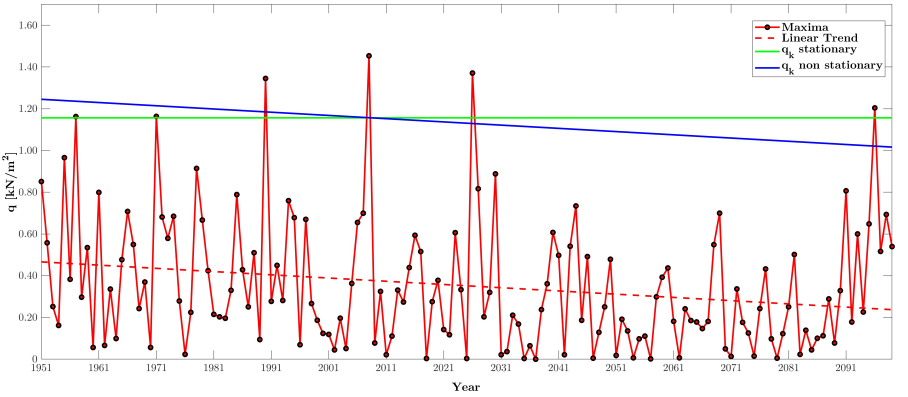

Figure 2.5: Annual maxima of ground snow loads based on climate projections - Stationary and non stationary characteristic loads.

of a linear model for location parameter

$$\mu(t) = \mu_0 + \mu_1 t \tag{2.17}$$

with constant scale parameter σ. However, the consequent decreasing value of the characteristic load obtained by the non-stationary model may result unsafe for structural requirements. This aspect is especially enhanced for long time series where particular attention should be devoted to check the homogeneity of the available data population. In Figure 2.5, the results presented above are reported considering a longer series of annual maxima of ground snow loads obtained from the analysis of climate projections provided for the control period (1951-2005) and the future period 2006-2100 (Scenario RCP4.5).

Moreover, it is important to underline that extremes in a changing climate are more sensitive to changes in the variability associated to the scale parameter than in the mean associated to the location parameter as demonstrated in [78]. Consequently, assuming a constant scale parameter, this important aspect is completely neglected.
In this study, the analyses are then oriented towards a correct definition of non-stationary extremes suitable for structural design [26]. In particular, trends in location and scale parameters will be assessed dividing the maxima data series in appropriate time windows and then checking the results in terms of characteristic loads. In Figure 2.6, the trend in characteristic values is reported for the same data in Figure 2.5, considering subsequent time window of 40 year shifted by ten years (1951-1990, 1961-2000,...,2051-2090).

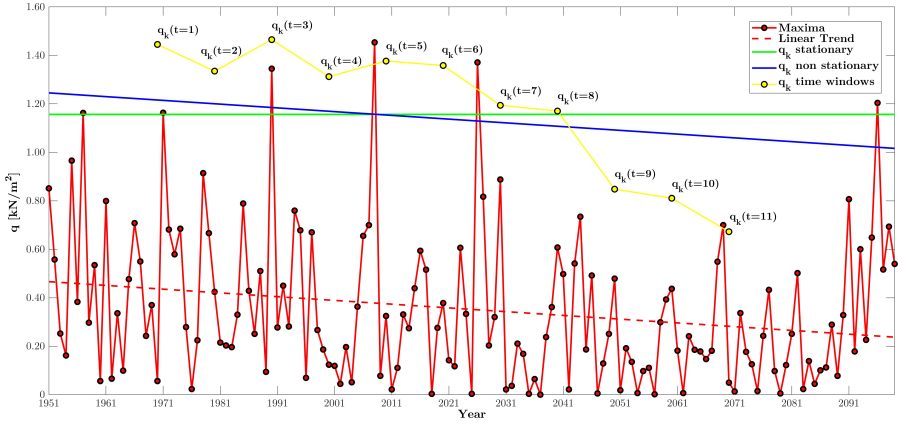

Figure 2.6: Annual maxima of ground snow loads based on climate projections - Stationary and non stationary characteristic loads with time windows.

Chapter 3

Climate change: evidence, models and effects

In this chapter, the topic of climate change is introduced, considering new evidence based on many independent scientific studies. Most recent climate models and scenarios for the evaluation of future changes are presented with their ability and drawbacks. Calibration strategies for the analysis of climate model simulations are then introduced. Finally climate change implications on structural design are discussed.

Contents

3.1 Observed changes in the climate system

The Earth's climate has always changed throughout its history. However, the current warming trend is considered of particular significance because it proceedes at a rate that is unprecedented over decades to millennia [67] and because it is extremely likely (greater than 95 percent probability [67]) that it is the result of human activity since the mid-20th century.
The Intergovernmental Panel on Climate Change (IPCC) confirms in its last report [67] that warming in the climate system is unequivocal with unprecedented observed changes in warming of the atmosphere and the ocean, diminishing of snow and ice, rising of sea levels and increasing of greenhouse gases concentrations. In particular,

- each of the last three decades has been successively warmer at the Earth's surface than any preceding decade since 1850;
- changes in many extreme weather and climate events, such as increase in the frequency of heat waves and heavy precipitation, have been observed since about 1950;
- the rate of sea level rise since the mid-19th century has been larger than the mean rate during the previous two millennia with high confidence;
- Greenland and Antarctic ice sheets have been losing mass and glaciers have continued to shrink almost worldwide over the last two decades;
- the atmospheric concentrations of carbon dioxide(CO_2), methane(CH_4), and nitrous oxide(N_2O), the so called greenhouse gasses, have increased to levels unprecedented in the last 800,000 years. Especially, carbon dioxide (CO_2) concentrations have increased by 40% since pre-industrial times, mainly from fossil fuel emissions but also from net land use change emissions.

Drivers of climate change are natural and anthropogenic substances and processes that alter the Earth's energy budget. The strength of climate change drivers is quantified as radiative forcing, which is the change in energy flux calculated in units watts per square meter W/m^2. The total radiative forcing is positive and is leading to surface warming. Best estimate of the global average radiative forcing in 2011 relative to 1750 is about 2.29 W/m^2 (with 90% interval from 1.13 to 3.33). Future climate projections require information about future emissions or concentrations of greenhouse gases; for this reason,

climate change scenarios are thus identified by their approximate total radiative forcing level in year 2100 relative to 1750.

3.2 Climate models and scenarios

3.2.1 Climate and weather predictability

A frequently asked question about climate change studies is "*If you cannot predict the weather next month, how can you predict climate for the coming decades?*" [67]. It is important to highlight that even if climate and weather are intertwined, they are two different things.
Weather is defined as the state of the atmosphere at a given time and place, and can change from hour to hour and day to day, while climate generally refers to the statistics of weather conditions over a long period of time, such as a decade or more.
Therefore, there is a distinction among weather forecasts, which provide forecasts of the detailed day-to-day evolution of future weather, and climate predictions that provide probabilities of long-term changes of the statistics of future climatic variables.
To make accurate weather forecasts, highly detailed information is needed about the current state of the atmosphere because small errors in the depiction of "initial conditions" typically leads to inaccurate forecasts beyond a week or two due to the chaotic nature of the atmosphere, as showed by Lorenz in [95] and [96]. Climate projections, instead, aim to provide information about the evolution of the statistics of weather and there is a sound scientific basis for supposing that these aspects of climate can be predicted [67].

3.2.2 Climate models and their characteristics

Climate models are considered our major source of knowledge about future climate [103]. They are process-based dynamical models [153], which operate on the entire globe or in limited region of the world, simulating the physics and chemistry of the atmosphere and oceans to obtain projections of temperature and other meteorological variables under various assumptions. Indeed, they can be run in different modes: considering observed changes in atmospheric composition to reproduce historical climate or according to different scenarios

of possible and plausible changes of forcing agents to simulate future climate. In most of the cases, these scenarios refer to changes in the emission of greenhouse gasses [153] and depend on economic and social development.
The output from climate models, in terms of climate projections of meteorological variables, drives forward climate science, helping scientists to understand changes affecting the Earth's climate and to underpin policy decisions for mitigation and local adaptation.
In practical terms, climate models are complex numerical computer models which consist of a set of equations representing the processes and interactions that drive the Earth's climate. Therefore, climate models abide fundamental physical principles, such as the first law of thermodynamics and the Stefan-Boltzmann Law, and comprise equations that describe the dynamics of the climate system such as the Clausius-Clapeyron equation and the Navier-Stokes equations. Since these equations are so complex that there is no known exact solution to them, they are discretized on a grid and solved numerically on big computers.
Earth is divided into a series of boxes, called grid cells, and the size of the grid cells is known as the spatial resolution of the model. Higher resolution models provide much more detailed information, however require also higher computational capacity. In general, increasing the spatial resolution of a model by a factor of two will require around 10 times the computing power to run in the same amount of time. A compromise with computation possibilities is done and the current resolution of global climate models is typically around 125 km in longitude and latitude in the mid-latitudes (Figure 3.1a), while regional climate models can reach a resolution of 12.5 km (Figure 3.1b). A similar compromise has to be made for the time step, how often a model calculates the state of the climate system. The finite resolution of climate models in space and time, implies that the effects of certain processes must be represented through "parameterizations" that are included into the numerical equations[153].

3.2.3 Global climate models

Global Climate Models (GCMs) , also known as General Circulation Models, describe several components of the climate system, such as the atmosphere the ocean, the cryosphere and the land surface.

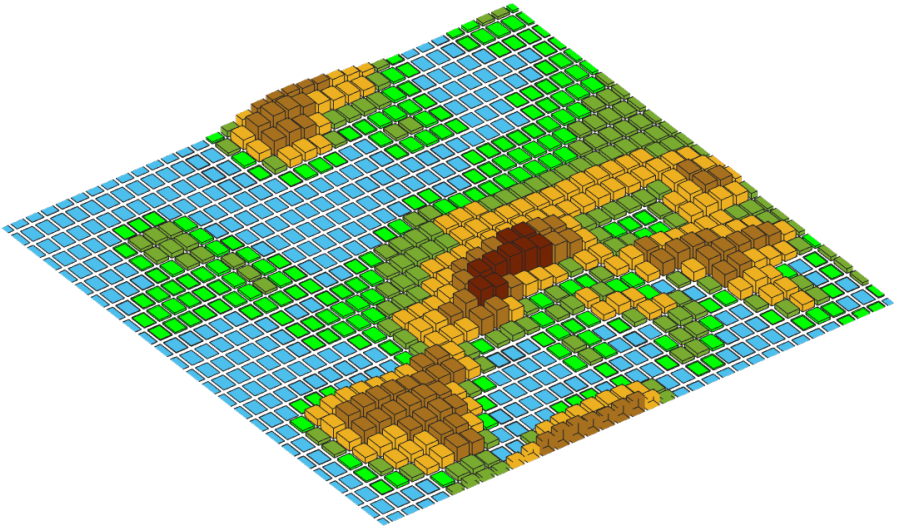

(a) Global Climate Model (GCM) - 125km x 125km grid

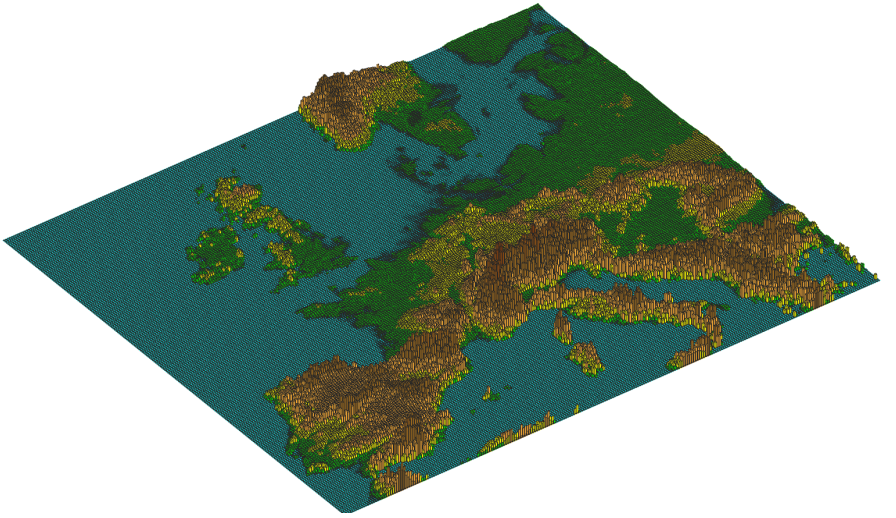

(b) Regional Climate Model (RCM) - 12.5km x 12.5km grid

Figure 3.1: Illustration of the European topography at different resolution.

Early GCMs were able to simulate only one of these components of the Climate System at each time but current coupled models such as the Atmosphere–Ocean General Circulation Models (AOGCMs) are able to describe interactions and provide a more comprenhisive representation of the climate system, near at the end of the spectrum of models currently available [67].
A key limitation of GCMs is the coarse resolution that doesn't allow to obtain information about future climate useful for practical planing and adaptation at local scale. Since running the GCMs to a finer scale can result too expensive, to obtain information at a more local scale Regional Climate Models (RCMs) are currently used.

3.2.4 Regional climate models

Regional Climate Models (RCMs) work by increasing the resolution of the GCMs in a small, limited area of interest. They are limited-area models with representations of climate processes comparable to those in the atmospheric and land surface components of AOGCMs, even if they are typically run without interactive ocean and sea ice [67].
Indeed, the response of the global circulation to large-scale forcings is simulated by the GCMs and is used to "drive" the RCM that takes into account sub-GCM grid scale forcings (e.g. complex topographical features and land cover inhomogeneity) in a physically-based way and to enhance the simulation of atmospheric circulations and climatic variables at finer spatial scales [67]. For this reason, a driving GCM is always associated to a RCM.
Therefore, RCMs are used to dynamically downscale GCMs simulations to provide more detailed information in some specific region. The added value of RCMs is expected in the simulation of topography-influenced phenomena and extremes with relatively small spatial or short temporal character.
In Figure 3.1 the European topography is illustrated for a typical GCMs of the fifth phase of the Climate Model Intercomparison Project (CMIP5), cell resolution 125 km x 125 km, and for the high-resolution RCMs developed by the EURO-CORDEX initiative [73], cell resolution 12.5 km x 12.5 km.

3.2.5 The EURO-CORDEX initiative

As part of the global COordinated Regional climate Downscaling EXperiment (CORDEX), the EURO-CORDEX initiative provides regional climate projections for Europe at the resolution illustrated in Figure 3.1b, also known as EUR-11 grid ($0.11° \sim 12.5$km).
The experiment is still on going and the available climate projections, provided for different climate models and scenarios, represent the most updated inputs for climate change impact and adaptation studies in Europe. Therefore, they will be used in the analysis presented in the next chapters.

3.2.6 Representative Concentration Pathways

Climate models are run according to different scenarios of potential changes of forcing agents to simulate future climate. As mentioned before, climate change scenarios are identified by their approximate total radiative forcing level in year 2100.
A new set of scenarios, the Representative Concentration Pathways (RCPs), was used for the new climate model simulations carried out under the framework of the fifth phase of the Coupled Model Intercomparison Project (CMIP5) of the World Climate Research Programme. An overview on the main characteristics of the Representative Concentration Pathways can be found in [150].
A set of four pathways were produced and they are identified by the radiative forcing level at the end of the century: 2.6 W/m^2(RCP2.6), 4.5 W/m^2(RCP4.5), 6 W/m^2(RCP6) and 8.5 W/m^2(RCP8.5).
RCPs provide information on all components of radiative forcing that are needed as input for climate modelling and atmospheric chemistry modelling (concentration and emissions of greenhouse gases and air pollutants, and land use change) resulting from different combinations of economic, technological, demographic, policy, and institutional futures.
Among them, we can identify a mitigation scenario leading to a very low forcing level, the RCP2.6, two stabilization scenarios, the RCP4.5 and RCP6, and one high greenhouse gas emissions scenario, the RCP8.5. The trajectories are illustrated in Figure 3.2.

In Figure 3.3, changes of global average surface temperature obtained by the CMIP5 multi-model ensemble, are illustrated for different RCPs, while Figure 3.4 shows the corresponding rise in global mean sea level.

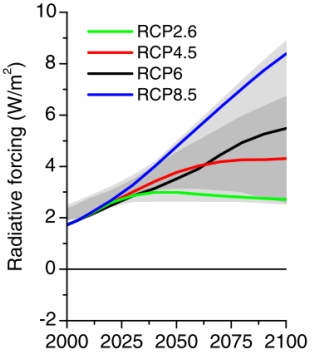

Figure 3.2: Trends in radiative forcing for different RCPs [150].

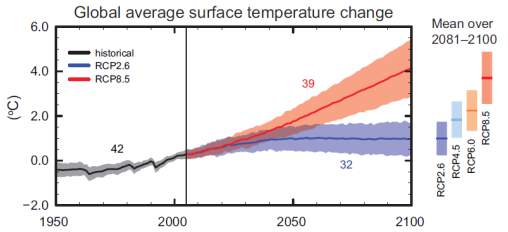

Changes for 2081-2100		
Scenario	Mean (°C)	5-95% Range
RCP2.6	1.0	0.3 to 1.7
RCP4.5	1.8	1.1 to 2.6
RCP6	2.2	1.4 to 3.1
RCP8.5	3.7	2.6 to 4.8

Figure 3.3: Global average surface temperature simulated changes relative to the reference period 1986–2005 [67]

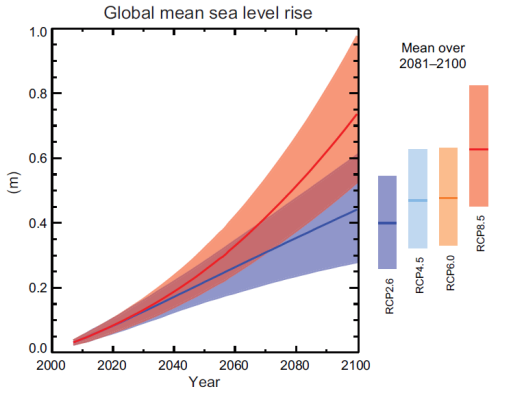

Changes for 2081-2100		
Scenario	Mean (m)	5-95% Range
RCP2.6	0.40	0.26 to 0.55
RCP4.5	0.47	0.32 to 0.63
RCP6	0.47	0.33 to 0.63
RCP8.5	0.63	0.45 to 0.82

Figure 3.4: Global mean sea level rise simulated changes relative to the reference period 1986–2005 [67].

3.3 Uncertainty in climate projections

Climate models, even the most informed and sophisticated ones, are approximations of the real climate system and therefore their projections are inherently uncertain [83]. Moreover, different models produce different projections of future climate and then a critical issue in climate change impact studies is the estimation of uncertainties associated with future predictions.
For any climate projection there is both an epistemic uncertainty that arises from the incomplete understanding of climate processes and then from the model limitations, and an aleatoric random part of uncertainty due, for example, to the natural variability of the climate. Hawkins and Sutton [55] identify three distinct main sources of uncertainty in climate predictions:

- Internal Variability of the climate system, which represents the natural fluctuations in the forecasts that arises in the absence of any radiative forcing of the planet and can have the potential to reverse trends that are associated with anthropogenic climate change;
- Model uncertainty, which represents the fact that different models may simulate somewhat different changes in the climate, in response to the same radiative forcing;
- Scenario uncertainty, related to future emissions of greenhouse gases, which causes uncertainty in future radiative forcing and hence in the climate.

The relative importance of each source of uncertainty depends on the investigated climate variable and varies with prediction lead time but also with spatial and temporal averaging scale, e.g. uncertainty contributions are different at global and regional scale. Analysing 14 different GCMs of the past CMIP3 multimodel ensemble under the previous generation of emission scenario [66], Hawkins and Sutton [56] partitioned the three sources of uncertainty for global decadal mean temperature and precipitation changes.

The results are reported in Figure 3.5 and Figure 3.6, for temperature and precipitation respectively, in terms of total (Figure 3.5a and 3.6a) and fractional (Figure 3.5b and 3.6b) uncertainty for projected changes calculated with respect to the period 1971-2000.
We can observe how internal variability (in orange) has a significant importance at the start of the century while scenario uncertainty (in green) becomes more

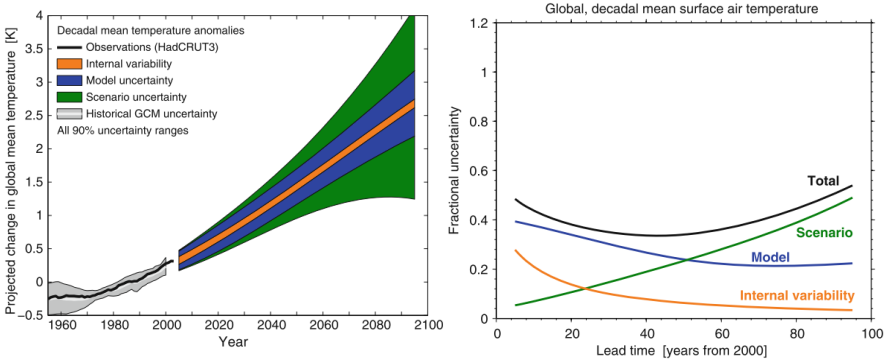

(a) Total Uncertainty **(b)** Fractional Uncertainty

Figure 3.5: Uncertainty in global decadal mean temperature change [56].

and more important throughout the century. Model uncertainty represents the dominant source of uncertainty for precipitation until the end of the century (Figure 3.6b) but for temperature (Figure 3.5b) scenario uncertainty becomes more important from mid-century. At regional scale, the contribution of scenario uncertainty is generally small and the internal variability is larger.

The results confirm that uncertainties in climate projections are largely dominated by the uncertainties in the model structure and parameters, as reported also in [83], and therefore, altough it is not possible to eliminate them, they are potentially reducible through progress in climate science [56].

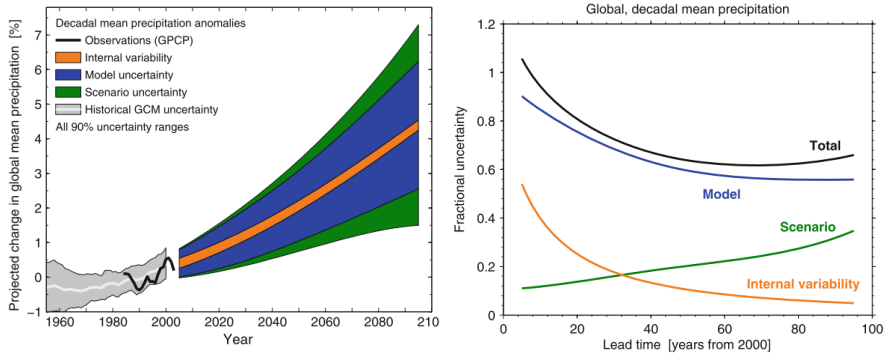

(a) Total Uncertainty **(b)** Fractional Uncertainty

Figure 3.6: Uncertainty in global decadal mean precipitation change [56].

A collection of different models, the so called multi-model ensemble, can be used to characterize the uncertainty in climate projections. A detailed review of the different approaches to combine climate models in multi-models ensemble can be found in [142].
However, the enormous computational capacity required to run high resolution climate models, doesn't allow to run many realizations of the same model. Theoretically, uncertain parameters in a single climate model may be perturbed to produce alternative simulations of past and future climate and climate change (perturbed physics models) but in practice, running enough simulations to adequately sample a complex model parameter space and, moreover, to test the sensitivity of the projections to different assumptions about the distributions of those parameters, is computationally challenging [20] and it becomes possible only with simplified models.
As stated in [83] to quantify uncertainty, one need also to decide whether a model is "*credible, plausible or consistent*" with the observations. Ensemble of simulations of past and current climate, driven by estimates of past radiative forcing and boundary conditions are then compared with observations to produce a metric of the model ability to reproduce past climate observations. In this way, discrepancies between model simulations ${x_i}^p$ and observations ${y_i}^p$ can be evaluated and consequently different calibration strategies can be set-up to adjust climate projections.
It is worth highlighting that even for high-resolution Regional Climate Model still remain a gap between the scale of simulated gridded values and point observations [157], thus the necessity to downscale climate model output to station scale for practical application.

3.4 Calibration strategies

In climate change studies, various calibration strategies are suggested for the analysis of climate projections but they can be essentially divided in two distinct calibration pathways [58]: the change factor or delta change approach, and the bias correction methods.

3.4.1 Delta change approach and weather generators

The delta change approach, also known as factor of change approach, is the simplest approach and has a long history in climate impact research. It assumes that the change from present to future in the observed climate variable ${y_i}^p$ is the same than the change predicted by the model, so that time series of future climate ${y_i}^f$ are generated by adding to observed time series a model derived climate change signal

$$ {y_i}^f = {y_i}^p + ({x_i}^f - {x_i}^p) \tag{3.1} $$

or by considering relative change,

$$ {y_i}^f = {y_i}^p \frac{{x_i}^f}{{x_i}^p}. \tag{3.2} $$

Eq. 3.1 is commonly adopted for temperatures, while Eq. 3.3 is used for precipitation, rainfall and snowfall.
The adoption of factors of change is usually combined with the use of weather generators. In this case, factor of changes for climate statistics are derived from the analysis of climate model output and then applied to observed climate statistics to generate future weather series. Indeed, weather generator (WG) are stochastic models based on regression relations between daily climatic variables, parameterised using current climate data, which are able to generate time-series of climatic variables with statistical properties similar to the input ones. By applying the change factors obtained from the analysis of climate model output to the WG parameters, future weather series are generated as described in [50] and [81].

3.4.2 Statistical Downscaling and Bias correction methods

Statistical downscaling and bias correction methods are becoming a core element of climate change impact studies [104]. A lot of different approaches and methodologies can be found in literature and no consensus exists on the appropriate use and evaluation of the different methods.

Even the terms "statistical downscaling" and "bias correction" and the collocation of a method in the two categories can generate a discussion. In general, downscaling climate model output is one of the major aim of the bias correction procedures and therefore statistical downscaling procedures may be considered as part of the bias correction methods. A complete and updated introduction to the main approaches can be found in [104], where instead of "statistical downscaling" and "bias correction", a distinction is done between perfect prognosis methods and model output statistics methods.
The underlying idea of bias correction methods is the identification of possible biases between observed and simulated climate variables, which become the basis for correcting both control and future climate model runs. In particular, a relationship between observed and modelled data series is derived and then applied to future model simulations, so assuming that discrepancies between model simulations and observations are constant over time. This assumption is considered one of the main drawback of these methods, since it cannot be verified.
A detailed presentation of specific bias correction methods of regional climate model simulations can be found in [144] and [103] starting from the simple linear scaling methods based on model output statistics and arriving to the more flexible quantile mapping methods, also known as probability mapping or statistical downscaling. Quantile mapping uses quantile based transformation of the distributions; in this way quantiles of the present day simulated distribution are replaced by the same quantile of the present-day observed distribution. In similar approaches, the cumulative distribution function of model simulations is duly adjusted to match the cumulative distribution function of the observed variable and the transfer function $f(x)$ can be derived by solving

$$\mathrm{CDF}_{obs}(f({x_i}^p)) = \mathrm{CDF}_{sim}({x_i}^p) \tag{3.3}$$

as described for example in [115] and [116]. However, classical bias correction techniques like quantile mapping, deterministically postprocessing the marginal distribution of the raw climate projections, are often characterized by inflation problems [102]. The problems arise from the attempt to explain local variability by gridbox variability and may have severe consequences such as the derivation of wrong variability and trends as discussed in [102] and [103]. The need for stochastic bias correction procedure is then demonstrated in [102] and a possible solution is to use a randomized downscaling specification as already suggested by Von Storch in [152].

3.5 Climate change implications on structural design

Structural design is often governed by climatic actions, thermal, wind, snow and ice loads. Therefore, alteration of them caused by climate change could significantly affect the design of new structures and infrastructures as well as the reliability of the existing ones designed in accordance to the provisions of current or past codes.
Structures shall withstand climatic loads during their life, which could be significantly greater than the design service life (DSL), assumed period for which the structure is to be used with anticipated maintenance but without major repair. Then, considering that design service life of buildings and other common structures is about 50 years, and the DSL of monumental buildings and bridges is about 100 years, structures designed in 2020 shall withstand climatic actions and extreme events expected in the period 2020-2070 (as for buildings), and in the period 2020-2120 as regards bridges and monumental buildings. As already remarked, most of them are going to last much longer, so being even more sensitive to climate change implications.
However, the definition of climatic actions on structures is currently based on extreme value analysis applied to past observations of the natural phenomena, under the assumption of stationary climate conditions. In design context, climate is considered as a stationary stochastic process varying in a neighbourhood of an unchanging mean state, so that statistical parameters of climatic actions can be considered nearly constant over time [82]. In this way, even if climate is not stationary, stationary return level and no changes in the frequency of extremes are assumed.
Accelerating changes in climate, emphasized by the recent studies on Climate Change [67] discussed in this Chapter, makes now the stationary assumption more questionable and alterations of frequency and intensity of extremes events as well as variations of statistical properties of extremes may be expected over time.
Changes in many extreme weather and climate events have been observed since about 1950 as reported in [67] and confidence has increased that extremes will become more frequent, more widespread and/or more intense during the 21st century [67]. Since it is expected that climate change will continue to alter climate extremes, relying only on past observations for the definition of climatic actions may result misleading and there is an urgent need to revise

current design provisions incorporating the projected climate change effects [138].

Therefore, in order to provide increased resilience of long-life structures and infrastructures to climate change consequences, the assessment of the impact of climate change is considered a key aspect also in the future evolution of structural Eurocodes, that will lead to the adoption of the second generation of Eurocodes in 2020-2023 [17].

The evaluation of the impact of climate change on climatic actions should start from the analysis of climate projections provided by the most recent climate models and scenarios, previously described in this chapter, that represent our major knowledge about climate change. Indeed, observed data series are not enough extended over the time to reflect the effects of climate change and it becomes necessary to rely on climate projections.

Chapter 4

Snow load on structures: state of art

In this chapter, previous researches about ground snow loads are reviewed and the current European Ground Snow Load map is derived comparing the definition in Eurocode EN1991-1-3:2003 and National Provisions.

Contents

4.1 Introduction

In this chapter, the development of snow load maps in European Standards is illustrated. Previous researches about ground snow loads that led to the adoption of the Eurocode EN1991-1-3:2003 [14] are reviewed. Moreover, the current European Ground Snow Load map is derived combining the definition reported in Annex C of Eurocode EN1991-1-3:2003 [14] and the National Provisions.
The state of the art concerning snow load on structures is thus investigated focusing the attention on the definition of ground snow loads, basic value of the load to be converted into roof snow load through appropriate coefficients taking into account the roof geometry and the wind exposure of the building. Indeed, the objective of the thesis is the evaluation of climate change impact on snow loads, and it is assumed that the most relevant impact will be on the basic climate variable and thus on ground snow load while the effects of roof geometries and wind exposure on the final value of roof load may remain unchanged and are not investigated in the present work.

4.2 Snow load in European Standards

The development of a harmonized ground snow load map for Europe was one of the main objectives of the pre-normative oriented research work that led to the publication of the Eurocode EN1991-1-3 in 2003 [14]. This Code superseded the previous pre-standard ENV 1991-2-3:1995, in which snow maps of CEN member states were based upon provisions, taken, almost directly, from national snow loading codes, available at that time [127]. The ENV document was deliberately drafted as an interim solution, calling for further investigations aimed at producing a harmonised snow map of Europe [127]. In 1996 the European Commission funded a specific pre-normative study, the European Snow Load Research Project [126, 125], focused on providing sound scientifically based answers to the following fundamental issues [114]:

- development of an European ground snow loads map;
- definition, identification and treatment of exceptional ground snow loads;
- study of conversion factors from ground to roof loads;

- definition of ultimate limit state (ULS) and serviceability limit state (SLS) combination factors for snow loads (ψ_0, $\psi_1 1$, ψ_2).

The EN1991-1-3:2003 is largely based on the results of this research project. In particular, the informative Annex C of the code presents the European snow maps, obtained by the research group for the eighteen countries that at the time of the research were members of the European Committee for Standardization (CEN): Austria, Belgium, Denmark, Eire, France, Finland, Germany, Greece, Iceland, Italy, Luxembourg, Netherlands, Norway, Portugal, Spain, Sweden, Switzerland, United Kingdom. In the Annex they were also included ground snow load maps supplied by three countries not directly part of the research group (Czech Republic, Iceland and Poland). The declared objective of the informative Annex was to help National Competent Authorities to redraft their national codes, establishing harmonised procedures to derive the snow maps, eliminating or reducing in this way the inconsistencies in ground snow load values encountered at borders between CEN member states, in view of enhancing harmonization.

4.2.1 The European Snow Load Research Project

As mentioned before the current version of EN1991-1-3 is largely based on the outcomes of the European Snow Load Research Project (ESLRP), reported in [126] and [125]. In that study, snow precipitation data were collected across the 18 CEN countries at approximately 2600 weather stations. Data series, generally longer than 50 years and not shorter than 30 years, consisting of water equivalent and snow cover depth measurements, converted into snow load through appropriate density functions defined for each CEN member, were deeply checked and used as the basis for the elaborations.
From snow data series, yearly maxima were extracted to be statistically processed according to a common approach, taking into account both zero and non-zero values (non-snowy winters and snowy ones), following the so-called "mixed distribution approach" proposed by Thom in [145]. Indeed, some countries like UK, Denmark, Spain, Portugal, France, Italy and Greece experience irregular snowfalls, which may have long periods, sometimes years between their occurrence and then may exhibit a significant number of "zero-years". The mixed distribution approach consists in combining the probability of not exceeding a given value of snow load, q_k, with the probability of

occurrence of snow within a winter, P_{snow}. In this way, the probability that the snow load takes a value less than or equal to q_k becomes:

$$P(X < q_k) = P_{snow}F_{snow}(q_k) + (1 - P_{snow}) \tag{4.1}$$

where F_{snow} is the CDF associated to snow load maxima in no-zero years and the probability of snow within a winter $P_{snow} = n/N$ can be easily calculated as the ratio between the number of no-zero years n and the years of observation N. Characteristic values of the load (loads having a probability of exceedance $p = 0.02$ per year, as defined in EN1990 – Basis of structural design [13]) are thus obtained by modifying 2.3 in

$$q_k = \mu - \sigma \log[-\log(1 - \frac{p}{P_{snow}})] \tag{4.2}$$

assuming a Gumbel or extreme value type I distribution, as limiting distribution of maxima. Indeed, they were also conducted comparative studies to evaluate the best fitting Probability Density Function (PDF) in the majority of weather stations, to be consistently adopted for the analysis across the whole European territory; the Gumbel distribution was then chosen and adopted for the calculation of characteristic loads. The extreme values analysis at each weather station was carried out excluding from the statistical sample exceptional values, specifying that ground snow load may be treated as accidental action for locations where exceptional loads may occur. Exceptional snow loads were defined in [126] as loads whose ratio with the characteristic load determined without the inclusion of that value is greater than 1.5. Among the different methods described in 2.2.1.2, the LSM was adopted to estimate extreme value parameters, location μ and scale σ. The availability of characteristic values of ground snow loads, derived according to a common statistical approach, allowed the identification, through an iterative process, of ten different climatic regions, with homogeneous climatic features (Iceland, Norway, Finland-Sweden, UK-Eire, Central West, Central East, The Alps, Mediterranean Region, Iberian Peninsula, Greece). The ten climatic regions together with the location of the 2600 investigated weather stations are shown in Figure 4.1.

The climatic regions were tailored in order to group areas in which a common relationship between the characteristic ground snow load and the altitude of the site where the weather station is located, was found to be satisfactorily

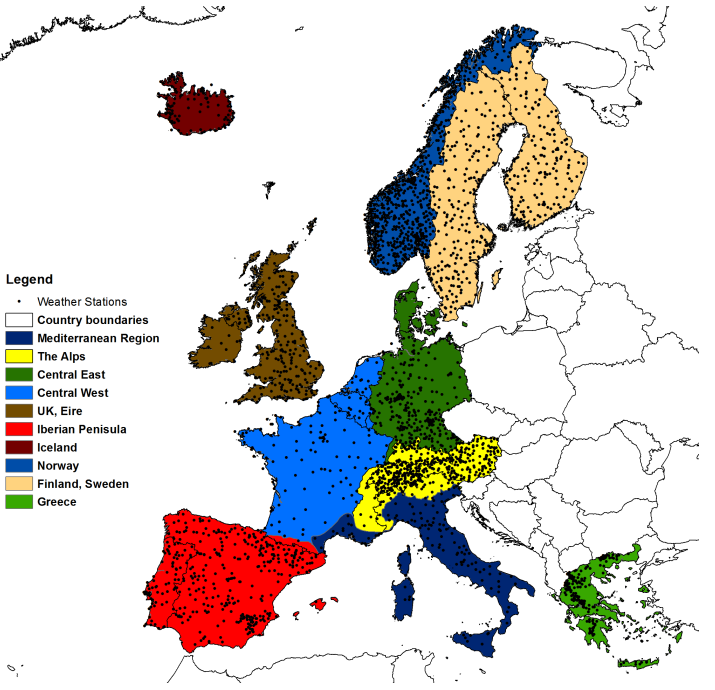

Figure 4.1: European Climatic Region and investigated weather stations in [126].

representing the variation of the load with altitude in the whole region. Suitable altitude functions were tested on the climatic regions: a parabolic curve was adopted for the Iberian Peninsula, Mediterranean Region, Greece, Alpine Region and Central East, a linear type altitude function was chosen for Sweden and Finland, UK and Eire and Central West, while for Iceland and Norway it was not possible to identify a clear altitude-snow load relationship and the ground snow load was presented in maps by means of isopleths. Finally, for each climatic region, different zones were defined in relation to the average altitude functions, assigning a number to each zone, which was used to modulate the load altitude correlation formula, to cover all the range of variation of loads at different altitudes in that region. Maps for each climatic region identifying the zones together with the load altitude relationships are included in the informative Annex C of the EN1991-1-3, not to be used for design purposes, but, as stated above, to serve as a basis for National Standard Bodies to derive their own maps. Implementing these laws in the corresponding zones, the European Ground Snow Load Map can be obtained for the 18 CEN member states, covered by the ESLRP map.

In Figure 4.2 the resulting map developed by means of a Geographic Information System (GIS) software is presented. The white spots in the investigated Countries identify sites at altitudes higher than 1500 m, for which the map does not apply.

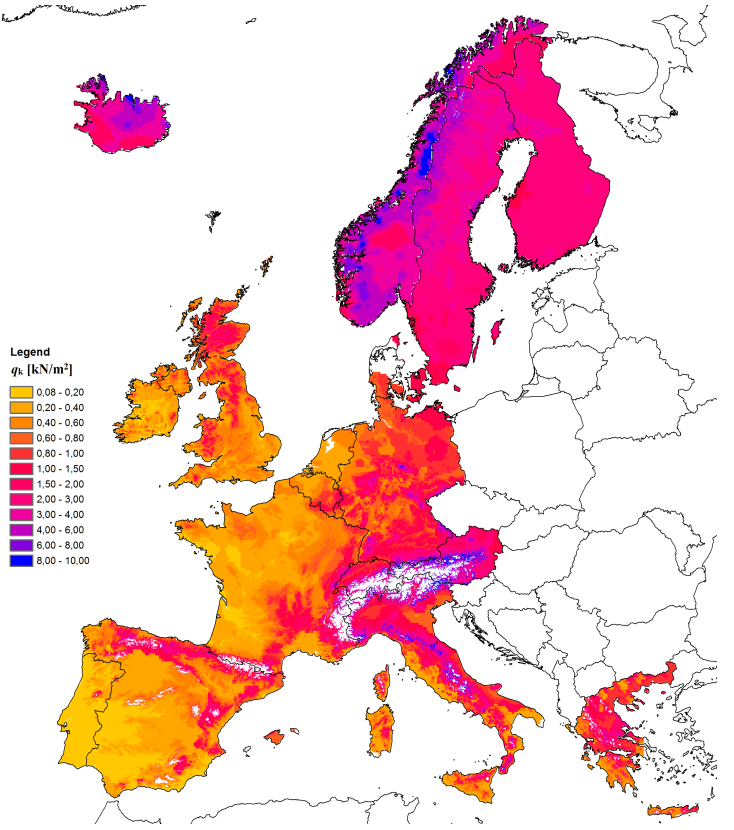

Figure 4.2: European Ground Snow Load Map according to [14].

4.2.2 Eurocode EN1991-1-3 and National Annexes

As stated in the foreword of the structural Eurocodes [13], these standards "*recognise the responsibility of regulatory authorities in each Member State and have safeguarded their right to determine values related to regulatory safety matters at national level where these continue to vary from State to State*". This is allowed by means of parameters left open in the Eurocode for national

choice, known as Nationally Determined Parameters (NDPs), to be used for the design of buildings and civil engineering works in the relevant country. These parameters and related choices are collected in a document, known as the National Annex (NA); ground snow maps are typically considered as "*safety matters*" to be regulated at national level and then information about their definition is given in these documents.
Therefore, in order to define the current version of European Ground Snow Load Map, the National Annex to EN1991-1-3 in force in CEN member states have been collected and analysed with the aim to evaluate the status of harmonization in the current group of 34 CEN member states. In particular, as presented in Table 4.1, it has been possible to examine the 30 published National Annexes out of 34 CEN member states. As we can observe in Table 4.1, different ways to define snow load maps are adopted by each National Standard Body: generally national maps are provided for the identification of zones together with altitude relationships, Bulgaria as well as Czech Republic provide a link to a website where a digital map can be consulted, other countries like Belgium, Cyprus, Hungary and Switzerland give an unique load altitude law for the whole territory while the Netherlands and Denmark provide only one value for all sites in the country. An altitude limit of 1500 m for the application of the snow map is maintained, when relevant, in most of the countries; only in Switzerland and in France the limit is extended up to 2000 m, in Spain altitude limits for each zone are given, while no altitude limits are given in Norway and Romania.

Country	**Annex**	**Snow Map Definition**
Austria	ÖNORM EN 1991-1-3/NA[4]	4 zones are defined with a load-altitude law
Belgium	NBN EN 1991-1-3/NA[10]	Minimum value equal to 0.5 kN/m^2 for $A <= 100m$. Altitude law for $100m < A < 700m$
Bulgaria	BDS EN1991-1-3/NA[9]	Ground snow load map at http://gis.mrrb.government.bg
Croatia	HRN EN1991-1-3/NA[25]	4 zones and altitude variation given in a table for 100 m intervals

Table 4.1: National Annexes to EN1991-1-3 [14].

Country	Annex	Snow Map Definition
Cyprus	CYS EN1991-1-3/NA[35]	Formula for load-altitude variation obtained from Annex C - Mediterranean Region
Czech Republic	ČSN EN1991-1-3/NA[36]	Minimum Value 0.7 kN/m^2, 8 zones are defined and values can be found in the digital map on http://www.snehovamapa.cz
Denmark	DS EN1991-1-3/NA[37]	1 kN/m^2 for all locations
Estonia	EVS-EN 1991-1-3/NA[42]	3 Zones are defined with constant snow load: 1.25, 1,5 and 1.75 kN/m^2
Finland	SFS EN 1991-1-3/NA[137]	Minimum values in a map. In area where the values are not constant, the intermediate values are obtained by linear interpolation in proportion to distances from the closest curves
France	NF EN 1991-1-3/NA[3]	8 zones are defined with minimum values. For altitude above 200m, different correction laws are given
Germany	DIN EN 1991-1-3/NA[39]	5 Zones are defined with minimum values and altitude correction laws are given for $A > 400m$, $A > 285m$ and $A > 255m$
Greece	ELOT EN 1991-1-3/NA[108]	3 Zones are defined with altitude correction law

Table 4.1: National Annexes to EN1991-1-3 [14].

Country	Annex	Snow Map Definition
Hungary	MSZT-EN1991-1-3/NA[62]	Minimum value 1.25 kN/m^2 and unique load altitude relationship for the whole territory
Iceland	IST EN1991-1-3/NA[63]	3 Zones are defined with constant minimum values (2.1, 3 and 5 kN/m^2) and a zone requiring site specific evaluation
Ireland	IS EN1991-1-3/NA[109]	Minimum Value 0.4 kN/m^2. 4 zones are defined and one altitude correction law for $A > 100m$
Italy	UNI EN1991-1-3/NA[41]	4 Zones with constant minimum values (1.5, 1.5, 1 and 0.6 kN/m^2) and altitude correction laws for $A > 200m$
Latvia	LVS EN1991-1-3/NA[88]	Minimum values are given in a map
Lithuania	LST EN1991-1-3/NA[92]	2 Zones are defined with constant minimum values equal to 1.2kN/m^2 and 1.6 kN/m^2
Luxembourg	ILNAS EN1991-1-3/NA[38]	Minimum value equal to 0.5 kN/m^2 for $A <= 100m$. Altitude correction law for $100m < A < 600m$
Netherlands	NEN EN 1991-1-3/NA[110]	0.7 kN/m^2 for all locations
Norway	NS EN 1991-1-3/NA[135]	Values and altitude relationship are given for each municipality

Table 4.1: National Annexes to EN1991-1-3 [14].

Country	Annex	Snow Map Definition
Poland	PN EN 1991-1-3/NA[117]	5 zones are defined with minimum values and altitude correction law
Portugal	NP EN 1991-1-3/NA[65]	3 zones are defined together with an altitude correction law
Romania	SR EN 1991-1-3/NA[122]	3 zones are defined with minimum values (1.5, 2 and 2.5 kN/m^2) for altitude below 1000m. Altitude correction laws for $A > 1000m$
Slovakia	STN EN 1991-1-3/NA[133]	5 zones are defined together with altitude correction laws
Slovenia	SIST EN 1991-1-3/NA[134]	5 zones are defined together with altitude correction laws
Spain	UNE EN 1991-1-3/NA[2]	7 zones are defined together with altitude correction laws
Sweden	SS EN 1991-1-3/NA[64]	8 Zones are defined and constant values are given for each zone (1 to 5.5kN/m^2)
Switzerland	SN EN 1991-1-3/NA[129]	Minimum value 0.9 kN/m^2 and unique load altitude relationship for the whole territory)
United Kingdom	BS EN 1991-1-3/NA[8]	6 zones are defined together with altitude correction laws

Table 4.1: National Annexes to EN1991-1-3[14].

Combining the information provided by each National Annex, the actual version of the European ground snow load map in force in CEN countries can be drawn; this map (Figure 4.3) has been developed by means of GIS software using a digital elevation model (DEM) having a resolution of 1km x 1km for the implementation of the altitude laws.

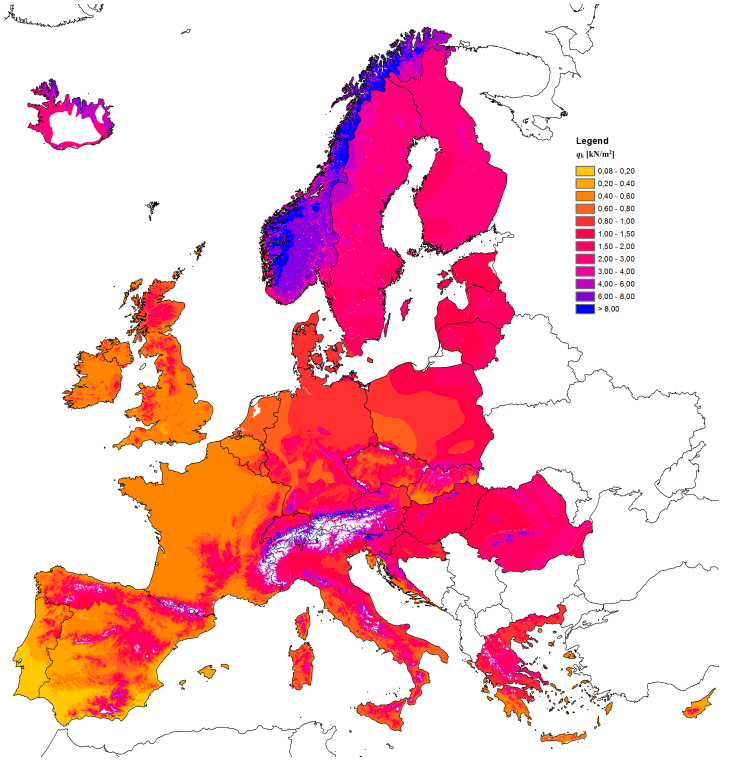

Figure 4.3: European Ground Snow Load Map according to CEN National Annexes.

Chapter 5

Harmonization of European snow load maps

In this chapter, the status of harmonization of European ground Snow Load maps is investigated.

Contents

5.1 National snow maps and EN1991-1-3: a comparison

The European ground snow load map obtained combining information provided by National Annexes to EN1991-1-3 and presented in Figure 4.3 has been compared with the ground snow loads maps provided in Annex C of EN1991-1-3 (Figure 4.2), to appreciate the effectiveness of the implementation of the latter in the derivation of national snow maps.

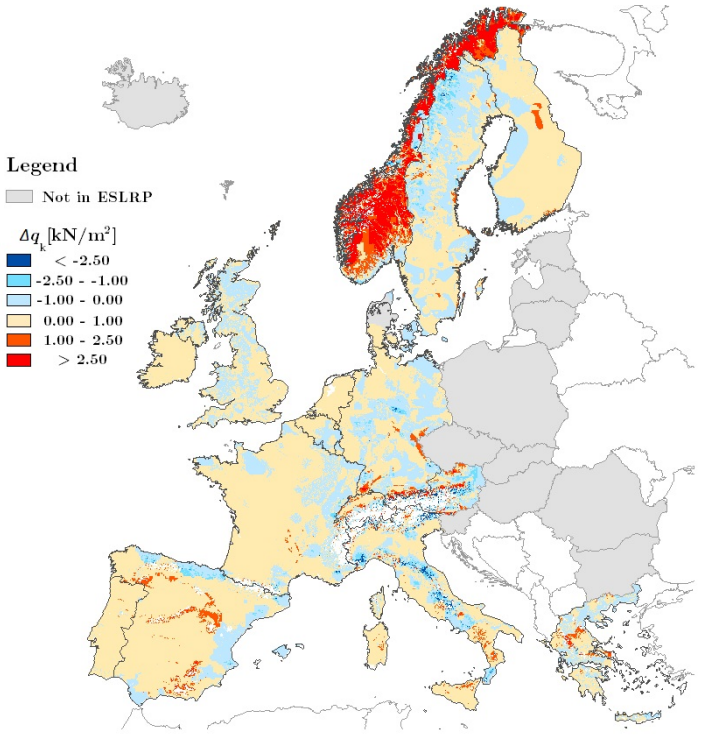

Figure 5.1: Comparison of European ground snow load maps in EN1991-1-3-Annex C and National Annexes to EN1991-1-3.

In Figure 5.1, the differences between characteristic ground snow loads in National Annexes and Annex C, Δq_k in kN/m^2, is plotted in a map for the 18 CEN member states at the time of the European snow load research project. The map shows that characteristic values in National Annexes are

generally higher than those obtained according to Annex C for Norway, Finland, Portugal, Spain, France, Netherlands, Denmark and Ireland (∼64% of the investigated European territory). In particular, in Norway load values result considerably higher, mainly due to the implementation of a load altitude relationship, which is not considered in the Annex C.
Moreover, comparing the results presented in Figure 5.1 with a population density map for the investigated territory (as shown in Figure 5.2) we can observe that in populated area with more than 10 inhabitants/km^2, higher characteristic values of snow load are obtained according National Annexes than with Annex C for the 71% of the region.
Considering that the snow load maps presented in Annex C, derived within the ESLRP, represent directly the results of the statistical analysis performed on observed data series, these positive differences in National Annexes denote an additional safety factor in the definition of snow load in National Annexes for large part of the populated European territory.

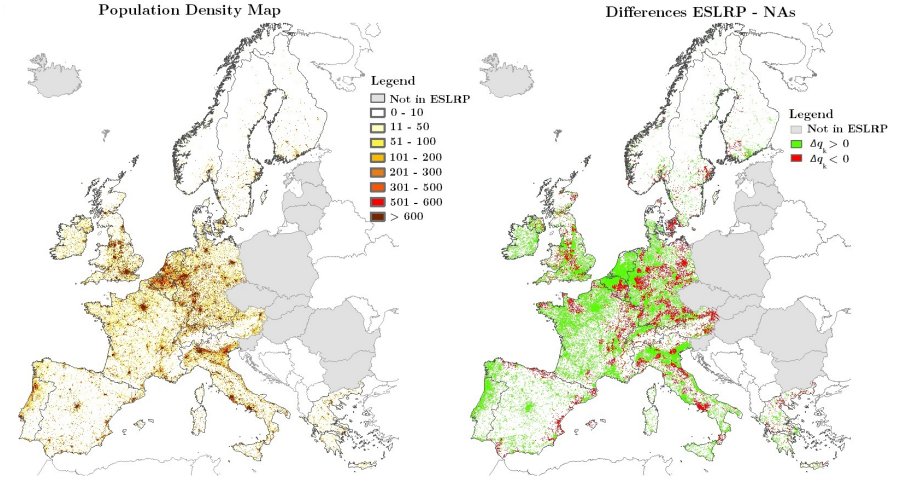

Figure 5.2: Differences in snow load definitions compared with a population density map.

Differences are mainly due to the different definition of zones and the adopted load altitude relationships. For example, German territory, according to EN1991-1-3-Annex C, falls for a large part within the Central East climatic region and for the remaining southern part in the Alpine climatic region, thus resulting in 8 zones, while in the German National Annex, only five zones are defined for the whole Country as showed in Figure 5.3.

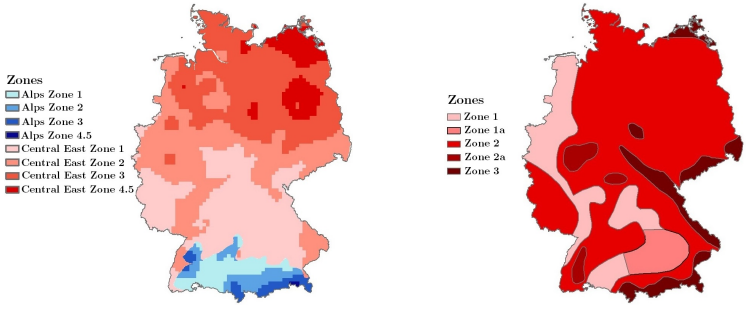

(a) EN1991-1-3-Annex C **(b)** German National Annex

Figure 5.3: German snow load map Zones.

Different load altitude relationships are also associated to each zone and the resulting snow load maps are shown in Figure 5.4, together with the differences between National Annex values and Annex C values. It is worth noting how for low altitudes, the threshold values given in the National Annex leads to higher values of the loads than those that were obtained by the statistical analysis of yearly maxima.

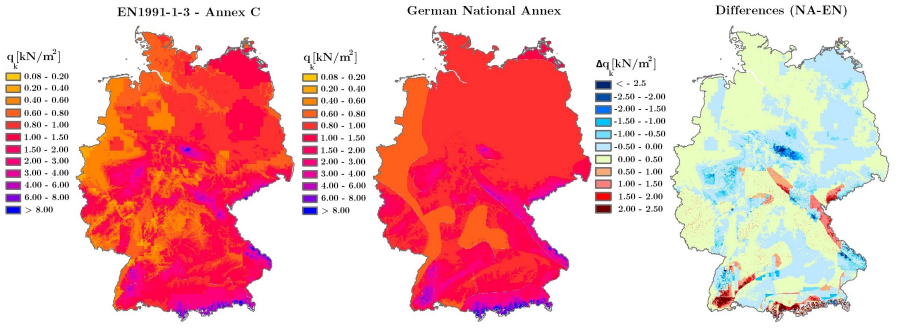

Figure 5.4: Comparison of characteristic ground snow load maps ESLRP – German National Annex.

5.2 Consistency in European Ground Snow Load map

In order to evaluate the degree of achievement of the objectives of the informative Annex C, based on the European snow loads research (in the years

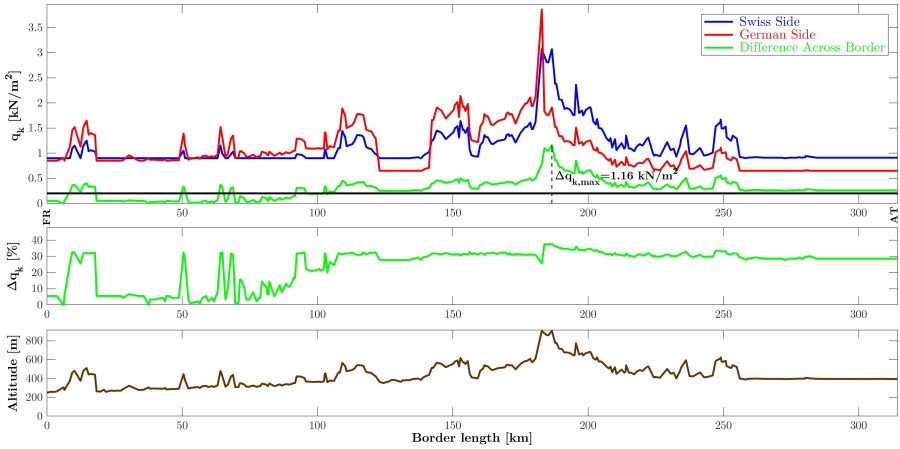

Figure 5.5: Comparison of characteristic ground snow load at Swiss-German border.

1996-1999)[126] and [125], in enhancing consistency eliminating differences in national maps towards their harmonization, a comprehensive analysis was carried out, on the basis of the maps presented in the previous paragraphs. More in detail, characteristic values of ground snow load can be easily compared across Country borders extracting them from the GIS map.
As an example, in Figure 5.5 the load values evaluated along the border between Switzerland and Germany (approximately 360 km from France to Austria) are plotted according the two National Annexes, together with the point altitudes. The blue solid line represents snow load values obtained according Swiss NA [129], the red solid line represents corresponding values obtained according German NA [39], while in green the absolute difference between the two is shown compared to a threshold value equal to 0.2 kN/m^2 (black line). Percentage differences calculated with reference to the Swiss side load are also illustrated in the same Figure 5.5. The maximum difference $\Delta q_{k,max}$ is 1.16 kN/m^2 (∼38% of the corresponding Swiss load value).

Figure 5.6 and Figure 5.7 show similar diagrams for the borders between France and Switzerland (approximately 570 km from Germany to Italy) and France and Spain (approximately 650 km from the south-western France and north-eastern Spain) respectively.

Analysing Figure 5.6, significant differences are found across the French-Swiss border in the section from 200 to 300km, with a maximum difference $\Delta q_{k,max}$ equal to 3.67 kN/m^2. Similar load values are instead obtained along the

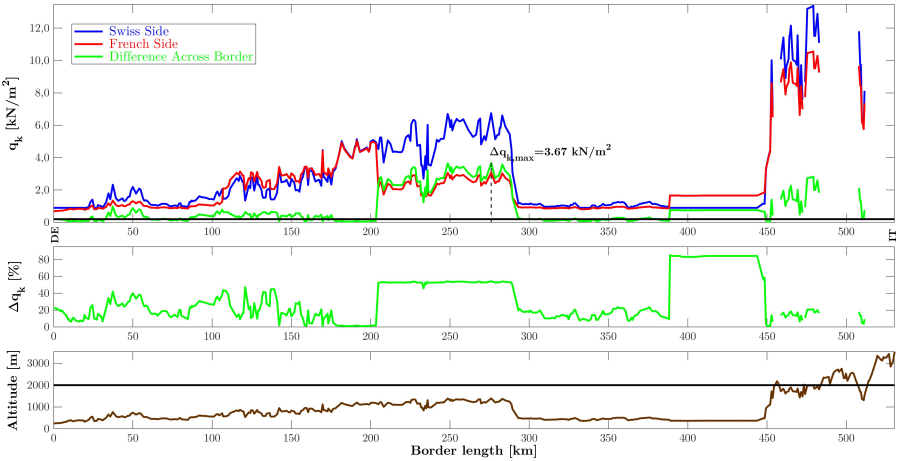

Figure 5.6: Comparison of characteristic ground snow load at French-Swiss border.

French-Spain border (Figure 5.7) with a maximum difference equal to 0.79 kN/m^2.

Therefore, the comparisons presented in Figures 5.5, 5.6 and 5.7 still show a lack of full consistency which is mainly due to the difference in the altitude correlation functions adopted in the two neighbouring countries, but also to the adoption of different minimum threshold values, which can be regarded as a safety related issue, which is left to national determination.

A further work to enhance the harmonization of the European snow load map

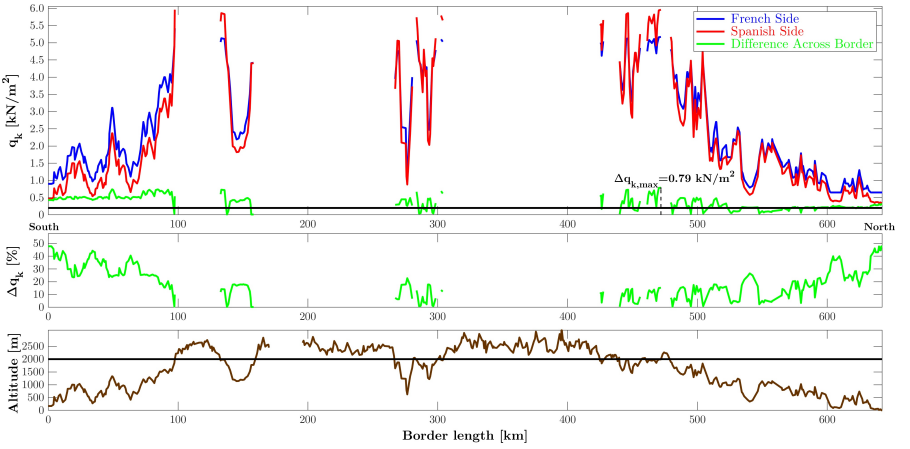

Figure 5.7: Comparison of characteristic ground snow load at French-Spanish border.

is then needed and the presented outcomes can serve as an input to National Standard Bodies (NSBs) for the possible further update of their maps in view of a fully harmonised European snow load map as requested by CEN in the response to the Mandate M/515 [17].
Concluding this section, it must be stressed that administrative borders can also correspond to climatic boundaries identifying different climatic regions, such as mountain ridge or mountain slopes. As an example, the French-German administrative border overlaps the boundary between West and East climatic regions defined by the ESLRP [126] and reported in Figure 4.1. Therefore, in the harmonization process the effort must focus on reducible differences across borders taking into account the potential presence of non reducible differences due to climatic reasons.

Chapter 6

Climate change impact on ground snow loads

In this chapter, climate change implications on snowfall extremes are described based on observations and climate models. Recent failures of lightweight roofs in Europe caused mainly by heavy snow loads are then discussed.

Contents

6.1 Climate change and snowfalls

6.1.1 Snowfalls response to climate change: theory

Snow is an important part of the climate system, and therefore it is also expected to change in a warming climate. One of the conventional remarks about global warming is that, as obvious consequence of it, a reduction of snow is expected. However, although a decrease in mean snowfall is expected in most regions due to the decrease of snowfall frequency, a contrasting response may be experienced for snowfall extremes [111]. Indeed, analysing daily precipitation extremes, the increase of surface air temperature due to global warming leads to a decrease of snowfall fraction but also to a an increase of precipitation rate according the Clausius–Clapeyron relation, which states that warmer air has a higher water vapor holding capacity [112]. According to this law, a scaling rate of about 6-7% K^{-1} warming can be predicted, considering the increase in atmospheric moisture content only. Heavy precipitation intensification that is now emerging in the observed record across many regions of the world confirms this theory [49].
A simple physically based theory is presented by O'Gorman in [111] to describe the response of snowfall extremes to climate change. Considering the dependency of the precipitation process on surface air temperature, the daily snowfall rate s can be expressed as a function of daily temperature T

$$s(T) = f(T)p(T) \tag{6.1}$$

where $f(T)$ is the snowfall fraction (fraction of precipitation that falls as snow at a given temperature) and $p(T)$ is the daily precipitation rate. The daily precipitation $p(T)$ is assumed to have a simple dependence on surface air temperature according to $p(T) = e^{\beta T}\hat{p}$ with $\beta = 0.06°C^{-1}$ and $\hat{p}$ normalized precipitation variable. The snowfall fraction dependence on temperature is instead taken from [48] and is given by $f(T) = \exp{-0.0000858(T + 7.5)^{4.12}}$ when T is between -4°C and 7°C.
In Figure 6.1, they are reported: the snowfall fraction function (in blue), the precipitation rate function (in green) and the snowfall rate function (in red). The optimal temperature for snowfall extreme in the theory, T_m is then evaluated as the temperature at which corresponds the maximum snow rate (with the above assumptions T_m results equal to -2.3°C). Temperature

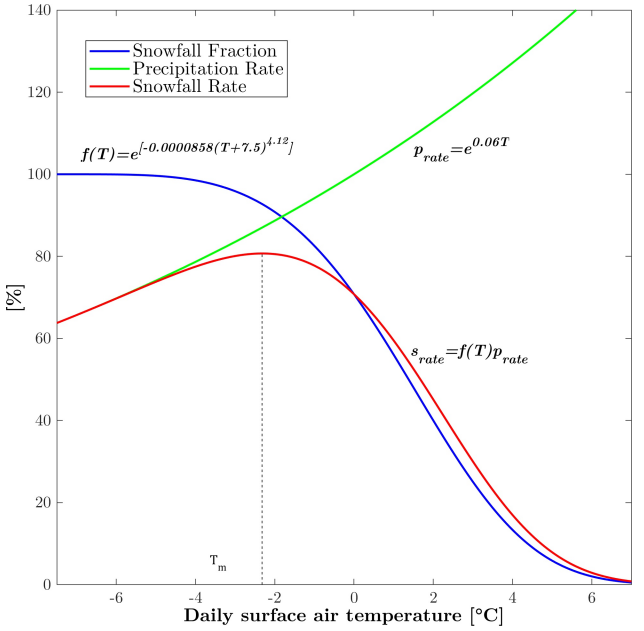

Figure 6.1: Snowfall rate as function of daily surface air temperature.

changes around this optimal value may thus lead to a decrease or an increase in snowfall extremes.

6.1.2 Global assessment

During the past four decades, the snow cover extent in the Northern Hemisphere has decreased, especially in spring and summer. In spite of this global trend, the trends in snow conditions have been variable on regional scales [119]. Climate change projections related to greenhouse gases emissions in the Northern Hemisphere mid to high-latitude continents indicate both a strong winter warming and an increase in winter precipitation. The increase in precipitation, if acting alone, would lead to an increase in snowfall and consequently to increased amounts of snow on ground. On the other hand, an increase in temperature will reduce the fraction of precipitation that falls as snow and will increase the melting of snow. Whether the snow amount on the ground will be actually reduced or increased depends on the balance between these competing factors [118].

General circulation models (GCMs) from the World Climate Research Programme (WCRP) provided within the third and fifth phase of the Coupled Model Intercomparison Project (CMIP3 and CMIP5) [141], generally agree in predicting a future decrease in snow cover duration and maximum snow water equivalent (SWE) in central Europe. The IPCC Working Group 1 conclusions state that generally the snow cover extent will be reduced [67]. However, snow cover sensitivity to changes in precipitation and temperature is highly related to topographic features such as elevation, aspect and terrain shading. Lemke et al. [90] found that the regional trends in snow conditions have been variable, although the Northern Hemisphere snow extent has decreased during the past four decades particularly in spring and summer. Where climate is cold enough, midwinter temperatures will remain substantially below zero even after a moderate warming. Thus, at least in the middle of the winter, the phase of precipitation and snow melting should be quite insensitive to temperature changes. Conversely, where winters are milder, even a modest warming will convert part of the snowfall to rainfall and increase the frequency and intensity of melting episodes. Changes in SWE induced by the expected global warming are thus more likely to occur in mild than in cold areas. According to Hosaka et al. [61], global climate projections reveal that in the late 21st century the snow water equivalent (SWE) will reduce in most regions and seasons, but SWE will increase from February to April in large parts of Siberia and northern parts of North America.
Krasting et al. [86] analysed projections of the Northern Hemisphere snowfall under RCP4.5 scenario in an ensemble of GCM simulations from CMIP5. Their analysis shows that most regions experience decreases in snowfall during the fall and spring, but in some regions, increases in midwinter snowfall are found. In particular, the multi-model ensemble trends show increasing snowfall tendency over Northern Europe and Canada in winter. However, the inadequate resolution of topography provided by GCM, greatly complicates the interpretation of results in regions of complex terrain and snowfall trends from such regions should be regarded with considerable caution.

6.1.3 Regional variability

Because of their current coarse horizontal resolution, GCMs could difficulty describe the variation of snow conditions in areas with significant orography or complex land-sea distribution while it is expected that it could be better

simulated by high-resolution regional climate models (RCMs).
Makkonen et al. [99] evaluated changes in extreme weather events for northern Europe according to a regional climate model (RCM) with horizontal resolution 49km, driven by two different GCMs and forced by the previous generation of emission scenarios [66]. Despite a widespread decrease in total annual snowfall in a warmer climate, the results suggest that extreme six hour snow precipitation will increase in most parts of the Nordic area. It is thus underlined in [99] how the increase of extreme snow precipitation intensities may initiate more severe snow and ice accretion on structures, such as power lines and communication towers. The extreme SWE is predicted to significantly decrease in most of the study area for the late 21st century (period 2071-2100) but increase in some highland areas. In conclusion, an updating of snow load maps in building codes, taking the local differences carefully into account, is recommended for an optimal structural design.
Raisanen and Eklund [119] analysed changes in snow amount in northern Europe by means of 11 RCMs with horizontal resolution $\sim$ 25km, from the ENSEMBLES climate change project [149] under the midrange emission scenario of the previous generation (A1B) [66]. They found that over the 21st century a large fraction of precipitation falls as rain, and episodes of snowmelt become more common. The amount of snow is generally reduced; however, the regional variability in this change is substantial within northern Europe. By the late 21st century, mildest areas (including Denmark, southern Sweden, southwestern Finland, western parts of the Baltic States and coastal Norway) are projected to lose the greater part of their snow. In some inland areas north of the Arctic Circle and over the Scandinavian mountains snowfall is expected to increase, although less than total precipitation. The largest increase, exceeding 20% in 2070–2099, is predicted in north western Sweden. Furthermore, about a half of the 11 simulations points towards an increase in SWE in northern Swedish Lapland in March. The study reveals that although snow cover is going to decrease due to melting, substantial amounts of snow are still likely to fall even in the late 21st century and different trends could happen to heavy short-term snowfalls as reported in [99].
Lopez-Moreno et al. [94] simulated changes in intensity and frequency of heavy snowfall events in the Pyrenees using a Surface Energy Balance Model driven by data from the HIRHAM RCM (resolution $\sim$ 50km) at the end of the 21st century under a lower (B2) and an higher (A2) emission scenarios of the previous generation [66]. They found that the projected changes in heavy snowfall depend largely on the elevation and the considered emission

scenario. Despite the marked decrease in snow accumulation and snow cover duration, heavy snow events will constitute an ongoing risk in many areas. For the highest emission scenario (A2) heavy snowfall intensity and frequency is expected to decrease between 1000 and 1500 m a.s.l.. Above 2000 m, the maximum intensity of single and multi-day events is expected to remain stationary, but may increase up to 30% at the higher elevation. For a more moderate emission scenario (B2) at 1500 m and above, an upward trend in the maximum intensity and frequency of snowpack is expected, and the frequency of the heavy snowfall events may increase by 20% to 30% above 2000 m.
In a recent study Frei et al. [51] investigate future snowfall in the Alps based on 12 high-resolution regional climate models (RCMs) data made available through the EURO-CORDEX initiative [73], with a resolution of approximately 12km, run under the medium emission scenario RCP4.5 and the highest emission scenario RCP8.5. Snowfall projections for the late 21st century reveal a robust signal of decreasing snowfall amounts over most parts of the Alps for both emission scenarios; in contrast, high-elevation regions could experience slight snowfall increases in midwinter for both emission scenarios despite the general decrease in the snowfall fraction.

6.1.4 Main trends

In effect, several literature studies based both on GCMs and on RCMs (e.g. Makkonen et al., 2007 [99], Lopez-Moreno et al., 2011 [94], Raisanen and Eklund, 2012 [119], Krasting et al., 2013 [86]) show that in some areas of the world, even in Europe, the snowfall is expected to increase.
However, the predicted changes are characterised by a small-scale heterogeneous pattern, making the trend of snowfall difficult to be predicted. Moreover, a reduction of snowfall is not directly linked to a reduction of snow load. In fact, the rain falling on snow can be stored within the snow pack, resulting in an increase in the total snow load [136].
A strategy for dealing with snow load risks in a changing climate encompassing monitoring and prediction is proposed by Strasser [136].Modern RCMs are able to provide valuable information at high resolution, which can be used as input for impact models. In particular, climate simulations developed in the framework of the Coordinated Regional Downscaling Experiment initiative over Europe (EURO-CORDEX [73]) offer the state-of-art climate projections

at the spatial resolution of about 11 km over the whole Europe. Projections at higher resolutions (up to 1 km) would be beneficial for more accurate local analyses and also in the view of developing operational warning systems [136].

6.2 Evidence of implications of climate change

As underlined in the previous paragraphs, one of the conventional remarks about global warming is that as an obvious consequence of it, a reduction of ground snow load should be expected. However, it should be considered that the snow load on ground often depends on local orographic situations that can determine increases of the height of local snow falls, even in case when the average snow height is reduced considering larger areas. Moreover, the capacity of the atmosphere to hold moisture increases with the temperature, and this phenomenon may lead to an increase of both the snow density and the occurrence of extreme snowfalls in regions where temperatures still remain below the freezing level during precipitation events.
The relevance of the above considerations are confirmed by catastrophic collapses of lightweight roof structures caused by snow that occurred in the last 15 years in Europe, although in some cases, snow overloads were accompanied by wrong constructional solutions or insufficient resistance of structural elements [6]. Indeed, snow loads can be in several cases the screening of the quality of the structure. Frühwald et al. [52] investigating 127 failure cases of wooden roofs in Scandinavian countries, Germany and US, found that insufficient or lacking design with respect to environmental actions was the reason for 11% of the considered collapses.

Strasser [136] reported 15 roofs collapses in Germany due to snow load in the period January – February 2006, characterized by an exceptional continuous snow cover, and among them the roof collapse of the ice rink of Bad Reichenhall which killed 15 people and injured 34 (Figure 6.2). Similarly on January 2006, the roof of an exhibition hall in Katowice (Poland) collapsed after heavy snowfall burying 235 people of which 65 perished (Figure 6.3) and the Basmanny Marketplace in Moscow collapsed after a snowstorm, killing 66 people and injuring 32 more people (Figure 6.4).

Vasek [151] reported about 200 collapses of timber and steel roofs in the first months of 2006 in the Czech Republic. That winter was the longest within 30

Figure 6.2: Roof collapse ice rink Bad Reichenhall [52].

Figure 6.3: Roof collapse Katowice Exhibition Hall.

Figure 6.4: Roof collapse Basmanny Marketplace in Moscow.

years and was characterized by continuous snowfalls with low temperatures. Melted snow laying on the roof was increased by the new snowfall, and in this way the weight of the snow could overcome the snow load value recommended by structural code.

Geis et al. [53] examined 1029 snow-induced building failure incidents in the United States between 1989 and 2009 and 91 international incidents between 1979 and 2009. The most commonly reported causes of snow-related failures were excessive snow (around 70% of total incidents), rain-on-snow (around 12% of total incidents), and building problems (around 9% of total incidents). It is also highlighted in [53] that the high number of incidents reported for new buildings (i.e., those constructed in the last 10 years) in both the U.S. and other Countries, indicates that a risk of snow-related failure can occur even in modern buildings designed according to current codes. Moreover, it is observed how the relationship between snow failures and snowfalls can be influenced by the increasing severity of snowstorms, experienced in US since 1950s [76], and expected in certain region of the world due to changes in global climate.

A very large number of roof collapsed, caused by snow, occurred in Northwest of United States during winter 2010-2011. Heavy snows resulted in nearly 500 problem roofs, of which 382 were full or partial collapses in the states of Connecticut, Massachusetts, New York and Rhode Island [113]. In New York City, roughly a 100 year mean recurrence interval snowfall event occurred. However, according to [113], the problem was not due to ground snow load in excess of those in ASCE 7-10 [1] ground snow load map but the significant

loading revealed "*hidden*" structural defects.
Recent building failures caused by snow, have led to study the reliability of existing structures subjected to extreme snow loads. After an unusually large number of collapses took place during the winter of 1999–2000 in Norway, Mel∅ysund et al. [107] examined the reliability of existing building stock. The investigations indicate a too low reliability for a considerable number of buildings according to Norwegian modern code provisions. Moreover, it is concluded that the future reliability of the buildings in these areas could decrease due to climate change scenarios.
Takahashi and Ellingwood [139] describe the importance of snow to dead load ratios in design, reliability indices are relatively high when the ratio of nominal snow to dead load S_n/D_n is low, and decrease when S_n/D_n becomes larger, therefore lightweight structures have a higher risk of failure than heavier structures. A critical analysis of design procedures in European standards is carried out by Holicky in [59] after the winter 2005/2006 when a large number of roofs collapsed in Europe. It appears from the presented reliability analysis that the partial factor design method provided in the European standards may not guarantee an adequate reliability level of lightweight roofs. For load ratios χ, given as a fraction of the characteristic value of the snow load s_k and the total load $G_k + s_k$, higher than 0.5 the reliability index β results less than the target reliability level equal to 3.8. In a follow-up study Holicky and Sykora [60] investigate a total of 249 roof collapses mostly in highlands and lowlands in the Czech Republic, taking into account information provided by the Police and the Fire Rescue Service of the Czech Republic. The main observed causes of structural damage are subdivided into human errors in design, execution and use, and insufficient code provisions. Insufficient code provisions seem to be the most common cause of structural damage and in several cases failure is due to underestimation of actual snow loads by snow load models recommended in standards. As presented in [59], the use of light-weight roof structures increases the significance of snow load and it may be characterized by an insufficient reliability level. In addition, the use of high-quality materials for heat insulation of roofs protects snow from melting and causes its accumulation (often non-uniform). A significant load due to the combination of snow and ice on roofs, not considered in design codes, is observed in several cases. The study points out that further refinement of the consideration of the snow loading in the design standards is needed.
A first attempt to evaluate potential risk and effects of climate change on the built environment based on climate projections has been carried out in Norway

[87]. The results present a high variability in the Norwegian territory; in most municipalities reduced snow loads are expected, however increased snow loads are foreseen for the central inland parts of southern Norway. An increase of current snow load values in the Norwegian NA to EN1991-1-3 [135] is then suggested for 34 municipalities, with the extreme case of Odda, a town in Hordaland Count, where the load is tripled (from 2.5 kN/m^2 to 7.5 kN/m^2). The recent failures of roofs in Europe, which were caused mainly by heavy snow load, naturally call for an estimation of the expected snow load on structures taking into account the implications of the climate change [33]. Only after such estimates it will be possible to proceed with further refinement of the definition of the snow loads in the design standards [32].

Chapter 7

Use of weather generators to assess impact of climate change on climatic actions

In this chapter, a new simple weather generator is presented for the assessment of future trends of climatic actions starting from regional climate model output. Application of the proposed technique on extreme temperatures and precipitation is shown for an Italian climatic region considering an ensemble of six Regional Climate Models.

Contents

7.1 Introduction

As discussed before, the evaluation of the impact of climate change on extremes is a crucial issue for the resilience of infrastructures and buildings and is a key challenge for adaptation planning. In this chapter, a suitable procedure for the definition of future trends of thermal actions at local scale starting from the output of Regional Climate Models (RCMs) is presented, considering the different sources of uncertainty affecting climate projections (emission scenarios, climate models, internal variability).
The methodology is based on the implementation of a new simple weather generator to RCM output in order to take into account the uncertainty in the model related to the internal climate variability, which can bear significant implications for interpreting regional to local changes especially at smaller spatial scales [7].
The results are presented for the Italian Mediterranean region proving the ability of the method to define factors of change for climate extremes as well as to assess their evolution in time, also allowing a sound estimate of the uncertainty range associated with different models.

7.2 General methodology

7.2.1 Definition of Weather Generator

Weather generators have been used extensively in water engineering design and hydrological impact studies [156] and they are currently used as statistical downscaling technique in climate change impact studies [130, 50, 81, 47]. They are statistical models based on regression relationships between daily climatic variables, which are able to generate time-series of climatic variables with statistical properties similar to the input(observed) ones. It is worth noting that stochastic weather generators are not weather forecasting algorithms, which operate by numerically integrating the physical equations describing the climate system, but they are tools able to generate time-series of synthetic weather with a number of statistics identical to the observations [130].
Originally they were used to simulate weather series long enough to be used for the risk assessment in hydrological or agricultural applications, to estimate

missing meteorological data and to extend weather series to unobserved locations. New interest in the application of weather generators is growing for the local assessment of climate change impacts. Indeed, even at highest resolution a gap remains between the scale of RCM predictions and real applications, and weather generator may be used to obtain site-specific climate change scenarios based on predicted changes of the weather generator parameters obtained from the analysis of climate model output. Future weather series at local scale are thus obtained perturbing the parameters of the weather generator, which usually consist of climate variable statistics, with factors of change derived from the analysis of climate model output. This approach assumes that the climate model is able to better represent the change in the statistical properties of the climate variable from the present to the future climate, rather than the real future weather series.
The original method can be resumed in the following steps:

- factors of change (FC) are derived from the analysis of climate model output comparing future period climate statistics with control period climate statistics;
- future weather series are generated implementing a stochastic weather generator whose parameters are modified according to the estimated factors of change;
- future weather series are used in impact models or are directly analysed to detect climate change impact on extremes.

However, the definition of weather generators requires to parametrise a series of climate processes involving a lot of climate variables whose changes are usually not possible to detect from climate model output. Moreover, the direct application of the FC derived from the climate model output seems to not take into account the internal variability of the climate model itself. Therefore a new simple method to generate future climate series and estimate factors of change for extreme statistics has been developed.
In this approach, instead of generating weather series from the statistics of the climate variables, climate data series are generated directly by sampling from the climate model outputs [34] according to the algorithm summarized in the flowchart reported in Figure 7.1.

The input data of the algorithm are the climate data series of daily maximum and minimum air temperatures ($T_{\mathrm{Max},CM}$ and $T_{\mathrm{Min},CM}$) and precipitation

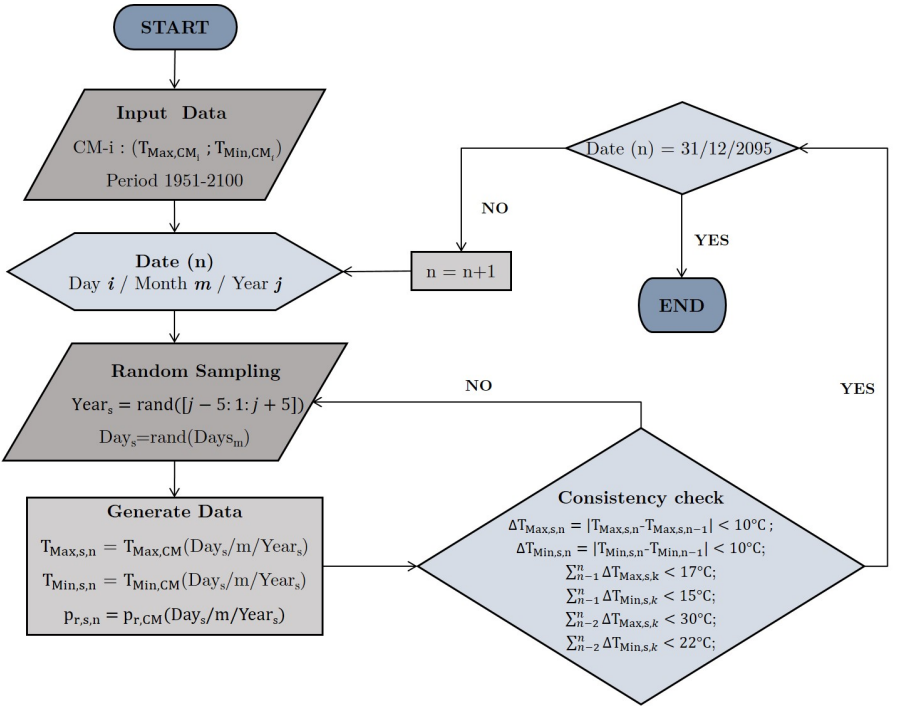

Figure 7.1: Flow chart of the weather generator algorithm.

($p_{r,CM}$) provided by high resolution regional climate models, selected, for example, from those provided by the EURO-CORDEX intitiative [73].
Then, daily data for day i of month m in year j ($T_{\mathrm{Max},s,n}$, $T_{\mathrm{Min},s,n}$, $p_{r,s,n}$) are randomly sampled from the daily data of the climate variables at the same month m in the period defined by the considered year plus and minus five years $[j-5,\, j+5]$. This time window of eleven years for the sampling interval has been considered as appropriate, being long enough to adequately represent the data population as well as short enough to exclude potential effects of climate change in the climate variables.
The random sampling procedure of temperatures and precipitation is implemented with some additional constraints in order to avoid the generation of unrealistic weather data series. In particular, constraints for maximum and minimum temperatures in two (Equations 7.1 and 7.2), three (Equations 7.3 and 7.4) and five consecutive days (Equations 7.5 and 7.6) have been defined from the analysis of the actual data, so requiring that the following inequalities are fulfilled by the generated data for day i:

$$\Delta T_{\mathrm{Max},s,n} = \mid T_{\mathrm{Max},s,n} - T_{\mathrm{Max},s,n-1} \mid < 10^{\circ}C, \tag{7.1}$$

$$\Delta T_{\mathrm{Min},s,n} = \mid T_{\mathrm{Min},s,n} - T_{\mathrm{Min},s,n-1} \mid < 10^{\circ}C, \tag{7.2}$$

$$\Delta T_{\mathrm{Max},s,n} = \sum_{k=n-1}^{n} \Delta T_{\mathrm{Max},s,k} < 17^{\circ}C, \tag{7.3}$$

$$\Delta T_{\mathrm{Min},s,n} = \sum_{k=n-1}^{n} \Delta T_{\mathrm{Min},s,k} < 15^{\circ}C, \tag{7.4}$$

$$\Delta T_{\mathrm{Max},s,n} = \sum_{k=n-3}^{n} \Delta T_{\mathrm{Max},s,k} < 30^{\circ}C, \tag{7.5}$$

$$\Delta T_{\mathrm{Min},s,n} = \sum_{k=n-3}^{n} \Delta T_{\mathrm{Min},s,k} < 22^{\circ}. \tag{7.6}$$

Then, implementing the algorithm in Figure 7.1, consistent climate data series of daily maximum and minimum air temperature ($T_{\mathrm{Max},s}$ and $T_{\mathrm{Min},s}$) but also precipitation ($p_{r,s}$) are generated for the period 1956-2095. Once generated these series, they can be analysed to derive factors of change for climate statistics evaluating also a confidence interval for the estimated changes. In particular, our interest is to evaluate climate change implication on extremes, therefore an extreme value analysis will be performed for each generated series.

7.2.2 Extreme Value Analysis and Factors of Change

As presented in paragraph 2.2 classical Extreme Value Theory provides a rigorous framework for the analysis of climate extremes and their return period under the assumption of stationary climate. However, the speed of current climate change, faster than most of past events, is making this assumption more questionable and concepts and models accounting for non-stationarity are thus becoming of increasing importance [21].

In this context, a procedure for the estimation of trends in extremes suitable for structural design has been set-up. Long annual maxima data series as those obtained from the analysis of climate projections are divided in appropriate subsequent time window of 40 years since observed series of 40 years are commonly used for the determination of structural loads. These subsequent time windows are shifted by ten years in order to evaluate changes in statistical parameters of extreme value distribution and return levels. In particular, in structural design we are interested in the characteristic value of the load, which it is recalled here that corresponds to the load having a 0.02 probability of exceedance in one year (50 years mean return period). The concepts of return level and return period are not changed for each time window and instead of evaluating changes in probabilities (return period) of an extreme event, changes are directly computed for the characteristic value of the load. In this way, the estimated changes can be used to update current load values given in structural Codes.
Following this approach, the generated climate data series of of daily maximum and minimum air temperature ($T_{\mathrm{Max},s}$ and $T_{\mathrm{Min},s}$) but also precipitation ($p_{r,s}$) are analysed according different time windows for a correct definition of non-stationary extremes suitable for structural design. In particular, the annual maxima data series are divided in appropriate time windows of forty year-long shifted by ten years (1956-1996, 1966-2006,..., 2056-2095) and for each time window t an extreme value analysis is carried out according to the block maxima approach assuming an extreme value Type I distribution with cumulative distribution function given in Equation 2.2. According to the least square method (LSM), the two distribution's parameters, μ and σ, are then estimated for each time window t, and by means of the Equation 2.6, with $p = 0.02$, characteristic values are calculated ($T_{\mathrm{Max},k}(t)$; $T_{\mathrm{Min},k}(t)$; $p_{r,k}(t)$).
Finally, factors of change are evaluated comparing the characteristic value of the investigated climate variable at the time window t with the corresponding value at the first time window ($t = 1$). In particular, a delta factor of change is defined for extreme temperatures

$$FC_{T_{\mathrm{Max},k}}(t) = T_{\mathrm{Max},k}(t) - T_{\mathrm{Max},k}(t = 1) \tag{7.7}$$

$$FC_{T_{\mathrm{Min},k}}(t) = T_{\mathrm{Min},k}(t) - T_{\mathrm{Min},k}(t = 1), \tag{7.8}$$

while a product factor of change is defined for extreme precipitation

$$FC_{p_{r,k}}(t) = \frac{p_{r,k}(t)}{p_{r,k}(t=1)}. \tag{7.9}$$

7.2.3 Factors of Change Maps

According to the presented procedure, factors of change for 50 years return period values of maximum and minimum temperatures and precipitation ($T_{\mathrm{Max},k}(t)$; $T_{\mathrm{Min},k}(t)$; $p_{r,k}(t)$) have been derived for a set of generated series obtained from an ensemble of high resolution of climate models. Combining the results, different percentiles of the factors of change ensemble can be easily evaluated, arriving to estimate changes in extremes together with their uncertainty range. The 25% percentile and 75% percentile can be taken as reference for the prediction interval and are thus calculated for each cell in the study region.

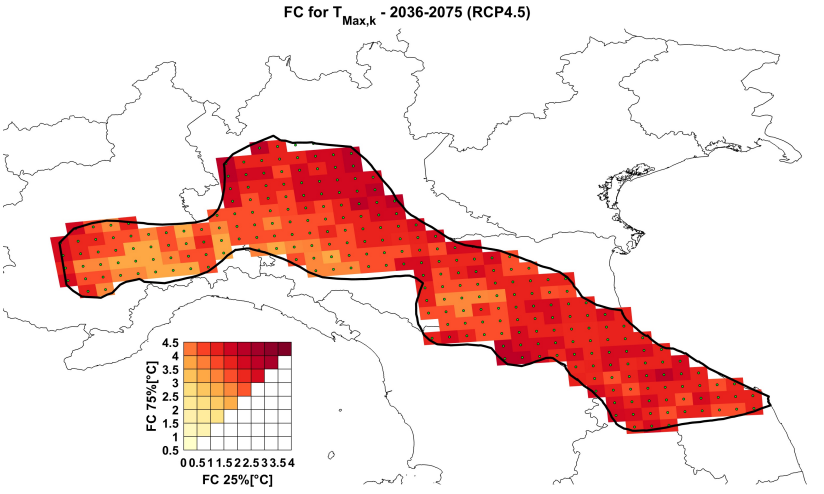

Figure 7.2: Bivariate factor of change map for $T_{\mathrm{Max},k}$.

Finally, factors of change maps can be drawn for each percentile and in order to better represent the results, bivariate color maps [143] are chosen. In this way, the two limit percentiles are drawn in the same map obtaining a convenient representation of the evolution of extremes together with the associated uncertainty interval. In Figure 7.2 an example of factors of change map is drawn for daily maximum temperature. These maps can provide

a guidance for potential amendments of the current climatic load maps in technical standards, e.g. maximum and minimum shade air temperature maps.

7.3 Case study

The procedure illustrated in the previous paragraph is applied here to investigate climate change impact on extreme temperatures and precipitation for an Italian climatic region .

7.3.1 Study area and dataset

The results of the analysis are presented for the geographical area which comprises the Zones 3-4 of the Mediterranean climatic region defined by the EN1991-1-3:2003 [14]. These zones are illustrated in Figure 7.3, together with the 272 cells at which climate projections are provided by the high resolution, $\sim$ 12.5kmx12.5km (EUR11-grid, see Figure 7.4), RCMs developed within the EURO-CORDEX initiative [73].

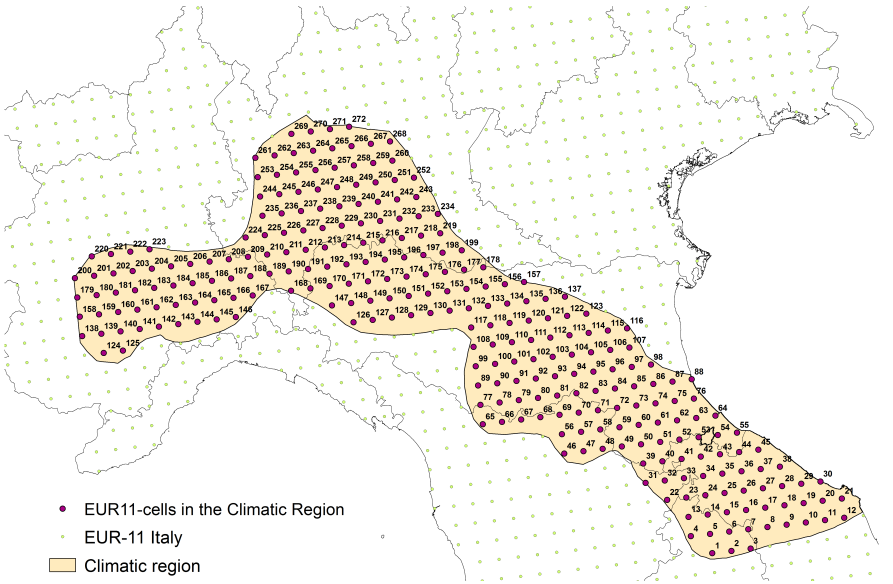

Figure 7.3: Investigated area in the Italian Mediterranean region.

Daily climate projection of maximum and minimum temperature ($T_{\mathrm{Max},CM}$ and $T_{\mathrm{Min},CM}$) are analysed for the control period 1951-2005 (*Historical Experiment*), where the model run is forced by observed atmospheric composition changes and for the future period 2006-2100 where run is forced by predicted atmospheric composition changes (*RCPs Experiment*).

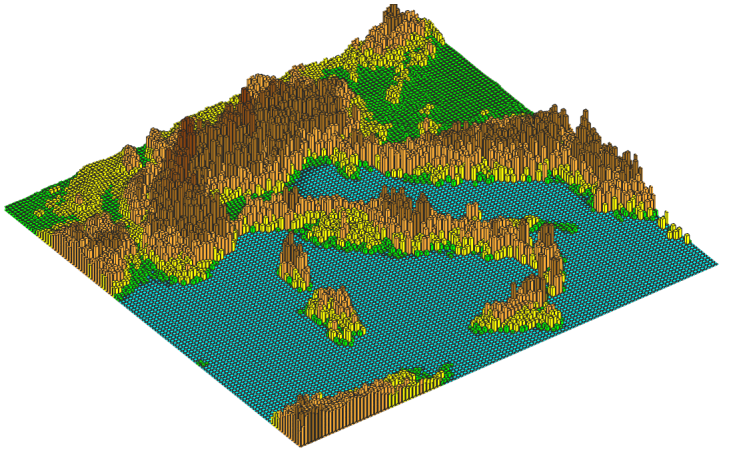

Figure 7.4: Illustration of the Italian topography at EUR11-grid resolution.

In particular, data provided by the Danish Meteorological Institute (DMI), the CLM Community (CLMcom), the Royal Netherlands Meteorological Institute (KNMI), the Max Planck Institute (MPI-CSC) and the Laboratoire des Sciences du Climat et de l'Environnement – Institute Pierre Simon Laplace (IPSL-INERIS), have been investigated for the so-called (*Historical Experiment*), the medium emission scenario (*RCP4.5 Experiment*) and the highest emission scenario (*RCP8.5 Experiment*). The model specifications of the analysed climate projections are reported in Table 7.1.

Dealing with multi-model ensemble, each climate model can be considered as an independent and plausible realization of the future climate, or suitable weights can be assigned to climate models based on their ability to reproduce past climate [142]. The results that will be presented in the following paragraphs are obtained combining with equal weights each individual component of the ensemble assuming that they are equally likely representation of future climate.

Institute	RCM	GCM	Experiment	Period
DMI	HIRHAM5	EC-EARTH	historical	1951-2005
			RCP4.5	2006-2100
			RCP8.5	2006-2100
CLMcom	CCLM4-8-17	CNRM-CM5-LR	historical	1951-2005
			RCP4.5	2006-2100
			RCP8.5	2006-2100
CLMcom	CCLM4-8-17	EC-EARTH	historical	1951-2005
			RCP4.5	2006-2100
			RCP8.5	2006-2100
KNMI	RACMO22E	EC-EARTH	historical	1951-2005
			RCP4.5	2006-2100
			RCP8.5	2006-2100
MPI-CSC	REMO2009	MPI-ESM-LR	historical	1951-2005
			RCP4.5	2006-2100
			RCP8.5	2006-2100
IPSL-INERIS	WRF331F	CM5A-MR	historical	1951-2005
			RCP4.5	2006-2100
			RCP8.5	2006-2100

Table 7.1: Overview on the analysed climate projections and their main characteristics.

7.3.2 Impact of climate change on extreme temperatures

Implementing the proposed procedure, described in the previous section, factors of change for the 50 years return period values of daily maximum and minimum temperatures ($T_{\mathrm{Max},k}(t)$; $T_{\mathrm{Min},k}(t)$) are estimated together with their uncertainty range [30].
In Figure 7.5 and 7.6 bivariate factors of change maps (25%-75% percentiles) are presented for the characteristic values of daily maximum temperature ($T_{\mathrm{Max},k}$) in four time windows (1976-2015, 1996-2035, 2016-2055 and 2035-2075) according to the RCP4.5 and RCP8.5 scenario respectively.
The mean factors of change percentiles (25%, 50%, 75%) for the study region obtained according the two different scenarios are collected for the different time windows in Table 7.2.
Similar maps are shown in Figure 7.7 and 7.8 for the characteristic values of daily minimum temperature ($T_{\mathrm{Max},k}$) while the mean factors of change percentiles (25%, 50%, 75%) are reported in Table 7.3.

The results show that a significant increase in extreme temperatures is expected with high confidence level in the near future. The increase is in line with the expectations for mean temperature (see Figure 3.3) but even more evident. Considering for example the time window 2036-2075, an increase of 2.75°C (with confidence interval 1.87°C - 3.55°C) and 3.37°C (with confidence interval

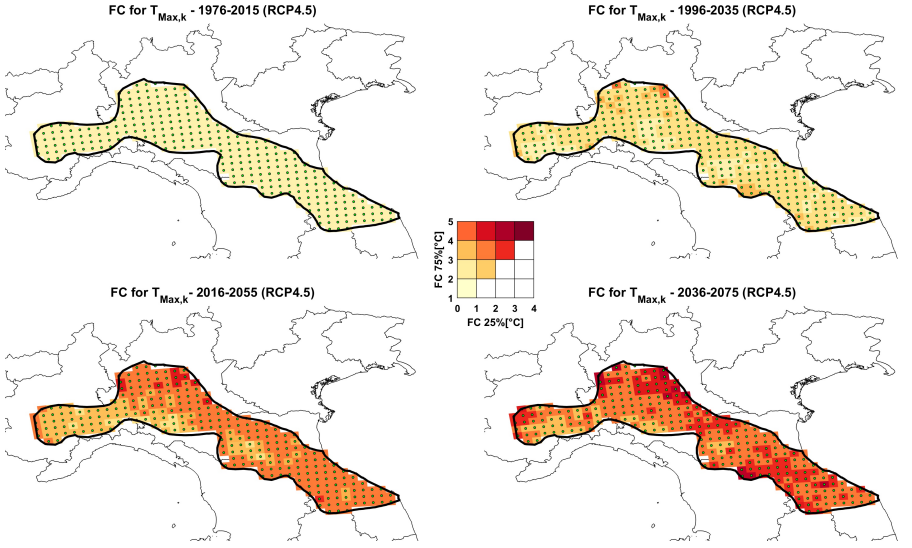

Figure 7.5: Delta Factors of Change (°C) for $T_{\mathrm{Max},k}$ – Confidence interval [25-75%] Map (Scenario RCP4.5).

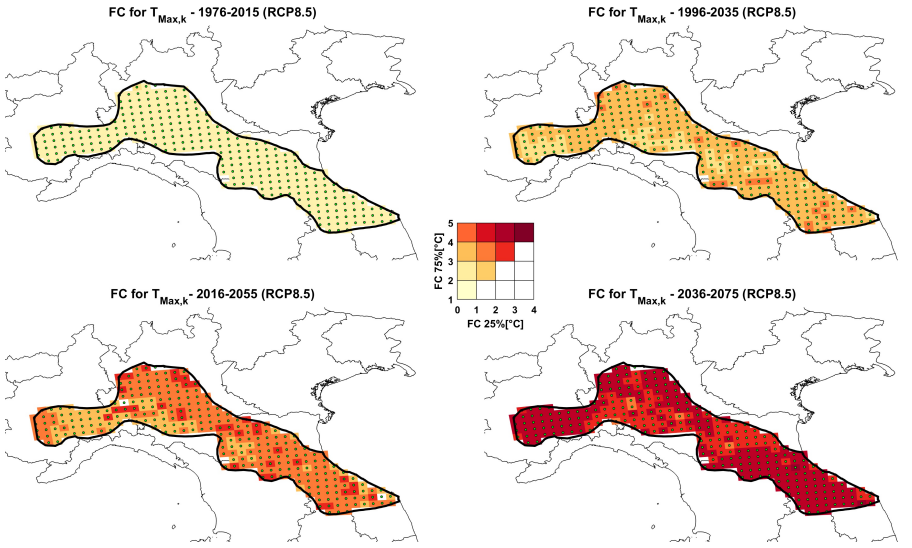

Figure 7.6: Delta Factors of Change (°C) for $T_{\mathrm{Max},k}$ – Confidence interval [25-75%] Map (Scenario RCP8.5).

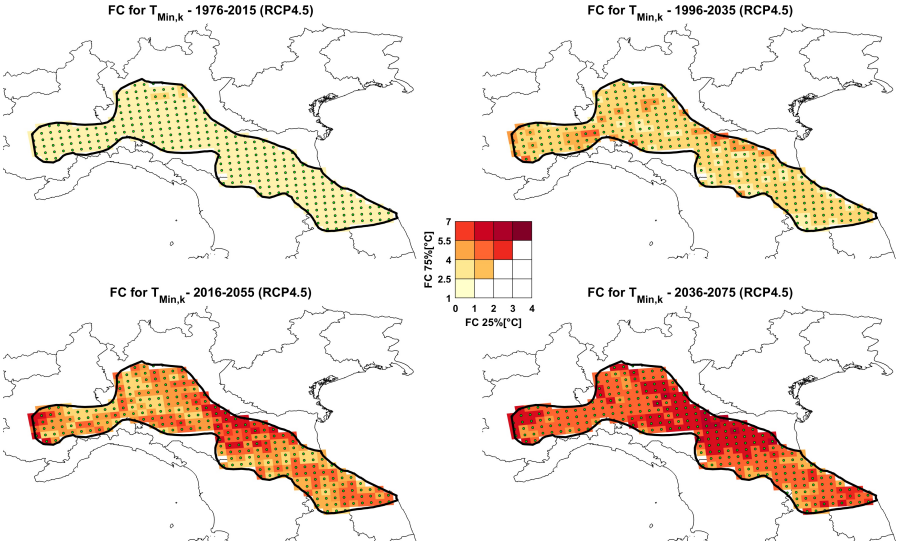

Figure 7.7: Delta Factors of Change (°C) for $T_{\mathrm{Min},k}$ – Confidence interval [25-75%] Map (Scenario RCP4.5).

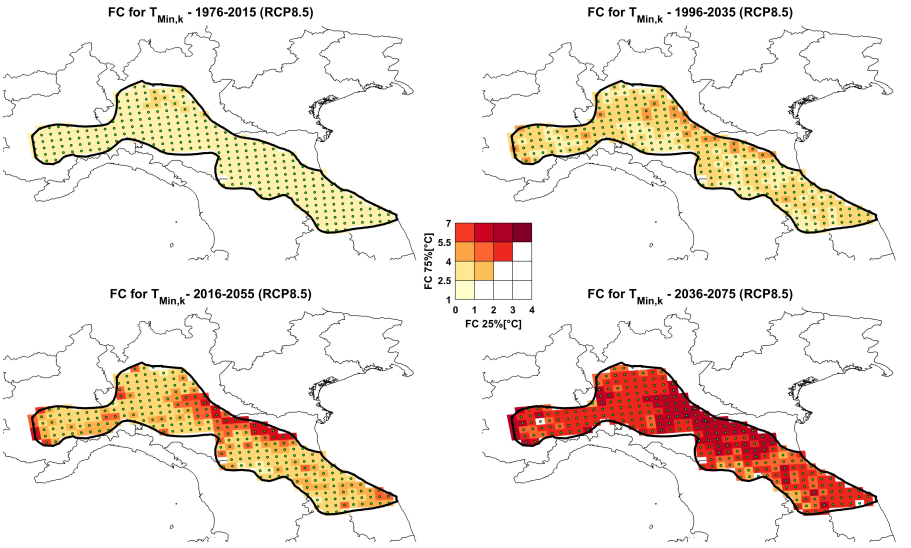

Figure 7.8: Delta Factors of Change (°C) for $T_{\mathrm{Min},k}$ – Confidence interval [25-75%] Map (Scenario RCP8.5).

Time window	RCP4.5			RCP8.5		
	25%	**50%**	75%	25%	**50%**	75%
1966-2005	0.04	**0.41**	0.82	0.03	**0.36**	0.72
1976-2015	0.31	**0.87**	1.42	0.35	**0.88**	1.42
1986-2025	0.45	**1.16**	1.87	0.81	**1.43**	2.06
1996-2035	0.65	**1.49**	2.25	1.26	**1.93**	2.67
2006-2045	0.89	**2.01**	3.10	1.44	**2.19**	2.85
2016-2055	1.33	**2.33**	3.31	1.77	**2.51**	3.19
2026-2065	1.58	**2.63**	3.63	2.00	**2.76**	3.54
2036-2075	1.87	**2.75**	3.55	2.47	**3.37**	4.17
2046-2085	2.18	**2.83**	3.67	3.93	**5.10**	6.08

Table 7.2: Mean of Factors of Change (°C) percentiles for $T_{\mathrm{Max},k}$ in the study region.

Time window	RCP4.5			RCP8.5		
	25%	**50%**	75%	25%	**50%**	75%
1966-2005	-0.30	**0.14**	0.73	-0.28	**0.15**	0.73
1976-2015	-0.23	**0.56**	1.60	-0.16	**0.63**	1.66
1986-2025	-0.12	**0.98**	2.48	-0.29	**0.84**	2.44
1996-2035	0.31	**1.57**	3.16	-0.08	**1.23**	2.92
2006-2045	0.65	**2.01**	3.89	0.24	**1.63**	3.39
2016-2055	1.01	**2.59**	4.52	0.83	**2.13**	3.67
2026-2065	1.48	**3.03**	4.87	1.55	**2.75**	4.19
2036-2075	1.59	**3.18**	5.22	2.29	**3.52**	5.23
2046-2085	2.40	**3.81**	6.02	2.83	**4.42**	8.55

Table 7.3: Mean of Factors of Change (°C) percentiles for $T_{\mathrm{Min},k}$ in the study region.

2.47°C - 4.17°C) is expected in the region for $T_{\mathrm{Max},k}$ according the RCP4.5 and RCP8.5 respectively.
In the same time window, even an higher increase is expected for $T_{\mathrm{Min},k}$: 3.18°C (with confidence interval 1.59°C - 5.22°C) for the RCP4.5 and 3.52°C (with confidence interval 2.29°C - 5.23°C) for the RCP8.5.

7.3.3 Impact of climate change on extreme precipitation

The outcomes of many recent studies call for an increase in precipitation extremes due to warming climate, resulting from the observational evidence of heavy rainfall intensifications in several regions all around the world [155, 40]. The observational evidence supports the thermodynamic law, often referred to as the Clausius-Clapeyron relationship, which states that warmer air has a higher water vapour holding capacity [49, 112]. According to this law, a scaling rate of about 6-7% K^{-1} warming can be predicted, considering the increase in atmospheric moisture content only.

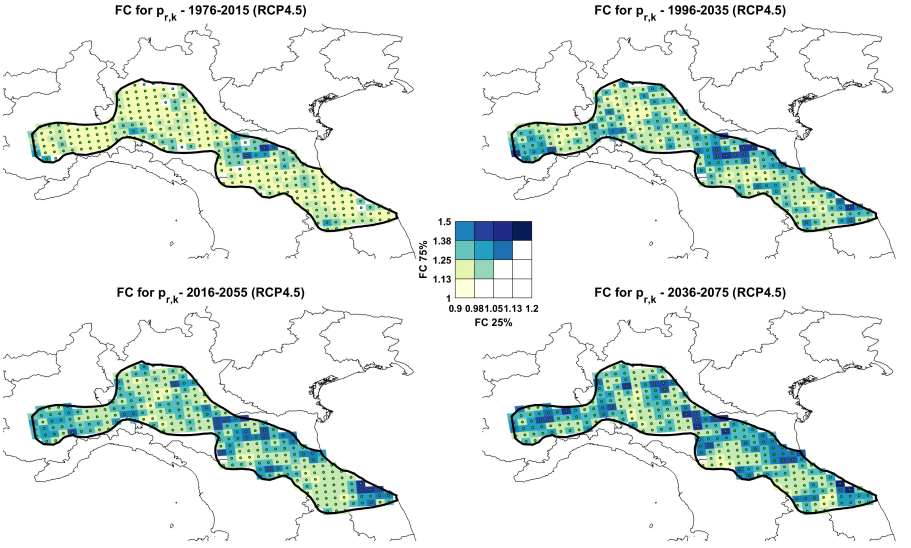

Figure 7.9: Factors of Change for $p_{r,k}$ – Confidence interval [25-75%] Map (Scenario RCP4.5).

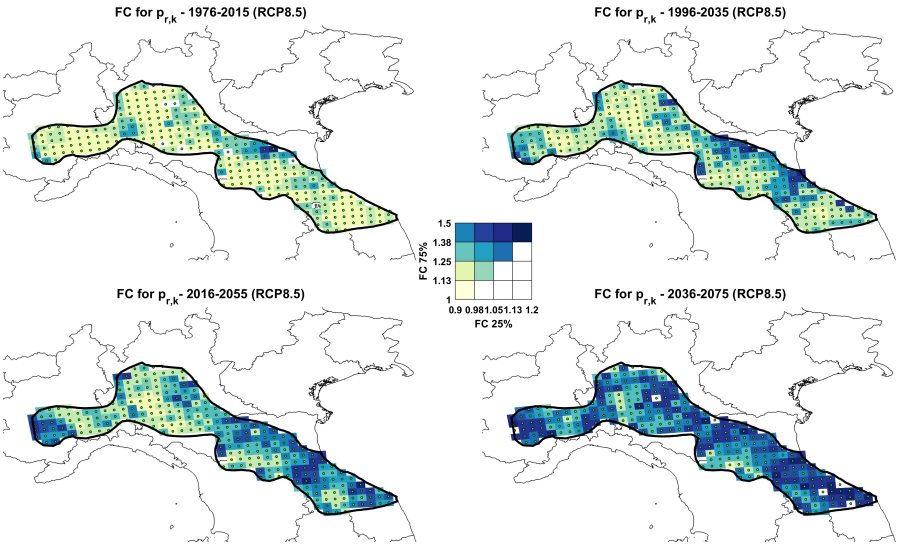

Figure 7.10: Factors of Change for $p_{r,k}$ – Confidence interval [25-75%] Map (Scenario RCP8.5).

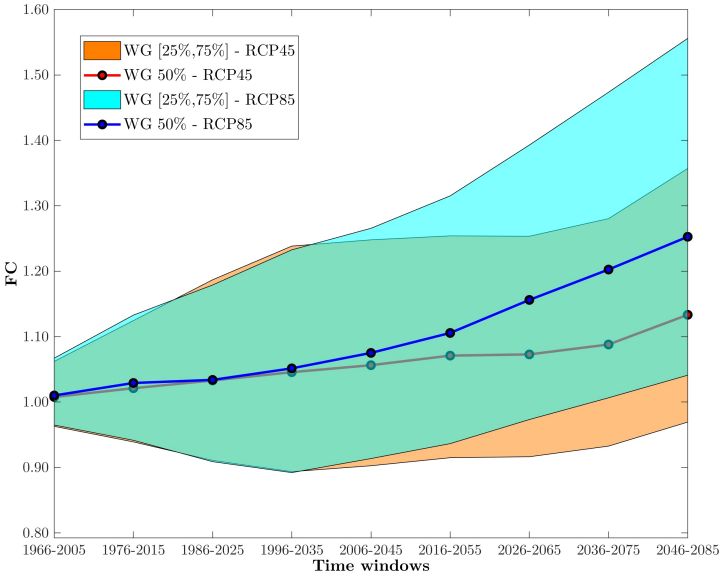

Figure 7.11: Factors of Change mean trends for $p_{r,k}$ in the study region.

Implementing the procedure which has been described in the previous section, factors of change for the 50 years return period values of daily precipitation ($p_{r,k}$) are derived together with their confidence interval. In Figures 7.9 and 7.10 factors of change maps for the 50 years return period values of precipitation ($p_{r,k}$) are presented in four time windows (1976-2015, 1996-2035, 2016-2055 and 2035-2075) according the RCP4.5 and RCP8.5 scenario.

Time window	RCP4.5			RCP8.5		
	25%	**50%**	75%	25%	**50%**	75%
1966-2005	0.96	**1.01**	1.06	0.96	**1.01**	1.06
1976-2015	0.94	**1.02**	1.12	0.94	**1.02**	1.12
1986-2025	0.91	**1.03**	1.19	0.91	**1.03**	1.18
1996-2035	0.89	**1.05**	1.24	0.89	**1.05**	1.23
2006-2045	0.90	**1.06**	1.25	0.91	**1.08**	1.25
2016-2055	0.91	**1.07**	1.25	0.94	**1.11**	1.32
2026-2065	0.92	**1.07**	1.25	0.97	**1.16**	1.39
2036-2075	0.93	**1.09**	1.28	1.01	**1.20**	1.47
2046-2085	0.97	**1.13**	1.36	1.04	**1.25**	1.56

Table 7.4: Mean of Factors of Change percentiles for $p_{r,k}$ in the study region.

As suggested in [49] and [112], averaging the results over all grid cells allows visualizing changes in heavy rainfall reducing the influence of unforced vari-

ability at grid box level where the signal may be obscured by high internal variability. Then, the resulting mean factors of change for the study region obtained according to different percentiles (25%, 50%, 75%) and different time windows are reported in Table 7.4. In this way, robust changes in extreme precipitation becomes more evident, as it is shown in Figure 7.11. Indeed, the results confirm that an increase in extreme precipitation could be very significant in the near future for the investigated region, especially in an high emission scenario (RCP8.5). For example, for the time window 2036-2075, an increase of 9% (FC=1.09) can be envisaged in the study region for $p_{r,k}$ assuming a RCP4.5 scenario, while, assuming a RCP8.5 scenario, it is expected an increase of 20% (FC=1.20).

Chapter 8

Estimation of ground snow load maxima from climate model ouput

In this chapter, a general procedure to evaluate future trends of snow loads on structures is illustrated, combining available outputs of climate models in terms of maximum and minimum temperatures and water precipitation, with local information of snowfall and snow melting conditions. The methodology, which is based on Monte Carlo simulations, is presented together with the results obtained for some Italian and German weather stations. Finally factors of change maps are shown for characteristic ground snow loads.

Contents

8.1 Introduction

As presented in section 6, the current definition of ground snow loads in structural Codes is based on the extreme value analysis of observed data series of annual maxima, usually no longer than 50 years and dating from 1950s to 1990s, under the more and more debatable assumption of stationary climate. Data series upon which the snow maps given in the Eurocodes are based, generally consist of water equivalent and snow cover depth measurements, converted into snow load through appropriate density functions; these series are suitable for the estimation of the characteristic ground snow load (50 years return period), but they are not enough extended over time to reflect the effects of climate change. At present it is therefore necessary to rely on climate projections provided by high resolution climate models, that represent our major source of knowledge about future climate.
However, climate model outputs, which are typically available, consist mainly of daily temperatures and precipitation and no direct relationship can be found with yearly maxima snow load.
Therefore, the first step of the present research has been the development of a general procedure to derive ground snow loads from the daily outputs of climate models, especially daily maximum and minimum air temperatures and precipitation.
The magnitude of loads imposed by snow depends upon a number of climatological and meteorological variables and may exhibit marked variations geographically, due to local effects within a particular region, and with time [72].
Then, the basic idea of the method is to reproduce the snow load formation process considering both climate data provided by the climate models and local information of snowfall and snow melting conditions derived from the elaboration of real measurements of actual meteorological events [29].
The methodology, which is based on Monte Carlo simulations, is presented in this chapter together with the results obtained for some Italian and German weather stations in reproducing observed data series. After the calibration and validation of the method, the procedure has been implemented on climate projections. Finally factors of change maps, as those reported in the previous section, are shown for the characteristic ground snow load in two different study regions, in Italy and in Germany.

8.2 Methodology

The proposed procedure for the estimation of ground snow loads consists of four steps which identify the following paragraphs:

- analysis of observed data series of daily temperatures, precipitation and snow cover depth, to derive conditional probability functions, linking snowfall and snow melting conditions at a given site with water precipitation data and air temperature;
- development of a predictive model to evaluate snow loads from available meteorological data, daily temperatures and precipitation, supplemented by the conditional probability functions of snowfall and snow melting;
- calibration and validation of the model predictions against observed data series;
- implementation of the model on projected data series provided by high resolution climate models.

8.2.1 Analysis of observed data series

First of all, relevant meteorological data recorded in the past, especially daily air temperatures and precipitation (water equivalent and snow cover depth), have been collected and analysed. The aim is to seek the conditions of maximum and minimum daily temperature, T_{Max} and T_{Min}, at which rainfalls or snowfalls are likely to occur and snow cover depth increases, in case of precipitation of height p_r, or decreases, in case of melting or increasing density of the snow cover. In particular, seven different situations have been identified comparing day n and day $n-1$:

- total melting of snow cover present at day $n-1$;
- partial melting of the snow cover present at day $n-1$;
- constant snow cover depth without precipitation;
- rainfall in absence of snow cover at day $n-1$;
- rainfall and total melting of the snow cover present at day $n-1$;
- precipitation on snow cover with snow depth decreasing;

- snowfall with increasing of snow cover;

and, following the flowchart reported in Figure 8.1, the daily measured data are allocated according to them.

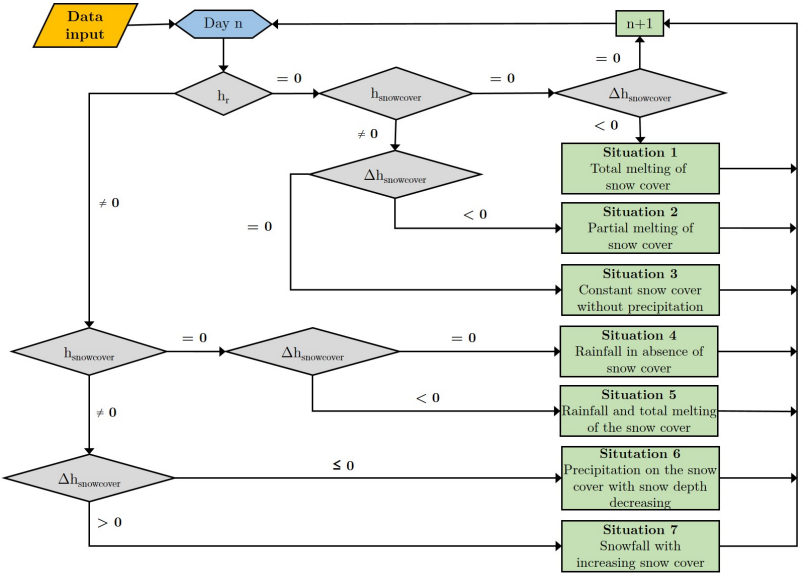

Figure 8.1: Flowchart for allocation of daily measured data.

Then, for each relevant situation, the frequency histogram $Z(\bar{T}_{\mathrm{Min}}, \bar{T}_{\mathrm{Max}})$ is derived according to the following conditions

$$Z(\bar{T}_{\mathrm{Min}}, \bar{T}_{\mathrm{Max}}) = \text{number of cases for which}$$
$$(\bar{T}_{\mathrm{Min}} - \frac{\Delta T}{2}) < \bar{T}_{\mathrm{Min}} < (\bar{T}_{\mathrm{Min}} + \frac{\Delta T}{2}) \cup (\bar{T}_{\mathrm{Max}} - \frac{\Delta T}{2}) < \bar{T}_{\mathrm{Max}} < (\bar{T}_{\mathrm{Max}} + \frac{\Delta T}{2})$$
$$\text{with} \quad -20^{\circ}\mathrm{C} < \bar{T}_{\mathrm{Min}} < 40^{\circ}\mathrm{C}; -20^{\circ}\mathrm{C} < \bar{T}_{\mathrm{Max}} < 40^{\circ}\mathrm{C}; \Delta T = 1^{\circ}\mathrm{C}. \tag{8.1}$$

The seven frequency histograms have been then converted into continuous surfaces $f_j(T_{\mathrm{Min}}, T_{\mathrm{Max}})$ by means of up to three two-dimensional Gaussian functions

$$f_j(T_{\mathrm{Min}}, T_{\mathrm{Max}}) = \sum_{i=1} a_i e^{\frac{-1}{2}\left[\frac{(T_{\mathrm{Max}} cos\beta_i + T_{\mathrm{Min}} sin\beta_i) - (\mu_{\mathrm{max},i} cos\beta_i + \mu_{\mathrm{min},i} sin\beta_i)}{\sigma_{\mathrm{max},i}}\right]^2} e^{\frac{-1}{2}\left[\frac{(T_{\mathrm{Min}} cos\beta_i - T_{\mathrm{Max}} sin\beta_i) - (\mu_{\mathrm{min},i} cos\beta_i - \mu_{\mathrm{max},i} sin\beta_i)}{\sigma_{\mathrm{min},i}}\right]^2} \tag{8.2}$$

being i the number of the Gaussian functions, which is assumed equal to the number of modes of the histogram. In Equation 8.2, each Gaussian function is defined by 6 parameters:

- a_i amplitude
- β_i angle of rotation with respect to x-axis (T_{Max});
- $\mu_{\mathrm{max},i}$ median value with respect to x-axis (T_{Max});
- $\mu_{\mathrm{min},i}$ median value with respect to y-axis (T_{Min});
- $\sigma_{\mathrm{max},i}$ standard deviation with respect to x-axis (T_{Max});
- $\sigma_{\mathrm{min},i}$ standard deviation with respect to y-axis (T_{Min}).

The parameters β_i, $\mu_{\mathrm{max},i}$, $\mu_{\mathrm{min},i}$ are derived from the peak values of the histograms, while the other parameters, $\sigma_{\mathrm{max},i}$, $\sigma_{\mathrm{min},i}$, a_i are estimated by means of least squares method and imposing the condition of unitary volume underlying the surface ($\sum_{i=1} a_i$). In Figure 8.2 they are shown, as an example, the results obtained in terms of frequency histogram and probability function derived from it, plotted for situation 7 (snowfall) at the Italian weather station of Bologna.

8.2.2 Definition of conditional probability functions of snowfall and snow melting

Once derived the probability distribution function f_j for each relevant situation, $j = 1, 2, .., 7$, conditional probability functions of snowfall and snow melting for given values of the daily temperatures, T_{Max} and T_{Min} are defined. In particular, it results that:

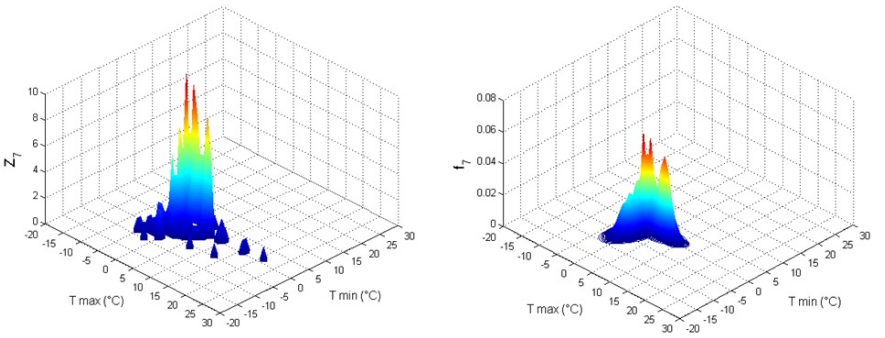

Figure 8.2: Frequency histogram for situation 7 (snowfall) Z7 and consistent probability function f7 (Bologna-Italy).

- the conditional probability function of snowfall in presence of precipitation is

$$P(\text{snowfall}(T_{\text{Max}}, T_{\text{Min}})|\text{precipitation}) = \frac{n_7 f_7}{n_7 f_7 + n_{4-5} f_{4-5}} \qquad (8.3)$$

  where n_7 is the number of cases of effective snowfall (situation 7) and f_7 is the consistent probability function previously defined; n_{4-5} is the number of cases of rainfall (situations 4 plus 5) and f_{4-5} is the consistent probability function (an example of such a function for the Italian weather station of Bologna is reported in Figure 8.3a);

- the conditional probability function of melting of snow cover in presence of snow cover is

$$P(\text{snowmelt}(T_{\text{Max}}, T_{\text{Min}})|\text{snowcover}) = \frac{n_{1-2} f_{1-2}}{n_3 f_3 + n_{1-2} f_{1-2}} \qquad (8.4)$$

  where n_{1-2} is the number of cases of snow melting (situations 1 plus 2) and f_{1-2} is the consistent probability function; n_3 is the number of cases of constant snow cover (situation 3) and f_3 is the consistent probability function previously defined (as an example, the conditional probability function obtained considering data of nine Italian weather stations is reported in Figure 8.3b).

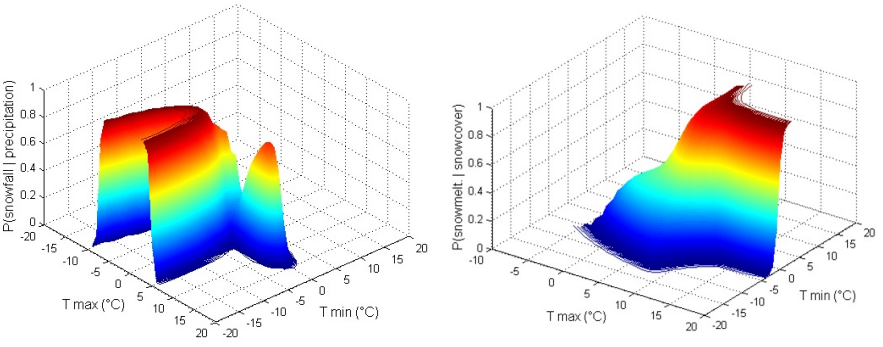

(a) Snowfall **(b)** Snow melting

Figure 8.3: Conditional probability function of snowfall and snow melting (Bologna, Italy).

8.2.3 Predictive model

A predictive model to evaluate ground snow loads has been then developed through a suitable Monte Carlo simulation, based on the previously determined conditional PDFs. The flowchart of the implemented algorithm is presented in Figure 8.4.

The input data of the algorithm are three relevant meteorological daily data: the maximum and minimum air temperature ($T_{\mathrm{Max},n}$ an d $T_{\mathrm{Min},n}$), and the precipitation in mm of water, $p_{r,n}$, at the day n. The probability of snowfall with increasing snow cover depth is estimated by checking the following conditions:

$$T_{\mathrm{Min},n} < 5°\mathrm{C} \quad \wedge \quad p_{r,n} \neq 0 \quad \wedge \quad P(\mathrm{snowfall}(T_{\mathrm{Max},n}, T_{\mathrm{Min},n})|\mathrm{prec.}) > R \tag{8.5}$$

where $0 \leq R \leq 1$ is derived from the randomly generated number, modified with the latin hypercube sampling technique. When conditions 8.5 are satisfied, the increase of the ground snow load Δq_n at the day n is estimated in terms of water equivalent measured by the rain gauge:

$$\Delta q_n = 0.01 \cdot p_{r,n} \quad [\mathrm{kN/m^2}] \quad \text{with} \quad p_{r,n} \quad \text{in} \quad [\mathrm{mm}] \tag{8.6}$$

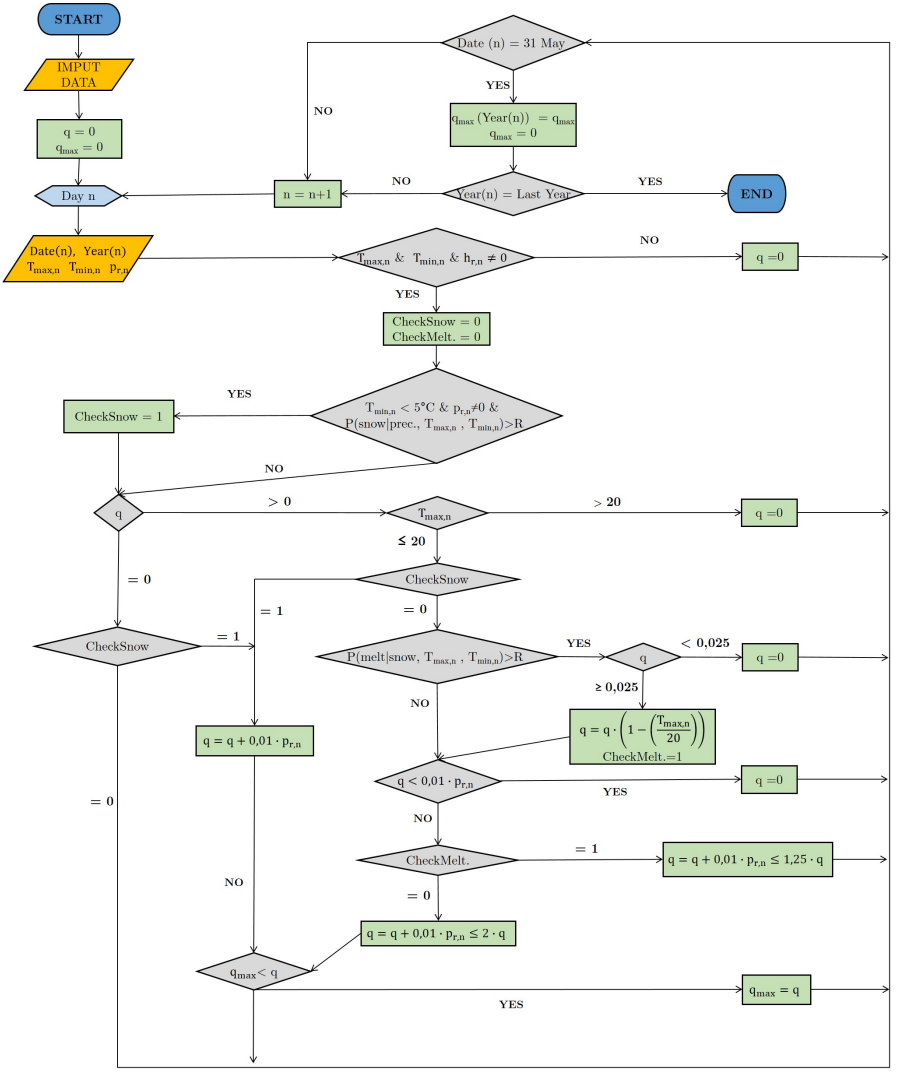

Figure 8.4: Flow chart of the algorithm for the estimation of yearly maximum ground snow load.

At the day $n+1$, several alternative and mutually exclusive events can happen regarding the snow load formation process, with an associated probability of occurrence:

- if snowfall conditions 8.5 are satisfied again, the ground snow load q_{n+1} is calculated as

$$q_{n+1} = q_n + 0.01 \cdot p_{r,n+1} \quad [\mathrm{kN/m^2}] \tag{8.7}$$

- if snow melting conditions are satisfied, i.e.

$$P(\text{snowmelt}(T_{\text{Max},n+1}, T_{\text{Min},n+1})|\text{snowcover}) > R \tag{8.8}$$

  snow melts, partially or totally, being R defined before: the melting is assumed to be proportional to the value of $T_{\text{Max},n+1}$, so that the updated ground snow load becomes

$$q_{n+1} = q_n(1 - \frac{T_{\text{Max},n+1}}{20}) \quad \text{where} \quad 0°\text{C} \leq T_{\text{Max},n+1} \leq 20°\text{C} \tag{8.9}$$

  but, if $T_{\text{Max},n+1} > 20°\text{C}$ or $q_n < 0.025 \quad \mathrm{kN/m^2}$ total melting is considered.

- if rainfall precipitation occurs in case of snow cover, the new ground snow load is given by

$$q_{n+1} = q_n + 0.01 \cdot p_{r,n+1} \quad [\mathrm{kN/m^2}] \quad \leq \quad 1.25 q_n \tag{8.10}$$

  but, if $q_n < 0.01 \cdot p_{r,n+1}$ total melting is considered.

All days of the year are considered, in order to estimate from the simulated snow load formation process the annual maximum ground snow load, q_{max}. Then, for each year, the process has been iterated 10000 times. In this way, the Monte Carlo simulation allows to obtain a series of 10000 values for maxima q_{max} for each year and, from them, the expected value of q_{max} is computed, i.e. the mean value of the simulated maxima for that year. However, since the results show that mean value and median are very close and that the

median value allows to better represent no snowy years, as best estimate of the maximum ground snow load for the examined year the median value q_{max} has been chosen instead of the mean value.
Concerning the number of iterations, calibration exercises to check the convergence of the method, proved that 10^4, 10^5 or 10^6 iterations give practically identical results. Finally, from the set of the N annual simulated maxima q_{max}, the characteristic value of ground snow load q_k, associated to the probability of 2% to be exceeded in one year [13], can be derived via extreme value analysis. In particular, an extreme value distribution Type I (Gumbel) with parameters μ and σ has been considered, so that the characteristic values is calculated by

$$q_k = \mu + \sigma\{-\log[-\log(1 - 0.02)]\}. \tag{8.11}$$

8.2.4 Calibration and validation of the methodology

8.2.4.1 Correction of snow precipitation measurements at the rain gauges

In order to compare the results obtained by means of the snow load algorithm on the basis of daily data of temperatures and precipitation at the rain gauges, with those obtained from the ESLRP [126], combining snow cover depth data with an empirical density law, a critical analysis of snow load measurements has to be done. In Figure 8.5: on the left, the time-dependent density law adopted for Italy (in case of snow cover duration $D > 10$ consecutive days) and on the right, the density function based on the height of snow cover adopted by Germany.

Indeed, several specific studies have been devoted in the last decades to assess the catching capability of rain, snow or mixed precipitation of different type of rain gauges as well as the influence of wind speed and the efficiency of wind shields [54, 120, 159]. A systematic outcome of these studies is that wind speed of 6 m/s at the gauge level (1.5 m above the ground) reduces the snow catching capability of approximately 60% [159] or 65% [120] in shielded condition, while in unshielded condition the reduction is higher, being around 80%. For these reasons, snowfall water equivalent (SWE) are often estimated

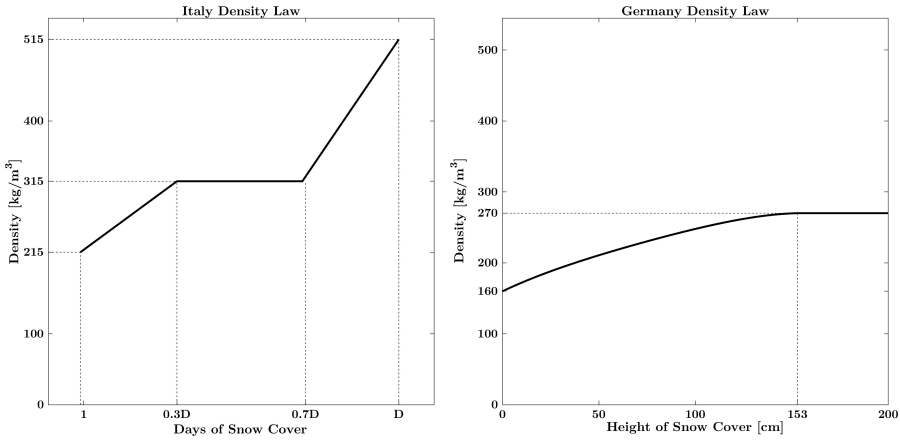

Figure 8.5: Density laws for Italy and Germany.

from snow cover depth measurements combined with the estimated snowfall density, according to the formula:

$$\text{SWE} = \rho_s h_s \quad [\text{kg/m}^2], \tag{8.12}$$

where ρ_s is the snow density in kg/m^3 and h_s is the height of snow cover in m. This is what was done for the evaluation of ground snow loads in Italy and Germany during the ESLRP [126]. Although snow density can be highly variable, it can be specifically assessed at a given location, so that the application of Equation 8.13 leads to acceptable results, even allowing to correct snowfall data recorded by precipitation gauges as it was done for example by Sevruk in [131, 132], and by Lendvai et al. in [91].
Comparing the daily increments of the snow loads, obtained in terms of water equivalent from the measurements of the snow height and the corresponding daily solid precipitations measured by the gauges in Italian weather stations, similar findings are systematically reached. For the sake of application of Equation 8.13, an empirical density law as presented in [91] has been adopted for the snow density. In particular, a reasonable value of $\rho_s = 250\text{kg/m}^3$ for the snow cover density at low altitudes in Italy is considered. This value was also adopted in [126] for snow duration $D < 10$ consecutive days. For example, analysing the winter season 1955-56 at the Bologna weather station and the winter season 1940-41 at the Spigno Monferrato weather station, the diagrams illustrated in Figures 8.6a and 8.6b, are obtained respectively. The graphs

allow to compare the daily variations of the snow load on the ground, obtained applying 8.13 ($\Delta q_s = \Delta h_s \rho_s$), represented by the orange lines, with the daily water equivalent of the precipitation measured by the gauge ($\Delta q_r = p_r \rho_w$, p_r in m and $\rho_w = 1000\text{kg/m}^3$), represented by the light blue lines.

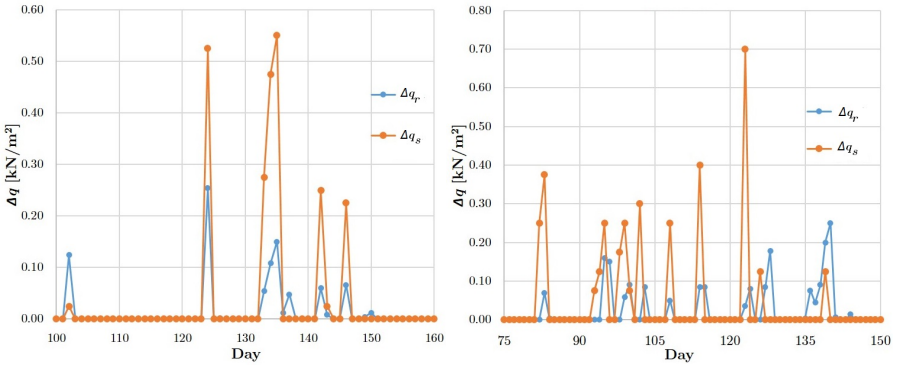

(a) Bologna 1955-1956 **(b)** Spigno Monferrato 1940-1941

Figure 8.6: Comparison of snow load variation in two consecutive days, from precipitation measurement at rain gauges(Δq_r) and snow cover depth (Δq_s).

Examining the diagrams in Figures 8.6a and 8.6b, it appears clearly that in Bologna the highest daily rates of snow accumulations are even five times the corresponding accumulation rates derived from the water equivalent of the precipitation measured at the gauge, and that in Spigno Monferrato they reach values up to fourteen. Obviously, as in the calculations it was assumed a snow density of 250 kg/m^3, these huge ratios cannot be justified by a simple overestimation of the actual snow density, because to match the aforementioned values, unrealistic values in the range 20-50 kg/m^3 should be adopted for the snow density. These systematic errors in solid precipitation measurements at the rain gauges are mainly due to wind field deformation in the neighbourhood of the gauge orifice [54], as summarized in Figure 8.7a; but also snow accumulation due to wind induced transportation phenomena shown in Figure 8.7b, could increase the snow cover height at the observation site [147], emphasizing the discrepancies between the measured height of the snow cover and that derived on the basis of the water equivalent obtained from gauge measurement.

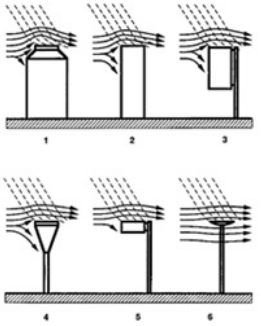

(a) Wind field deformation at the rain gauge[54]

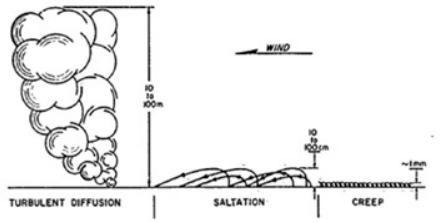

(b) Wind induced transportation phenomena[106]

Figure 8.7: Main reasons for systematics errors in solid precipitation measurements.

On the basis of the aforementioned considerations, a suitable correction factor, $k \geq 1.0$, should be introduced, as proposed by Sevruk in [131], to convert water equivalent measurement at the rain gauge into snowfall water equivalent. As recalled, the correction factor mainly depends on the type of the rain gauge employed for the measurements, and on its wind protection, if any; on the location of the weather station, and on the average wind conditions during the precipitation events, so resulting a specific property of the weather station. As the present study focuses on the extreme values of the snow load, a suitable correction factor, k_{corr}, affecting the characteristic values has been introduced,

$$k_{corr} = \frac{q_{k,\mathrm{ESLRP}}}{q'_k}. \tag{8.13}$$

This factor aims to convert characteristic snow loads derived from precipitation measurements at the rain gauges (q'_k) into the correct load values obtained from the true amount of snow water equivalent ($q_{k,\mathrm{ESLRP}}$) [126].

8.2.4.2 Calibration of the model on selected weather stations: deterministic approach

In order to calibrate the presented methodology and derive the appropriate correction factors to take into account the systematic errors in snowfall precipitation measurements at the rain gauges presented in the previous paragraph,

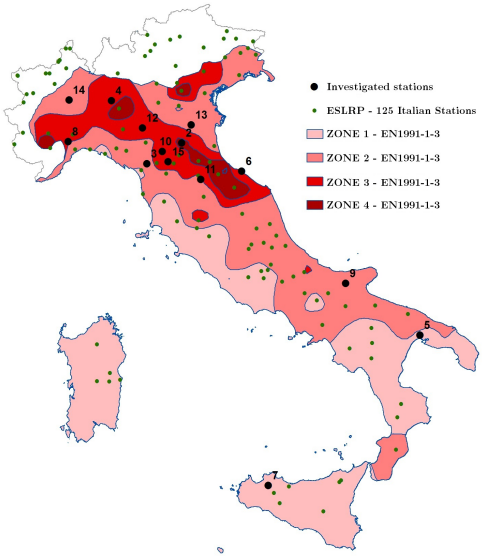

N.	Station	Lon(°)	Lat(°)	Alt(m)
1	Ascoli Piceno	13.56	42.90	136
2	Bologna	11.36	44.50	51
3	Castelnuovo Garfagnana	10.43	44.12	276
4	Lodi	9.51	45.32	80
5	Massafra	17.13	40.58	116
6	Pesaro	12.91	43.92	11
7	San Giuseppe Jato	13.19	37.97	450
8	Spigno Monferrato	8.36	44.55	476
9	San Severo	15.39	41.68	87
10	Pavullo	10.84	44.35	682
11	Camaldoli	11.83	43.80	1111
12	Parma	10.33	44.80	56
13	Ferrara	11.63	44.83	15
14	Vercelli	8.38	45.33	135
15	Poretta Terme	10.99	44.15	349

Figure 8.8: The fifteen Italian weather stations considered in the calibration and the zonation of the Italian Mediterranean region according to EN1991-1-3.

the snow load algorithm has been initially tested against observed data series of daily temperatures and precipitation at selected weather stations, whose data were collected in the database of the University of Pisa during the ESLRP [126, 125]. In this way, the snow loads derived with the proposed methodology can be easily compared with those collected for the same weather stations during the ESLRP [126, 125].
In particular the long-time series of observed daily temperatures, precipitation and snow cover depth at fifteen Italian weather series have been considered. The location of these stations is shown in Figure 8.8 together with the zonation of the Italian Mediterranean region obtained according to the Annex C of EN1991-1-3 [14], where the ground snow load at sea level (to which different zones are referred) is increasing from zone n.1 to zone n.4.

Implementing the snow load algorithm on the observed series of daily maximum and minimum temperature and precipitation, series of the annual maxima snow loads are derived for the investigated stations. From them, following the same assumptions of the ESLRP[126], here described in 4.2.1, the characteristic values of ground snow loads are derived. The results are thus reported in terms of characteristic load values (q_k) and correction factors (k_{corr}) in Table 8.1 for the investigated stations.

N.	Station	q_k' [kN/m^2]	$q_{k,\mathrm{ESLRP}}$ [kN/m^2]	k_{corr}
1	Ascoli Piceno	0.68	1.12	1.65
2	Bologna	0.99	1.67	1.69
3	Castelnuovo Garfagnana	1.14	1.14	1.00
4	Lodi	0.76	1.19	1.57
5	Massafra	0.16	0.54	3.38
6	Pesaro	0.67	1.07	1.60
7	San Giuseppe Jato	0.50	0.94	1.88
8	Spigno Monferrato	0.88	2.40	2.73
9	San Severo	0.46	0.74	1.61
10	Pavullo	1.45	3.89	2.68
11	Camaldoli	2.37	4.15	1.75
12	Parma	1.08	1.56	1.44
13	Ferrara	0.72	1.00	1.39
14	Vercelli	0.92	1.08	1.17
15	Poretta Terme	1.87	2.73	1.46

Table 8.1: Characteristic load values q_k and correction coefficients k_{corr} for the investigated Italian weather stations.

It must be underlined that k_{corr} is a characteristic of the considered site, and, therefore, it may be considered constant for sites characterized by similar climatological conditions. In effect, it assumes typically values around 1.70 (mean value 1.69), that are comparable with the typical values present in literature [54, 131, 132, 91]; for instance, if the values reported in [131] for the Alpine region are analysed, the mean correction factor is also about 1.69 and factors up to 2.44 can be found, which are not far from the value determined for Spigno Monferrato, 2.73. Moreover, the high value of the conversion factor in Spigno Monferrato was anticipated by the analysis of the daily increments, as illustrated in the already discussed Figure 8.6b. A separate discussion is necessary for the Massafra weather station, characterized by $k_{corr} = 3.38$. In effect, Massafra is an exceptional case, due to the particular site location, which is in Southernmost part of Italy, in the Taranto gulf, very close to sea, and it is characterized by a very low number of snowfall events in the investigated period.
The methodology has been then tested against observed data series also at some German weather stations. In this case, the results reported in Table 8.2 show slightly lower values, around 1.40, for the correction factors.

N.	Station	q'_k (kN/m^2)	$q_{k,\mathrm{ESLRP}}$ (kN/m^2)	k_{corr}
1	Bad Reichenhall	2.06	2.43	1.18
2	Braunlage	3.30	4.88	1.48
3	Braunschweig	0.54	0.87	1.61
4	Karlsruhe	0.55	0.70	1.27
5	Teterow	0.65	0.98	1.51
6	Wasserkuppe	3.03	3.68	1.21

Table 8.2: Characteristic load values q_k and correction coefficients k_{corr} for the investigated German weather stations.

8.2.4.3 Calibration of the model on selected weather stations: Bayesian approach

The calibration of the methodology which consists in the identification of the appropriate conversion factor for characteristic ground snow loads, can be also performed following the so called Bayesian approach. In this case, the conversion factor is considered as a random variable K at which is assigned a prior distribution $\pi(k)$ characterising the epistemic uncertainty coming from our lack of knowledge. According to the values reported in [131] a prior distribution for the correction factor to be applied to snowfall precipitation at the rain gauges, can be defined. In Figure 8.9 the resulting normal PDF, $N(\mu$=1.69, σ=0.37), is showed.

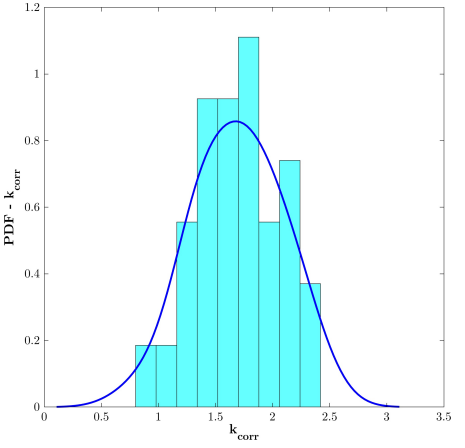

Figure 8.9: PDF for correction factor according to the values reported in [131].

Then, in the snow load algorithm described in paragraph 8.2.3 precipitation

data $p_{r,n}$ in case of snowfall, are corrected and eq.8.6 becomes

$$\Delta q_n = 0.01 \cdot p_{r,n} \cdot k_{corr} \quad \text{kN/m}^2 \quad \text{with} \quad p_{r,n} \quad \text{in} \quad [\text{mm}], \tag{8.14}$$

where in the Monte Carlo simulation k_{corr} is sampled from the previously defined PDF. However, as discussed before, the correction factor is site specific and it can be identified comparing the model predictions obtained by means of the algorithm, which represents our forward model G, in terms of characteristic ground snow load, with that obtained from observed snow water equivalent measurements during the ESLRP. Since errors in the estimation of q_k are inevitable in practice, $q_{k,\text{ESLRP}}$ may not match the true value of the model prediction $G(k_{corr,true})$, so that, assuming a model error $\varepsilon \sim N(0,\ \sigma_\varepsilon)$, the measurement data takes the form

$$q_{k,ESLRP} = G(k_{corr,true}) + \varepsilon. \tag{8.15}$$

The Bayesian approach seeks to estimate the updated density of the random variable K given a set of observations, in this case represented by $q_{k,\text{ESLRP}}$. Then, the Bayes rule takes the form

$$\pi(k|q_{k,\text{ESLRP}}) = \frac{\pi(q_{k,\text{ESLRP}}|k)\pi(k)}{\int(q_{k,\text{ESLRP}}|k)\pi(k)dk}, \tag{8.16}$$

where $\pi(k)$ is the prior probability density of K, $\pi(q_{k,\text{ESLRP}}|k)$ is the likelihood function, and $\pi(k|q_{k,\text{ESLRP}})$ is the posterior probability density of K. The likelihood function can be expressed from the probability distribution of the model error π_ε

$$\pi(q_{k,\text{ESLRP}}|k) = \pi_\varepsilon(q_{k,\text{ESLRP}} - G(k)). \tag{8.17}$$

Since the likelihood and thus the posterior distribution cannot be analytically derived in a closed form, sampling techniques are commonly used to estimate it. Therefore, the Bayesian updating has been performed by means of a Markov Chain Monte Carlo (MCMC) algorithm. The algorithm of the MCMC consists of sampling from the posterior distribution with the help of a random walk, constructing a Markov chain that has the desired PDF as its equilibrium

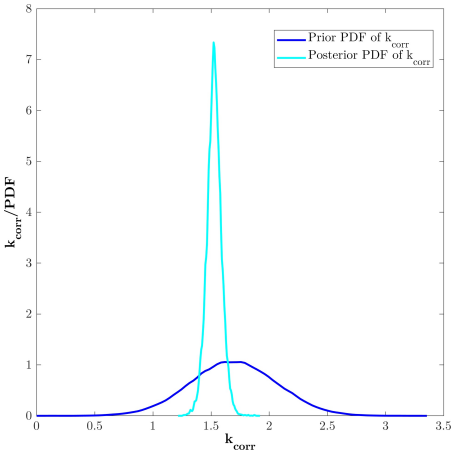

Figure 8.10: Bayesian updating of the correction factor PDF.

distribution [146, 140]. In Figure 8.10 the results of the Bayesian updating for k_{corr} are reported for a German weather station, Braunlage, while in Figure 8.11, they are reported in a Gumbel probability paper: the snow load maxima together with the fitted Gumbel Extreme Value distribution, in green for the ESLRP, in red for the snow load algorithm with the prior distribution for k_{corr} and in cyan with the posterior distribution.

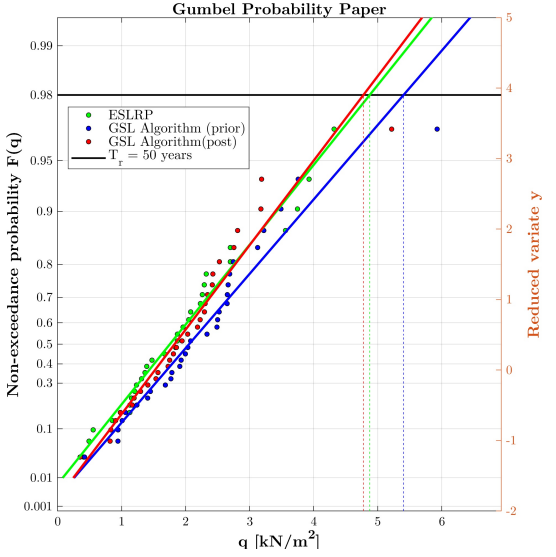

Figure 8.11: Comparison of extremes in the control period (Braunlage weather station).

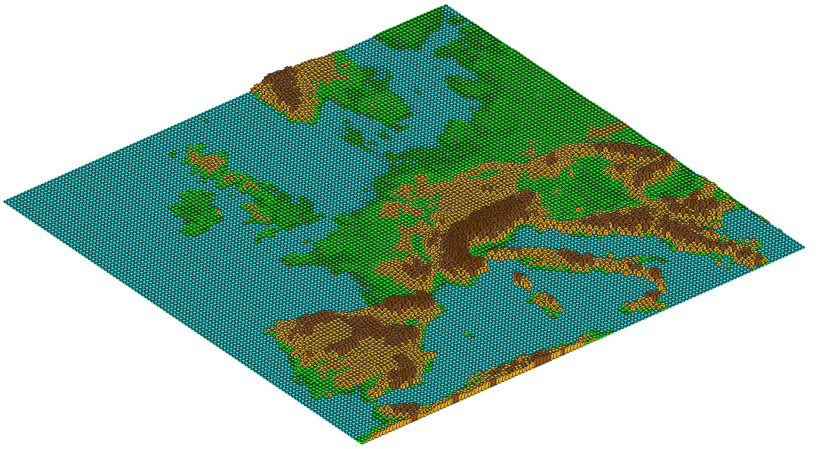

Figure 8.12: Illustration of the European topography at E-OBS redolution (25km x 25km grid).

8.3 Implementation on observed data series

Before arriving to the definition of future snow maps by applying the illustrated methodology to climate projections, a study of the actual trend of ground snow loads has been carried out on the basis of observed data series of daily temperatures and precipitation provided by the European Climate Assessment & Dataset project (E-OBS dataset) [57]. The E-OBS dataset is an European land-only daily high resolution gridded data set for mean, maximum and minimum surface temperature, precipitation and sea level pressure. It is based on observations collected at more than 10000 weather stations, and provides data on a regular grid that at the highest resolution reaches the 0.22°rotated grid (EUR22, about 25x25km as shown in Figure 8.12) which contains four cells of the EUR11 grid used by the EURO-CORDEX and illustrated in Figure 3.1b. The E-OBS dataset improves previous products with its spatial resolution and extent, time period, number of contributing stations [57] and it is commonly used as observational reference dataset for the evaluation of RCMs output at the European scale, as described in [84]. The dataset is continuously updated and in the latest version v.17.0, contains data from 11422 stations and spans the period from 1950-01-01 to 2017-12-31.

However, gridded data represent area averaged data, rather than point process data, and this has a large impact on the analysis of extremes especially for precipitation data, depending on the local orography. The analysis of gridded

precipitation data can lead to an underestimation of magnitudes of extremes compared with stations observations as illustrated in [57] for the E-OBS dataset. Mannshardt-Shamseldin et al. [101] confirm that return values computed from rain gauge data are typically higher than those computed from gridded data and develop regression relationships between the two sets of return values.

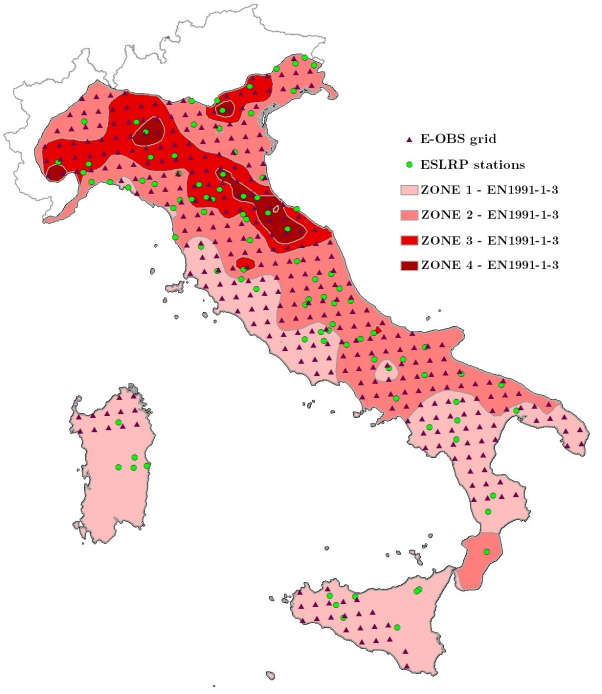

Zone EN1991-1-3	k_{corr}
1	2.63
2	1.42
3	1.96
4	1.69

Figure 8.13: E-OBS – Grid Cells and ESLRP weather stations for Italian Mediterranean region.

Therefore, first a calibration method for the analysis of gridded datasets, able to take into account the expected underestimation of extremes and the effects of local orography has been especially studied for Italy comparing the characteristic ground snow loads obtained by:

- the European Snow Load Research Project (ESLRP) for the 96 Italian weather stations in Mediterranean climatic region defined by the Annex C to EN1991-1-3 [14], period 1951-1990;

- the analysis of observed gridded data of daily temperatures and precipitation provided by the E-OBS dataset for the period 1951-1990, according to the predictive model illustrated in the previous paragraph 8.2.3 and assuming, consistently with the discussion in 8.2.4, a constant correction factor, k_{corr}, for each of the four climatic zones defined by EN1991-1-3 for the Mediterranean region. In this case, the correction factor for a given zone has been set equal to the mean value for the zone, according to the Table presented in Figure 8.13.

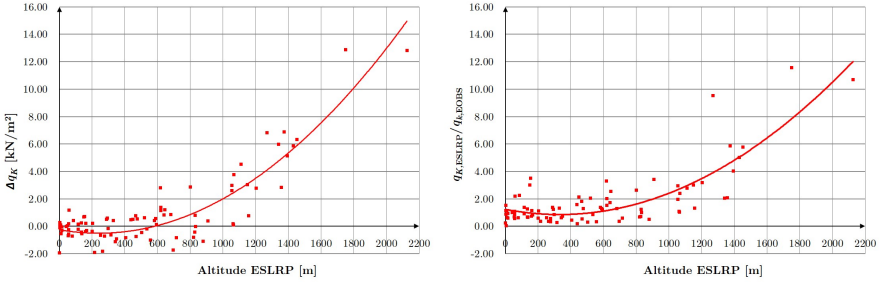

(a) Δq_k - Altitude

(b) $\frac{q_{k,\mathrm{ESLRP}}}{q_{k,\mathrm{EOBS}}}$ - Altitude

Figure 8.14: Comparison of $q_{k,\mathrm{ESLRP}}$ and $q_{k,\mathrm{EOBS}}$ for Italian Mediterranean Region.

In Figure 8.13, the locations of the investigated Italian weather stations (green points) are shown together with the E-OBS grid cell points and the zonation of the Italian Mediterranean region defined by the Annex C of EN1991-1-3:2003. The results of the comparison confirm that, for the study region, the characteristic values computed by the analysis of the gridded data (E-OBS dataset for the period 1951-1990) are typically lower than the values obtained by point-data (ESLRP for the same period) and the magnitude of the underestimation mainly depends on the local orographic. In fact, indicating with $q_{k,\mathrm{ESLRP}}$ the snow load estimated using ESLRP data and with $q_{k,\mathrm{EOBS}}$ the snow load estimated using E-OBS gridded data, the differences $\Delta q_k = q_{k,\mathrm{ESLRP}} - q_{k,\mathrm{EOBS}}$ and the ratios $\frac{q_{k,\mathrm{ESLRP}}}{q_{k,\mathrm{EOBS}}}$ clearly show an increase with the site altitude, as reported in Figure 8.14a and 8.14b respectively.
Subsequently, starting from these results, a calibration procedure has been defined in two steps:

- first, a regression analysis is carried out in order to derive an altitude relationship for $q_{k,\mathrm{EOBS}}$ data in each climatic zone (purple lines in Figure

8.15). A quadratic law as in ESLRP is assumed

$$q'_{k,\mathrm{EOBS}}(A) = [a + (\frac{A}{b})^2] \quad \text{in} \quad [\mathrm{kN/m^2}], \tag{8.18}$$

where A is the altitude of the site in [m] and a and b are two dimensionless coefficients determined via regression analysis;

- second, a correction rule is defined for each climatic zone as

$$q_{k,\mathrm{EOBS},corr}(A) = q'_{k,\mathrm{EOBS}}(A) + \Delta q_k(A) \quad \text{in} \quad [\mathrm{kN/m^2}], \tag{8.19}$$

where the functions $\Delta q_k(A)$ (red lines in Figure 8.15) are calculated as the difference between the altitude function for $q_{k,\mathrm{ESLRP}}$ data, defined in [126], and the altitude function $q'_{k,\mathrm{EOBS}}(A)$ defined by eq.8.18.

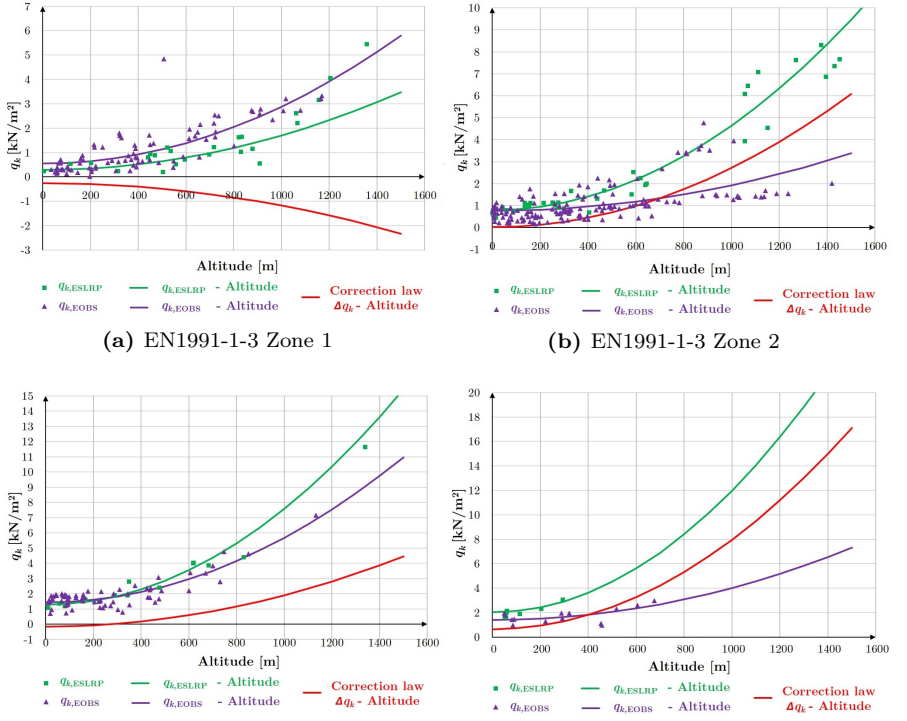

(a) EN1991-1-3 Zone 1

(b) EN1991-1-3 Zone 2

(c) EN1991-1-3 Zone 3

(d) EN1991-1-3 Zone 4

Figure 8.15: q_k - Altitude curves for Italian Mediterranean region.

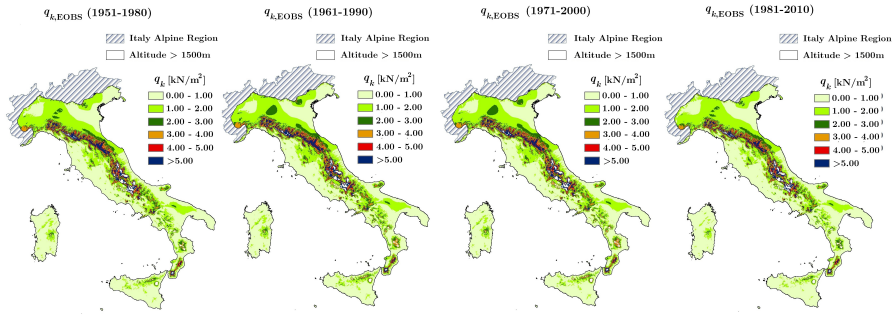

Figure 8.16: Ground snow load maps according different time windows of E-OBS data.

Once these relationships are available, it is possible to draw, according to the results obtained by the analysis of gridded data, the snow load map on the ground consistent with the current version of snow map present in the Annex C of EN1991-1-3, based on the results of ESLRP.
The outcomes of the elaboration of E-OBS gridded data ($q_{k,\mathrm{EOBS},corr}$) obtained according the methodology described in the previous section are presented in Figure 8.16. In particular, the characteristic ground snow loads are derived considering consecutive time windows of thirty years, shifted ten years by ten years (1951-1980, 1961-1990, 1971-2000 and 1981-2010).
Then, assuming as reference period 1951-1980 ($q_{k,rif}$), the actual trend of variation of characteristic ground snow loads and its dependence on the time period is estimated. For each subsequent time period analysed, the results are illustrated in Figure 8.17 in terms of differences ($q_{k,\mathrm{EOBS}} - q_{k,rif}$) and in Figure 8.18, in terms of percentage difference ($\frac{q_{k,\mathrm{EOBS}} - q_{k,rif}}{q_{k,rif}} \cdot 100$).

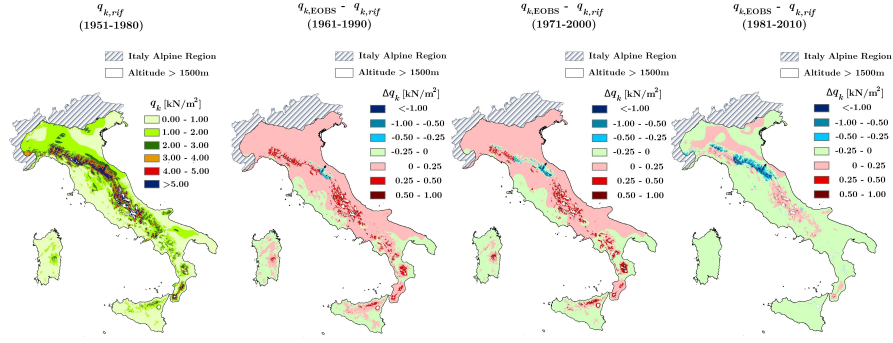

Figure 8.17: Trends of ground snow load obtained using different periods of E-OBS data, differences with respect to 1951-1980.

When examining these maps, it appears clearly that trends are different depending on the region. However in some northern and eastern Italian regions a constant or increasing trend is obtained, while in western and southern Italian regions they generally tend to decrease.

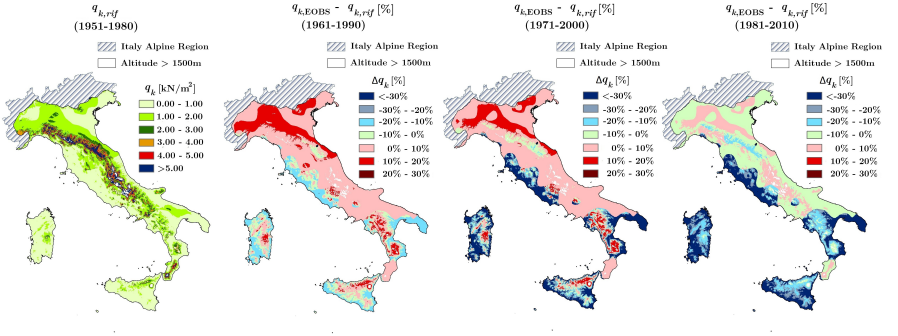

Figure 8.18: Trends of ground snow load obtained using different periods of E-OBS data, percentage differences with respect to 1951-1980.

8.4 Implementation on climate projections

8.4.1 Trends at selected weather stations

The estimation of future trends of ground snow loads at specific weather stations can be carried out starting from the analysis of climate projections provided by high resolution regional climate models as those presented in Table 7.1. In particular, the following procedure is followed:

- first, in order to take into account the main sources of uncertainty in climate projections, data are collected for an ensemble of different climate models considering different climate change scenarios. New weather series are also derived by means of the weather generator illustrated in the previous section 7;
- second, each generated series of daily maximum and minimum temperatures (T_{Max} and T_{Min}), and precipitation (p_r) are analysed according to the algorithm presented in paragraph 8.2.3 to simulate the snow load formation process and estimate yearly maxima ground snow loads;

- third, for each series of yearly maxima ground snow loads an extreme value analysis is performed according to the block maxima approach and considering subsequent time windows of forty year-long shifted by ten years (1956-1995, 1966-2005,...,2056-2095). In particular, an extreme value Type I distribution, with CDF given in Equation 2.2, is assumed and fitted according the least square method (LSM) as in [126]. The two distribution's parameters, $\mu(t)$ and $\sigma(t)$, are thus estimated for each time window t, and by means of the Equation 2.6 with $p = 0.02$ characteristic values are calculated ($q_k(t)$);
- factors of change, $FC_{q_k}(t)$, are evaluated comparing the characteristic value of ground snow load at the time window t with the corresponding value at the first time window ($t = 1$)

$$FC_{q_k}(t) = \frac{q_{k,CM}(t)}{q_{k,CM}(t=1)}; \tag{8.20}$$

- finally, for a given time window t the characteristic ground snow load $q_k(t)$ is derived by multiplying the characteristic value obtained by observed data ($q_{k,\mathrm{ESLRP}}$)[126] in the first time window (t=1) with the corresponding factor of change

$$q_k(t) = FC_{q_k}(t) \cdot q_{k,\mathrm{ESLRP}}. \tag{8.21}$$

As an example, in Figure 8.19 trends are shown for a German weather station, Braunlage, where long time series of observations are also available, according to different scenarios (RCP4.5 and RCP8.5). In this way, the trend estimated from the analysis of climate projections for the first three time windows (1956-1995, 1966-2005 and 1976-2005) can be compared with the trend derived from the real trend derived from the analysis of observed data series.
Trends are thus shown for the different climate models (solid lines) together with the corresponding prediction intervals (25%-75%). The mean ensemble result (in green) show a decreasing trend for characteristic ground snow loads at the investigated station, well reproducing the observed trend for the first three time windows (black dashed lines).

Similar results are obtained for other weather stations (in Figure 8.20 the results for Braunschweig weather station are shown).

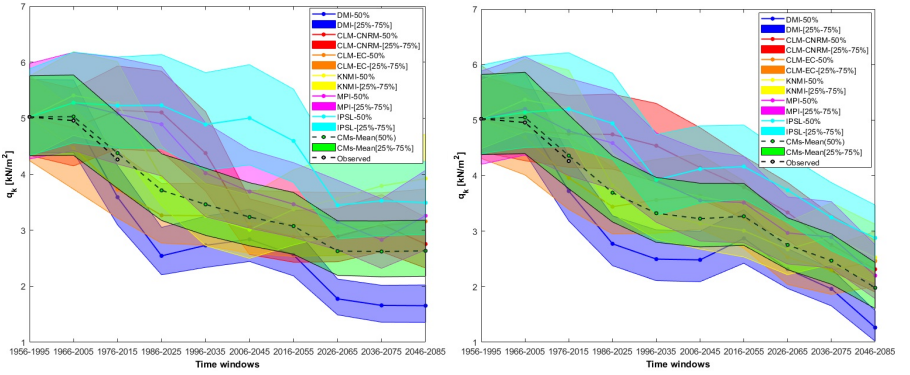

(a) historical-RCP4.5 **(b)** historical-RCP8.5

Figure 8.19: Observed and future trends for q_k according different RCMs - Braunlage weather stations.

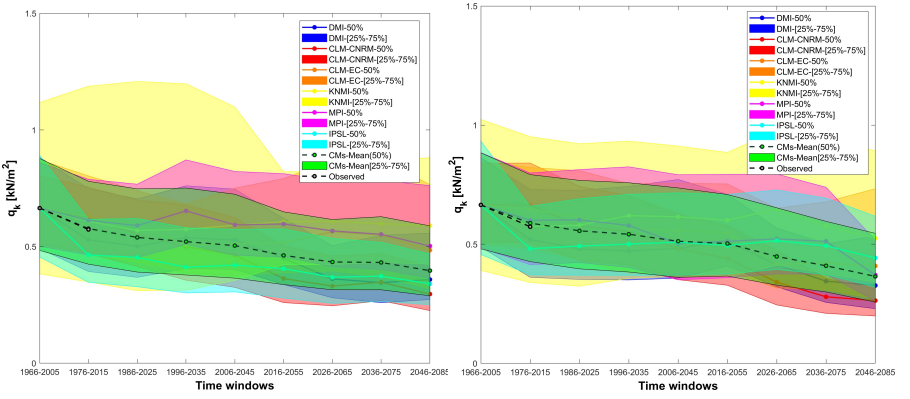

(a) historical-RCP4.5 **(b)** historical-RCP8.5

Figure 8.20: Observed and future trends for q_k according different RCMs - Braunschweig weather stations.

8.4.2 Factors of change maps

In order to provide guidance for potential amendments of the current snow load maps in technical standards, factor of change maps are drawn following the procedure presented in the previous section 7 for temperature and precipitations. In particular, bivariate color maps are chosen to better represent results,

considering the 25% percentile and 75% percentile as reference percentiles for the prediction interval.

8.4.2.1 Italian Mediterranean Region

In Figure 8.21 and 8.22, factor of change maps for characteristic ground snow load (q_k) are presented in three time windows (1991-2030, 2011-2050, and 2031-2080) for the same study region and dataset presented in paragraph 7.3.1, according to the RCP4.5 and RCP8.5 scenario respectively. In the same Figures, on the top row left, the current snow load map for the study region, obtained implementing the load-altitude relationship in the Annex C of EN1991-1-3 [14]

$$q_k = (0.498Z - 0.209)[1 + (\frac{A}{452})^2] \quad \text{where} \quad Z \quad \text{is the zone number} \quad (8.22)$$

is also reported to directly compare the snow load map at which change factors should be applied.
The outcomes show a general decreasing trend for the study region even if trends can be different depending on the areas and on the investigated time windows and scenario. In the near term future (1991-2030) a constant or increasing trend (FC_{50}>0.95) is expected in around 15% of the region (RCP4.5) and 7% (RCP8.5). However, a decrease is expected in the long-term future (2041-2080) for the whole region.

Time window	RCP4.5			RCP8.5		
	25%	**50%**	75%	25%	**50%**	75%
1961-2000	0.91	**0.98**	1.03	0.91	**0.98**	1.03
1971-2010	0.85	**0.95**	1.04	0.84	**0.94**	1.04
1981-2020	0.80	**0.92**	1.04	0.78	**0.90**	1.02
1991-2030	0.76	**0.88**	1.01	0.72	**0.84**	0.99
2001-2040	0.73	**0.85**	0.98	0.69	**0.81**	0.95
2011-2050	0.69	**0.82**	0.95	0.67	**0.78**	0.91
2021-2060	0.67	**0.79**	0.92	0.65	**0.76**	0.88
2031-2070	0.64	**0.76**	0.89	0.61	**0.72**	0.85
2041-2080	0.62	**0.73**	0.85	0.56	**0.68**	0.80

Table 8.3: Mean of Factors of Change percentiles for characteristic ground snow load q_k in the study region.

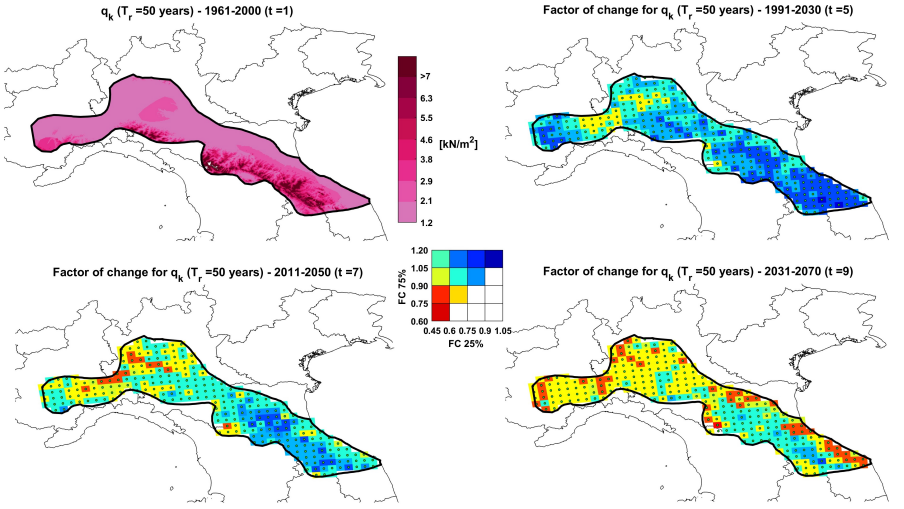

Figure 8.21: Factors of Change for q_k – Confidence interval [25-75%] Map (Scenario RCP4.5).

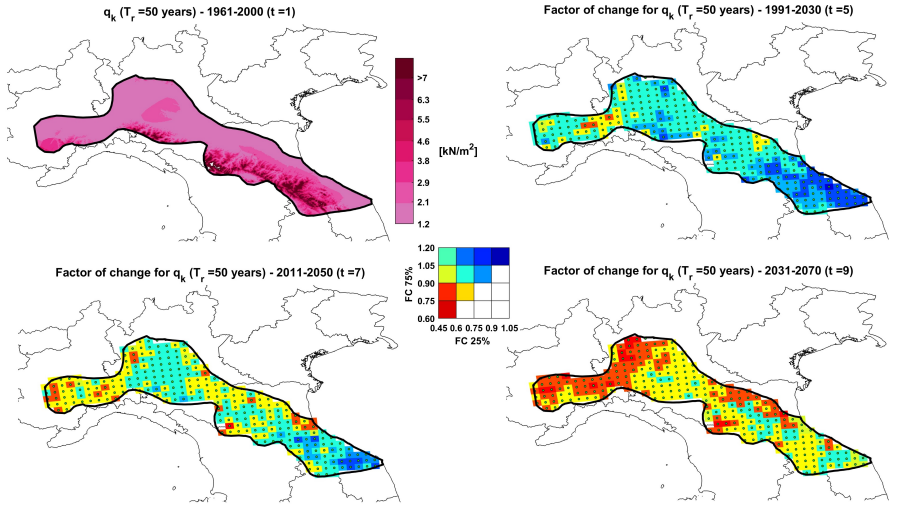

Figure 8.22: Factors of Change for q_k – Confidence interval [25-75%] Map (Scenario RCP8.5).

As it was done in the previous section 7 for precipitation, the results are averaged over all grid cells to better visualize changes in ground snow load, reducing the influence of unforced variability at grid box level.
The resulting mean factors of change for the region obtained according the investigated time windows and percentiles are reported in Table 8.3 and shown in Figure 8.23.
The results confirm a general decrease of ground snow loads in the study region, around 10% to 15% in the mid term future (1991-2030) and 25% to 30% in the long term future (2041-2080).

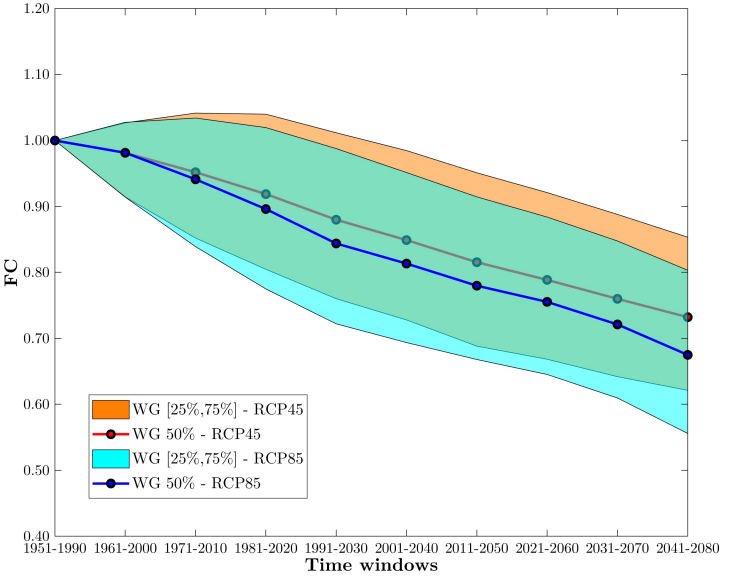

Figure 8.23: Factors of Change mean trends for q_k in the study region.

8.4.2.2 German Central East Region

The analysis can be extended to other European climatic region. As an example in Figure 8.24 and 8.25, the results obatained in terms of factors of change (FCs) maps for characteristic ground snow load (q_k) are presented for the zone 4 of the central East region defined in in the Annex C of EN1991-1-3 [14] and located in the Northern East Germany (Figure 5.3).
These Figures show FCs in three time windows (1991-2030, 2011-2050, and 2031-2080) derived according to the RCP4.5 and RCP8.5 scenario respectively together with the current snow load map (on the top row left) obtained

implementing the load-altitude relationship in the Annex C of EN1991-1-3 [14]

$$q_k = (0.264Z - 0.002)[1 + (\frac{A}{256})^2] \quad \text{where} \quad Z \quad \text{is the zone number,} \quad (8.23)$$

to directly compare the snow load map at which change factors should be applied.

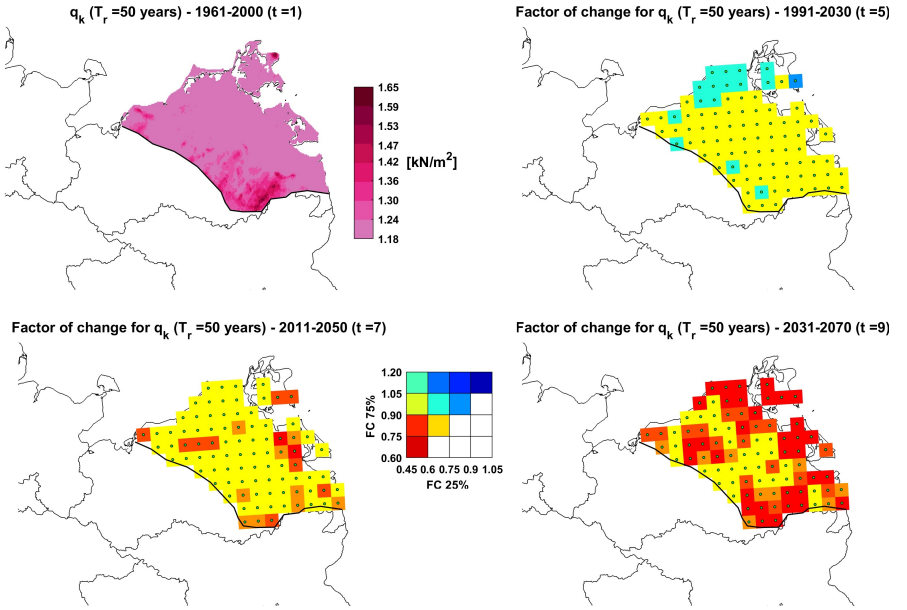

Figure 8.24: Factors of Change for q_k – Confidence interval [25-75%] Map (Scenario RCP4.5).

The outcomes show a general decreasing trend for the study region even if the magnitudes can be different depending on the areas and on the investigated time windows and scenario.

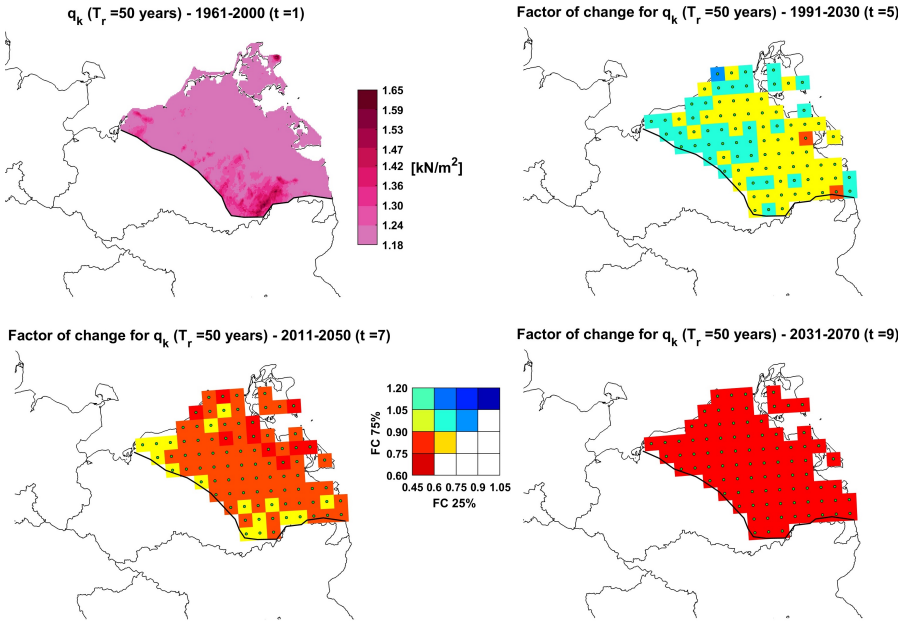

Figure 8.25: Factors of Change for q_k – Confidence interval [25-75%] Map (Scenario RCP8.5).

Chapter 9

A stochastic downscaling technique for the local assessment of future trends of snow loads

In this chapter, a stochastic technique for bias correction and downscaling of climate projections is presented. An application of the method for the local assessment of future trends of ground snow loads is also discussed in comparison with the factor of change approach.

Contents

9.1 Introduction

As presented in paragraph 3.4 different calibration methods have been used in climate change studies to obtain reliable projections of weather variables from climate models, but they can be essentially divided in two calibration pathways: the factor of change approach, and the bias correction methods [58].
The factor of change approach has a long history in climate research and its application supplemented by an *ad hoc* weather generator has been illustrated in the previous sections of this work to estimate future trends in extreme temperatures, precipitation and ground snow loads considering the uncertainty in the prediction.
Classical bias correction techniques, such as quantile mapping, employs a quantile-based transformation of distributions, defining a transfer function to adjust the CDF of model simulations. Then, bias correction methods deterministically postprocess the marginal distribution of the raw climate projections and when they are used to downscale climate projections at the local scale of station data, inflation problems occurs [102]. The problems arise from the attempt to explain local variability by gridbox variability and may have severe consequences such as the derivation of inflated variability and trends as discussed in [102] and [103]. Therefore, the need for stochastic bias correction procedures is then demonstrated in [102] and a possible solution is to use a randomized downscaling specification as already suggested by Von Storch in [152].
In this section, a stochastic procedure, suitable for a probabilistic assessment of future trends in climatic actions, is proposed, aiming to combine the advantages of Regional Climate Model simulations and weather generators [28].
The key idea is to generate downscaled series by adding to the Regional Climate Model outputs an error random term derived comparing observations y_i^p and model simulations x_i^p for current and past climate.

9.2 Methodology

First, climate data are collected in terms of daily climate projections from high resolution RCMs and observations. In particular, daily maximum and minimum

temperatures (T_{Max}, T_{Min}) and precipitation (p_r) have been investigated considering data provided by:

- an ensemble of RCMs developed by the EURO-CORDEX initiative and already described in Table 7.1, for the control period 1951-2005 (*Historical Experiment*) where climate models are forced to run according observed atmospheric composition changes, and for the future period 2006-2100 (*RCPs Experiment*) considering a medium emission scenario (RCP4.5) and the highest emission scenario (RCP8.5);
- observed data series given in the database of the Italian Meteorological Institutes for some relevant weather stations. Results for Bologna weather station will be presented and discussed in the following.

9.2.1 Definition of monthly PDFs for the climate model error

Recorded daily series of maximum and minimum air temperature and precipitation are collected for the investigated weather stations (WS) and compared with the climate model simulations (CM) provided for the considered historical period 1951-1990 in the corresponding grid cell. The monthly error PDFs are then defined according the following steps:

- firstly, observed data (WS) and climate model outputs (CM), are collected for each month m in the control period, and then ordered for each year j belonging to the investigated period;
- subsequently, daily errors are computed as differences between the ordered observed values and the ordered climate model outputs:

$$\varepsilon_{T_{\text{Max}},m} = T_{\text{Max,WS},m} - T_{\text{Max,CM},m} \tag{9.1}$$

$$\varepsilon_{T_{\text{Min}},m} = T_{\text{Min,WS},m} - T_{\text{Min,CM},m} \tag{9.2}$$

$$\varepsilon_{p_{r,m}} = p_{r,\text{WS},m} - p_{r,\text{CM},m} \tag{9.3}$$

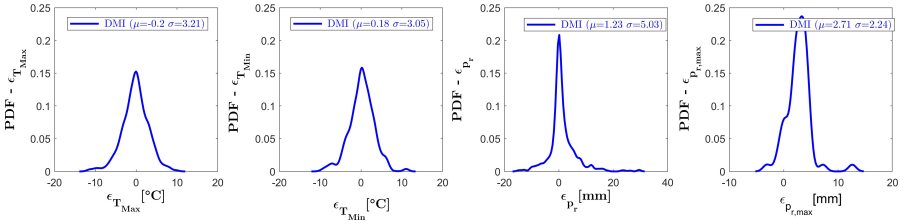

Figure 9.1: Monthly error PDFs for daily maximum and minimum temperature and precipitation (February– Model 1).

- finally, errors computed at the previous step are grouped for each month m and an empirical cumulative density function is constructed;
- the previous steps are repeated for precipitation monthly maxima defining a different CDF for the climate model error in precipitation maxima.

As an example, in Figure 9.1 empirical PDFs for daily temperatures (T_{Max}, T_{Min}), precipitation and precipitation maxima (p_r, $p_{r,\text{max}}$) are presented for February and Model 1. Similar functions are obtained for other months and climate models.

9.2.2 Generation of weather data series

Climate data series are generated by adding an error term sampled from the empirical distribution functions previously defined to the climate model output for day i month m and year j. Then, for temperatures, we have:

$$T_{\text{Max,WG}}(i/m/j) = T_{\text{Max,CM}}(i/m/j) + \varepsilon_{T_{\text{Max}},m} \tag{9.4}$$

$$T_{\text{Min,WG}}(i/m/j) = T_{\text{Min,CM}}(i/m/j) + \varepsilon_{T_{\text{Min}},m} \tag{9.5}$$

while for precipitation a different sampling is implemented for common days

$$p_{r,\text{WG}}(i/m/j) = p_{r,\text{CM}}(i/m/j) + \varepsilon_{p_r,m} \tag{9.6}$$

and monthly maxima of climate models

$$p_{r,\mathrm{WG}}(i/m/j) = p_{r,\mathrm{CM}}(i/m/j) + \varepsilon_{p_{r,\max},m} \tag{9.7}$$

The random sampling from error functions is implemented with some physical constraints to avoid generation of unrealistic weather data series. In particular for maximum and minimum air temperatures, the following constraints are defined starting from the analysis of observed data series:

$$|T_{\mathrm{Max,WG}}(i/m/j) - T_{\mathrm{Min,WG}}(i/m/j)| \leq 15^{\circ} \tag{9.8}$$

$$|T_{\mathrm{Max,WG}}(i/m/j) - T_{\mathrm{Max,WG}}(i-1/m/j)| \leq 10^{\circ} \tag{9.9}$$

$$|T_{\mathrm{Min,WG}}(i/m/j) - T_{\mathrm{Min,WG}}(i-1/m/j)| \leq 10^{\circ} \tag{9.10}$$

9.2.3 Estimation of ground snow load maxima

The generated weather data series of daily maximum and minimum temperature (T_{Max}, T_{Min}) and precipitation (p_r) can be used as input data to estimate ground snow loads according the algorithm presented in paragraph 8.2.3. Implementing the algorithm for the period 1951-1990, annual maxima are obtained and assuming an extreme value Type I distribution for maxima as in [126], the characteristic value of the load q_k (50 year return period) can be evaluated, according the eq. 8.11.
In Figure 9.2, the resulting CDFs for maxima obtained from the analysis of raw climate projections (dashed lines in Figure 9.2a) and 50th percentile of the generated series (solid lines in Figure 9.2b) are compared with the observed CDF derived from the ESLRP at Bologna weather station (green solid line). It appears clearly from the comparison that the generated series are able to reproduce the observed CDF for maxima, minimizing the significant errors resulting from the analysis of raw climate projections.

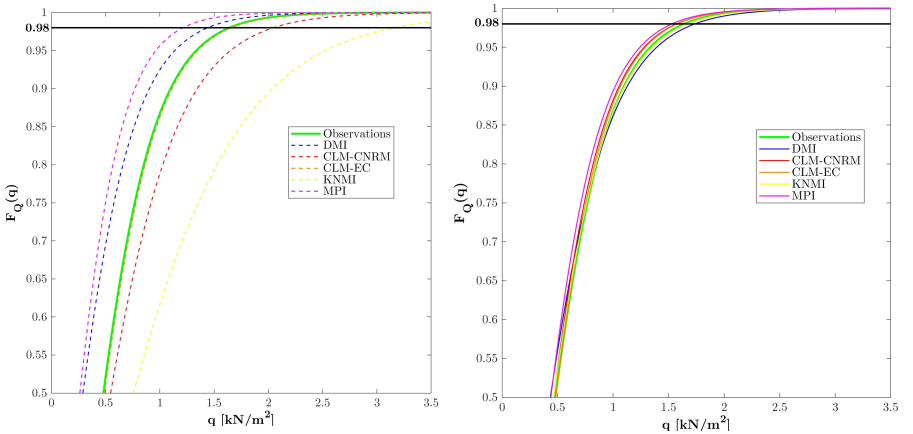

(a) Raw climate projections

(b) Generated series 50th percentile

Figure 9.2: CDFs for annual maximum ground snow load at Bologna weather station.

9.3 Assessment of future trend of ground snow loads

Extending the analysis to the future period, annual maxima ground snow loads can be estimated for the whole period 1951-2100, starting from the generated series of daily temperatures and precipitation. To evaluate variations of climatic actions over time, snow load maxima are then analysed in moving time windows suitable for structural design, as discussed in section 2 for non stationary extremes under climate change.

In particular, the maxima data series are divided in appropriate time windows, each one forty year-long and shifted by ten years (1951-1990, 1961-2000,. . . ,2051-2090) from the adjacent ones. For each time window an extreme value analysis is carried out according to the block maxima approach and assuming an extreme value Type I distribution. The results are summarized in Figure 9.3 in terms of prediction interval (25%-75%) for q_k, for the investigated climate models in the moving time windows, according the two different considered emissions scenarios (RCP4.5 and RCP8.5).

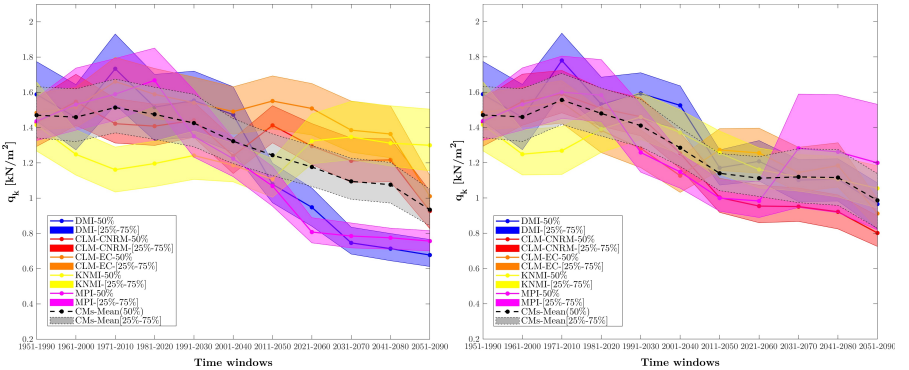

(a) historical-RCP4.5 **(b)** historical-RCP8.5

Figure 9.3: Uncertainty assessment of future trends in characteristic ground snow loads at Bologna for different climate models (25%-75% prediction interval).

9.4 Comparison with the factor of change approach

The proposed probabilistic correction technique has been finally compared with the factor of change approach in order to verify the preservation of the climate change trends simulated by the models. First, factors of change ($FC(t)$) are calculated as ratio between the characteristic values at each time window, $q_{k,\mathrm{CM}}(t)$, and the corresponding one at the first time window, $q_{k,\mathrm{CM}}(t=1)$, obtained from the analysis of raw climate projections. Then, for a given time window t the characteristic ground snow load $q_k(t)$ is derived by multiplying the characteristic value obtained by observations ($q_{k,\mathrm{ESLRP}}$)[126] the first time window (t=1) with the corresponding factor of change

$$q_k(t) = FC(t) \cdot q_{k,\mathrm{ESLRP}} \tag{9.11}$$

In Figure 9.4, the variation over time derived from the factor of change approach supplemented by the *ad hoc* weather generator, presented in the previous sections, and from the proposed stochastic technique are compared for the two investigated RCPs. In particular, the results obtained for different climate models have been combined assuming equal weights, so considering that each individual component of the ensemble is an equally likely representation of future climate. Then, mean trends (50%) as well as prediction interval

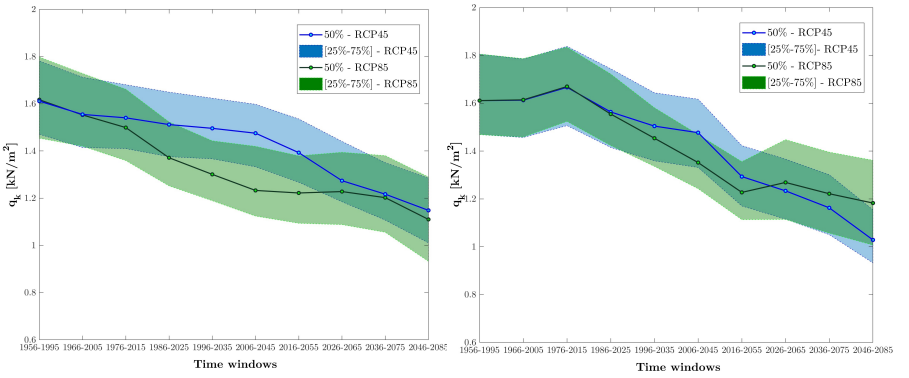

(a) Factor of change approach and weather generator

(b) Stochastic downscaling

Figure 9.4: Comparison of ensemble prediction interval of future trends in characteristic ground snow loads at Bologna weather station.

(25%-75%) are plotted for the RCP4.5 (in blue) and for the RCP8.5 (in green), according to the two different methodologies in Figure 9.4a and 9.4b.

The comparison shows that similar trends and prediction intervals are obtained demonstrating that the proposed technique not only preserves the climate change signal simulated by the uncorrected climate model ensemble derived according the factor of change approach, but also allows to estimate prediction intervals for the climatic action trends. This result combined with the capability of the methodology to reproduce recorded past climate extremes, highlights its suitability for probabilistic assessment of impacts of climate change on climatic actions.

Chapter 10

Bayesian approach for snow map refinement

In this chapter, a technique for snow load map refinement is proposed. Ground snow loads derived starting from gridded climate data as those provided by climate models, are combined with observed point measurements and then suitably updated following the Bayesian approach.

Contents

10.1 Introduction

The analysis of gridded climate data like those provided by climate models may lead to an underestimation of extremes especially for precipitation [101] as it has been shown in paragraph 8.3 for the E-OBS dataset [57]. Hence, the necessity to set-up a proper methodology to adjust area averaged data on the basis of point measurements. In this chapter, a technique for snow load map identification by refining the snow load map derived from the analysis of gridded climate data will be illustrated.

10.2 Methodology

The key idea of the proposed methodology is to combine the prior estimates provided by the gridded climate data with the point observations in a Bayesian framework [31].
Then, for its application on ground snow loads, it is based on the definition of a prior random field of characteristic ground snow loads. The load is defined on the sea level of a homogeneous climatic region. The prior distribution of the random filed is derived from the analysis of gridded climate data and the subsequent update is carried out with available point measurements. Definition of the a priori random field and its refinement can be briefly summarized in the four steps as follows:

- analysis of gridded data of daily maximum and minimum air temperatures and precipitation as those provided by the E-OBS gridded dataset [57] for the period 1951-1990 and evaluation, using the algorithm defined in paragraph 8.2.3, of annual maxima of ground snow loads;
- estimation of characteristic values of ground snow load at the sea level for each point of the E-OBS grid from the results of the analysis;
- definition of a prior random field for the characteristic ground snow loads at sea level of the given climatic region;
- Bayesian updating of the prior random field with the characteristic ground snow loads obtained from point measurements of snow load at the weather stations as those collected during the European Snow Load Research Project (ESLRP)[126].

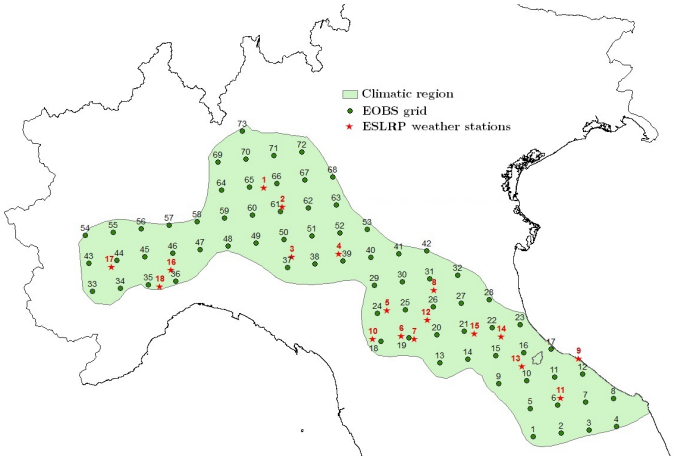

Figure 10.1: E-OBS grid points and ESLRP weather stations in Zone 3-4 of the Mediterranean climatic region defined by EN1991-1-3.

In the following paragraphs, the four phases will be fully described, using as reference the results obtained for the same study region presented in paragraph 7.3.1 (Zones 3-4 of the Mediterranean climatic region, as defined by the EN1991-1-3) and illustrated again in Figure 10.1, where the 73 E-OBS grid cell points and 18 ESLRP weather stations are specified as well.

10.2.1 Analysis of gridded climate data

As mentioned before, the a priori random field for ground snow loads is derived analysing the gridded data provided by the E-OBS dataset [57] for the period 1951-1990, using the algorithm presented in paragraph 8.2.3, which allows to estimate for each grid point a set of N=40 annual maxima of snow loads, through a suitable Monte Carlo simulation. Of course, once obtained the above mentioned set of yearly simulated maxima for a given grid point, the characteristic value of the ground snow load q_k is derived, via extreme value analysis, according the definition given in EN1990 [13], as the value having a probability of 2% to be exceeded in one year, i.e. the value characterized by a return period of around 50 year (eq.8.11).
Since the part of the grid considered in the present study belongs to the Mediterranean region, where q_k depends on the site altitude, the characteristic values of ground snow loads are subsequently reported at the sea level through

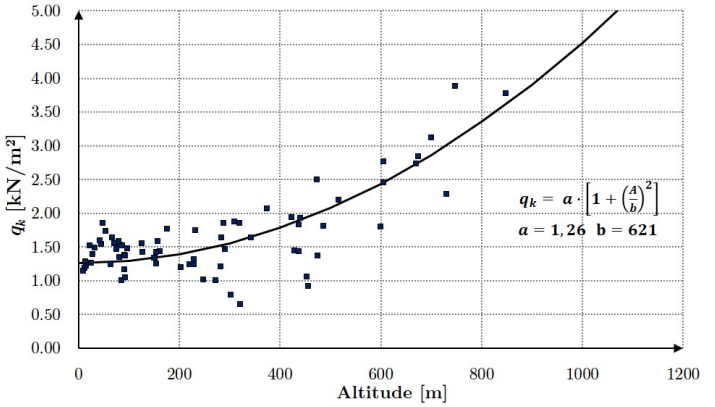

Figure 10.2: Characteristic Ground snow load - Altitude relationship (Mediterranean Region - Zones 3-4).

a suitable altitude relationship. In the present study, the relationship proposed in EN1991-1-3[14] has been adopted:

$$q_k(A) = a[1 + (\frac{A}{b})^2] \quad \text{in} \quad [\text{kN/m}^2] \tag{10.1}$$

where A is the altitude of the site in [m] and a and b are the dimensionless coefficients determined via regression analysis. In Figure 10.2 it is shown the outcome of the regression analysis for Zones 3 and 4 of the Mediterranean region used for actual snow load maps.

10.2.2 Definition of the prior random field

10.2.2.1 Introduction

For each climatic region, a homogeneous random field is defined for the characteristic ground snow load as the transformation of a Gaussian random field

$$Q(x, \omega) = \Psi(q(x, \omega)) \quad x \in D, \quad \omega \in \Omega \tag{10.2}$$

in which

D is the spatial domain;

x is the spatial variable;

Ω is the space of possible outcome;

ω is the actual realization;

q is a Gaussian random field;

Q is the random field of characteristic ground snow loads.

Ψ is the transformation map from Gaussian field into the distribution of the characteristic ground snow load field calculated as

$$\Psi = F_Q^{-1}(\Phi_q(q)), \tag{10.3}$$

where F_Q^{-1} is the inverse CDF of the distribution of Q and Φ_q is the CDF of the Gaussian distribution of q. Herein we supposed log-normal distribution for Q so $\Psi(q) = \exp(q)$ but the proposed procedure can also be implemented assuming different types of distribution for Q.

Assuming second order stationarity of the field, a fully description is obtained by the first two moments [89]:

$$\mu_Q(x) = \mathrm{E}[Q(x, \omega)] \tag{10.4}$$

$$Cov_Q(x_1, x_2) = \mathrm{E}[(Q(x_1, \omega) - \mathrm{E}[Q(x_1, \omega)])(Q(x_2, \omega) - \mathrm{E}[Q(x_2, \omega)])] \tag{10.5}$$

mean and covariance of the marginal distributions of the spatially fixed random variables $Q(\omega)$.

The spatial dependency between two points x_1 and x_2 is then only described by the covariance $Cov_Q(x_1, x_2)$ or by the semi-variogram $\gamma_Q(x_1, x_2)$

$$\gamma_Q(x_1, x_2) = \frac{1}{2}\mathrm{Var}[Q(x_1, \omega) - Q(x_2, \omega)] \tag{10.6}$$

and it can be assumed to be a function of the distance h between the two points. In order to calculate the covariance function, the experimental semi-variogram $\gamma_Q(h)$ is evaluated as

$$\gamma_Q(h) = \frac{1}{2n(h)} \sum_{i=1}^{n(h)} (Q(x_i) - Q(x_i + h))^2 \tag{10.7}$$

where $n(h)$ is the number of pairs of points whose distance is h. A set of lags h_i separated by the lag distance d is then defined and all pairs of samples whose distance falls in the range $h_i \pm d$ are used to estimate the average semi-variance $\gamma_Q(h_i)$ at the average lag h_i. The lag distance d is assumed equal to the grid spacing as suggested in [68], and the distance of reliability for the experimental semi-variogram is $h_{\max}/2$, where $h_{\max}$ is the maximum distance in the region considered in the analysis [74]. Once estimated the experimental semi-variogram, a theoretical model is fitted

$$\gamma_Q(h) = c(1 - e^{\frac{-h}{a}}) \tag{10.8}$$

where c is the sill and a is the range of the variogram, and the covariance function is defined [24] as

$$Cov_Q(h) = c - \gamma_Q(h) \tag{10.9}$$

The semi-variogram and the covariance function of Q so derived for the study region, illustrated in Figure 10.1, are reported in Figure 10.3.

10.2.2.2 Representation of the random field

According to [89] the random field $q(x, \omega)$ can be separated into a deterministic part, the mean $\mu_q(x)$, and in a decomposed fluctuating random part

$$q(x, \omega) = \mu_q(x) + \sum_{i=1}^{N} \sqrt{\lambda_i} \psi_i(x) X_i(\omega). \tag{10.10}$$

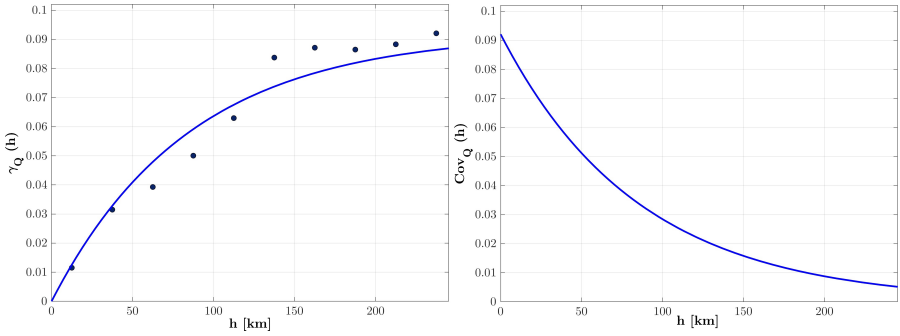

(a) Semi-variogram $\gamma_Q(h)$ **(b)** Covariance function $Cov_Q(h)$

Figure 10.3: Semi-variogram and covariance function of Q (Mediterranean Region - Zones 3-4).

The fluctuating part is decomposed using the Karhunen-Loeve (KL) expansion [75] [93], which allows a separation of the stochastic and spatial terms. The spatial function $\psi_i(x)$ are the orthogonal eigenfunctions and λ_i are the corresponding eigenvalues of the following eigenproblem

$$\int_{-\infty}^{\infty} Cov_q(x_1, x_2)\psi_i(x_1)dx_1 = \lambda_i\psi_i(x_2) \tag{10.11}$$

and the stochastic terms $X_i(\omega)$ are mutually uncorrelated random variables satisfying

$$\mathrm{E}[X_i(\omega)] = 0, \quad \mathrm{E}[X_i, X_j] = \delta_{ij}. \tag{10.12}$$

As the variance of each term in the KL expansion in 10.11 is λ_i, the total variance will be $\sigma_t^2 = \sum_{i=1}^{N} \lambda_i$ and the expansion can be truncated after M terms, provided that the residual variance $\sigma_r^2 = \sum_{i>M} \lambda_i$ is sufficiently small. The random field is then approximated by the following expression

$$q(x, \omega) \approx \mu_q(x) + \sigma_c \sum_{i=1}^{M} \sqrt{\lambda_i}\psi_i(x)X_i(\omega), \tag{10.13}$$

where the correction factor σ_c is estimated as $\sigma_c = \sqrt{\frac{\sigma_t^2}{\sigma_t^2 - \sigma_r^2}}$, in order to obtain a suitable estimate of effective total variance for the approximate field [123].

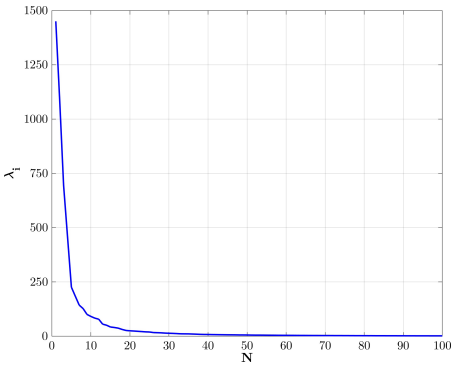

Figure 10.4: Decay of eigenvalues λ_i (Mediterranean Region - Zones 3-4).

To decide the number of terms of the series to be considered, reference could be made to the decay rate of the eigenvalues λ_i depending on i [158]. For example, the decay rate of eigenvalues λ_i for the snow load q obtained for the study region is reported in Figure 10.4. According to the graph, the expansion has been truncated at $M = 30$.

The eigenfunctions ψ_i can be discretized by projection into some V subspace spanned by the spatial basis functions $[\Phi_j]_{(j=1)}^{N}$

$$\psi_i(x) \approx \sum_{j=1}^{N} v_{ij}\Phi_j(x). \tag{10.14}$$

In this way, the eigenproblem in eq.10.12 can be solved using the Galerkin method by requiring the residual to be orthogonal to the approximating subspace, V

$$< \Phi_j, \int_{-\infty}^{\infty} Cov_q(x_1, x_2)\psi_i(x_1)dx_1 - \lambda_i\psi_i(x_2) >= 0. \tag{10.15}$$

Defining $C_{q,(\alpha,\beta)} = \int_{-\infty}^{\infty}\int_{-\infty}^{\infty} Cov_q(x_1, x_2)\Phi_\alpha\Phi_\alpha dx_1 dx_2$ and adopting the hat functions for the spatial basis functions $\Phi_i(x_j) = \delta_{ij}$, we arrive to the following generalized eigenvalue-eigenvector problem

$$GC_qGv_i = \lambda_i Gv_i, \tag{10.16}$$

in which G is the Gramian matrix defined as

$$G_{ij} = \int_{-\infty}^{\infty} \Phi_i(x)\Phi_j(x)dx \tag{10.17}$$

and C_q is the covariance matrix of the underlying Gaussian random field, which is calculated from the previously defined covariance matrix C_Q. Assuming a log-normal distribution for the random field, C_q is obtained applying the following transformation

$$C_q(x_i, x_j) = \ln(1 + \frac{C_Q(x_i, x_j)}{\mu_Q(x_i)\mu_Q(x_j)}); \tag{10.18}$$

while for different distribution it can be calculated using the NORTA method [11].
Finally, the mean $\mu_q(x)$ of the underlying Gaussian random field is calculated, as the covariance matrix, by the transformation of the mean vector $\mu_Q(x)$ of the log-normal random field

$$\mu_q(x_i) = \ln(\frac{\mu_Q(x_i)^2}{\sqrt{\mu_Q(x_i)^2 C_Q(x_i)}}); \tag{10.19}$$

where $\mu_Q(x)$ contains the characteristic ground snow loads at sea level for each point of the mesh k defined for the investigated area. They have been obtained using kriging as spatial interpolation technique, starting from the values at the grid points i and the semi-variogram γ_Q previously defined

$$\mathrm{E}[Q(x_k, \omega)] \approx \sum_{i=1}^{n} k_i \mathrm{E}[Q(x_i)] \tag{10.20}$$

The optimal solution for the coefficients k_i is found by using the Lagrange multiplier λ and then solving the system of $n + 1$ equation[85]

$$\begin{cases} \sum_{i=1}^{n} k_i \gamma_Q(h_{ij}) + \lambda = \gamma_Q(h_{ij}), \quad i = 1, 2.., n, \\ \sum_{i=1}^{n} k_i = 1 \end{cases} \tag{10.21}$$

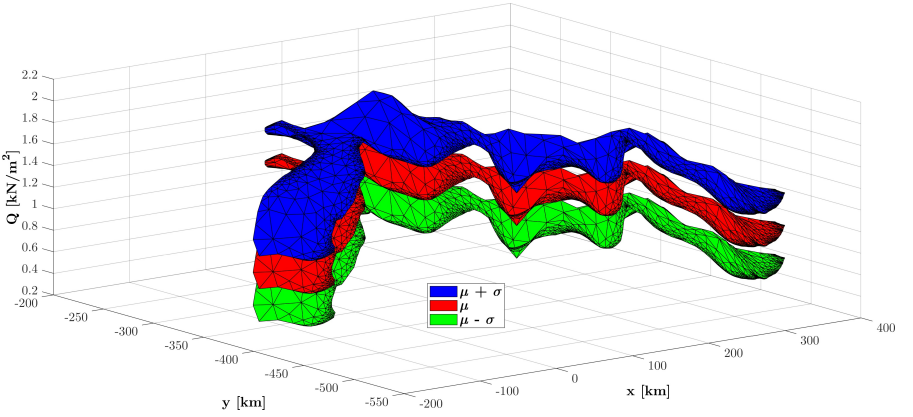

Figure 10.5: Prior random field (Mediterranean Region - Zones 3-4).

In Figure 10.5, it is reported in red the mean of the prior random field μ_Q obtained for the investigated region, as well as the $\mu_Q + \sigma_Q$ and the $\mu_Q - \sigma_Q$ values, in blue and in green, respectively.

10.2.3 Bayesian updating of the random field

The prior random field $Q(x, \omega)$ previously defined for characteristic ground snow loads at sea level on the basis of the analysis of gridded dataset, can be updated by the information provided by the point measurements of snow load at the weather stations via the well-known Bayes-rule:

$$f_{X|Q_m} = \frac{f_{Q_m|X} f_X}{\int f_{Q_m|X} f_X dX} \tag{10.22}$$

in which

f_X is the prior distribution of the input random variables $X_i(\omega)$

$f_{Q_m|X}$ is the likelihood function. Assuming the presence of a model error in the estimation of characteristic ground snow load $\varepsilon_m \sim N(0, \sum_\varepsilon)$ such that

$$Q_{true} = Q_m + \varepsilon_m \tag{10.23}$$

the likelihood can be expressed from the probability distribution function (PDF) of the model error f_ε [105]

$$f_{Q_m|X} = f_\varepsilon(Q - Q_m) \tag{10.24}$$

where Q are the predictions at the measurement points, calculated assuming the prior distribution of $X_i(\omega)$ and Q_m are the characteristic ground snow loads obtained from point measurements of snow depth at the weather stations. In the calculations, these values have been assumed independent so $\sum_\varepsilon$ is a diagonal covariance with entries $\sigma_i^2 = (\alpha Q_{m,i})^2$, where α is the coefficient of variation of $Q_{m,i}$. The characteristic values are calculated considering, as in the previous sections, an extreme value distribution type I (Gumbel) for annual maxima ground snow loads [126]

$$Q_{m,i} = \mu_i + \sigma_i\{-\log[-\log(0.98)]\} \tag{10.25}$$

where the two parameters μ and σ of the Gumbel distribution are estimated by means of the method of moments (MOM):

$$\mu_i = \bar{X}_i - \frac{\sqrt{6}}{\pi}\mathrm{COV}_i\bar{X}_i \cdot 0.57721, \tag{10.26}$$

$$\sigma_i = \frac{\sqrt{6}}{\pi}\mathrm{COV}_i\bar{X}_i. \tag{10.27}$$

The mean value of annual maxima ($\bar{X}_i$) for the investigated weather station can be assumed to be known, assuming that all kind of uncertainties are included in the coefficient of variation COV_i. According to the outcomes of the ESLRP[126] in the climatic region considered here, COV_i can be considered as normally distributed with mean equal to 0.7 and standard deviation equal to 0.05. Under these assumptions, the coefficient of variation of $Q_{m,i}$ can be estimated using the Monte Carlo method and solving equation (26). A value for $\alpha = 0.046$ is then obtained.

$f_{X|Q_m}$ is the posterior distribution of the input random variables $X_i(\omega)$.

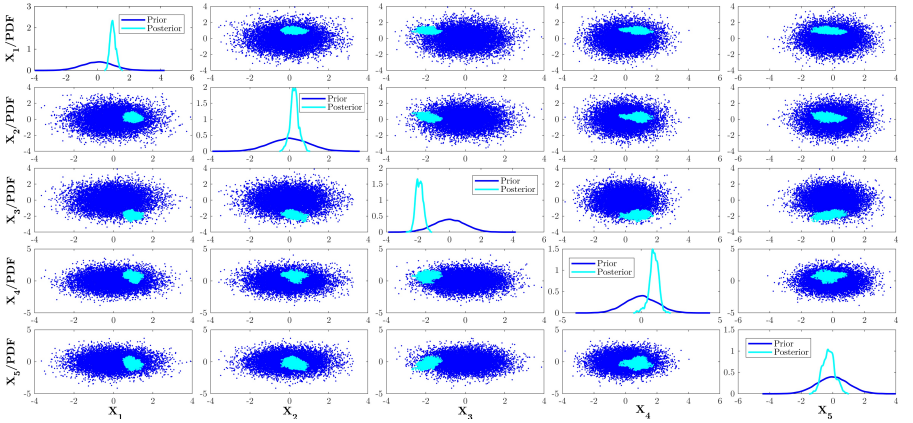

Figure 10.6: Results of the MCMC for the first five X_i (Mediterranean Region - Zone 3-4).

Nevertheless, the posterior distribution $f_{X|Q_m}$ doesn't have a closed form and it is described using sampling techniques. One of the most widely used approaches is the Markov Chain Monte Carlo (MCMC) method [158], which has been also used in the present study. An extensive review of the method can be found in [140].
The adaptation of the MCMC algorithm to the sampling of the posterior distribution $f_(X|Q_m)$ is immediate. In practice, at a given step k the random walker is at the sample points x_i^k and following a proposal distribution may move to x_i^* with a probability of acceptance r given by

$$r = \min[1, \frac{f_{Q_m|X}(x_i^*)f_X(x_i^*)}{f_{Q_m|X}(x_i^k)f_X(x_i^k)}] \tag{10.28}$$

Once obtained the updated samples of $X_i(\omega)$ also the representation of the random field can be updated using the eq. 10.13. In Figure 10.6, results of the MCMC for the first five $X_i(\omega)$ are illustrated for the study region.

Then, in Figure 10.7 the prior and posterior mean of the random field for the investigated region are plotted, together with the characteristic ground snow loads obtained during the ESLRP for the relevant weather stations.
Finally, in Figure 10.8, the box plot of prior and posterior realizations of random field at the measurement points, the 18 weather stations, are drawn, again together with the ESLRP data.

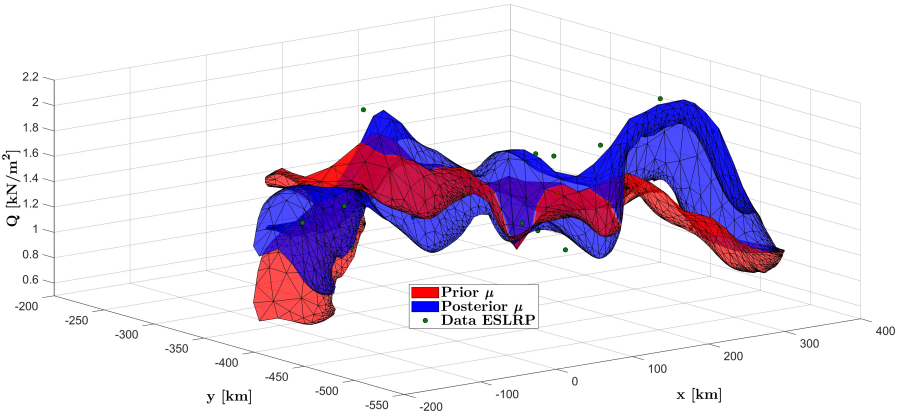

Figure 10.7: Prior and posterior mean of the random field (Mediterranean Region - Zones 3-4).

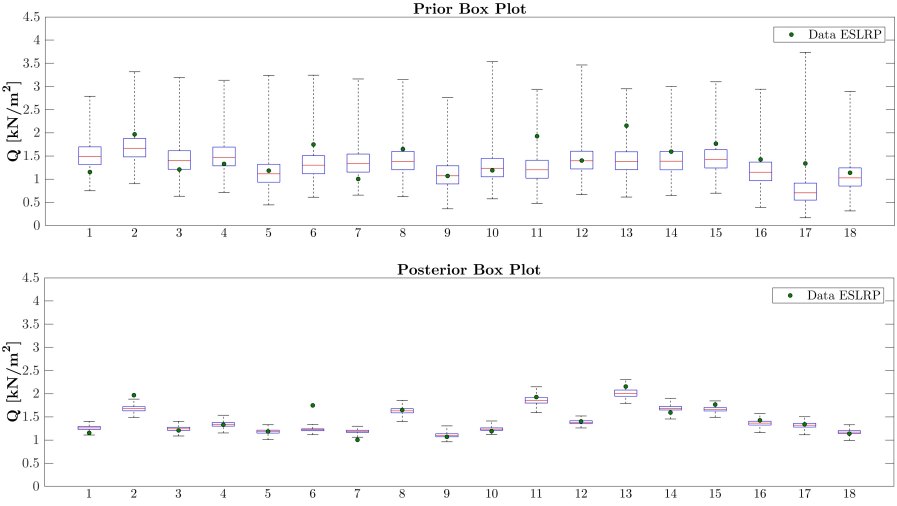

Figure 10.8: Box plot of prior and posterior realizations of random field at the measurement points (Mediterranean Region - Zones 3-4).

10.3 Results

The analysis of the graphs reported in Figure 10.7 and 10.8 clearly shows that the updating technique which is proposed here leads to refined snow maps; in effect, in the neighbourhood of the weather stations, for which measured data

are available, the updated map is much more closer to extreme values obtained from measured data then the prior one, so avoiding the underestimation of the extremes, which is typical of the area averaged data maps.
The methodology illustrated for ground snow load above is general and can be also applied for different climatic variables.
Moreover, the proposed Bayesian approach allows a sequential, continuous and dynamical update process. This can be achieved by recalculating the covariance matrix from the posterior samples and by then repeating the update when new measurements become available.

Chapter 11

Bayesian hierarchical models for snow loads under climate change

In this chapter, a Bayesian hierarchical model for extreme snow loads is set-up in order to take into account the variation of the extreme value process over a climatic region. The main features and the potentialities of the proposed method are highlighted referring to a relevant case study, concerning the updating of snow load maps.

Contents

11.1 Introduction

As discussed in section 2 there is an urgent need for a better evaluation of climate extremes and their evolution over time, to achieve a more detailed assessment of their potential consequences for infrastructures and buildings. Dealing with climate extremes, generally recorded at a spatial scale, a key strategy in extreme value analysis to overcome difficulties caused by the scatter of data is the spatial modelling [12]. The main advantage in spatial modelling is the pooling of information but it can be also useful for interpolation to sites where little or no data may have been collected. Then, the implementation in a Bayesian framework, enables inferences and predictions to incorporate uncertainties in process variation and parameter estimates.
In this chapter, in order to characterize the spatial behaviour of the extreme value process, a Bayesian hierarchical model for extreme snow loads derived from the analysis of Regional Climate Model (RCM) output is set-up [27]. The model is then applied to different time windows forty-years long to assess the time evolution of extreme value parameters. Finally the obtained results are compared in terms of characteristic values of ground snow loads evaluating their evolution in time and providing a quantification of the uncertainty in the predictions.
In the study, an ensemble of six different RCMs described in Table 7.1 is investigated to evaluate the variability in climate model simulations [128], considering the period 1951-2100 (Historical experiment and RCPs experiment). The results will be presented in the following paragraphs for the geographical area already presented in paragraph 7.3.1 and shown in Figure 7.3, which comprises the Zones 3-4 of the Italian Mediterranean climatic region defined by the Annex C to EN1991-1-3 [14].

11.2 Spatial hierarchical model for extreme snow loads

There has been considerable recent interest in spatial hierarchical models to characterize the spatial behaviour of climate data. Aim of these models is to describe how the marginal distribution of a quantity of interest varies with its location [23]. Rather than applying a spatial model directly to the data, hierarchical models assume that there is a latent spatial process that is

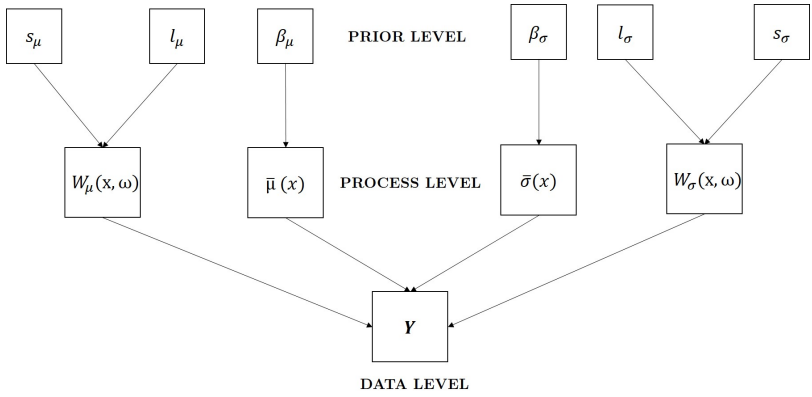

Figure 11.1: Diagrammatic representation of the Hierarchical Model.

characterized by a spatial model for the parameters of the marginal distribution at each location. An extensive review of such models for spatial data can be found in [5].
Hierarchical spatial modelling for extremes has begun to be studied recently, one of the first work in this field is reported in [5], while successive developments are available in [22] and [23], and are increasingly used for the capability to borrow strength from neighbouring locations when estimating parameters in extreme value analysis, usually characterized by small amount of data. The Bayesian Hierarchical Model is formulated through what has now become the standard three-level hierarchical formulation [124]:

- Data Layer, which is the base layer where data, in this case the annual maxima ground snow loads, are modelled at each location according to the extreme value theory;
- Process Layer, where the latent process that drives the extremes for the study region is formulated;
- Prior Layer, where information about the parameters controlling the latent process are given in terms of prior distributions.

In order to assess the evolution in time of extreme value parameters, the hierarchical model for extreme snow loads has been implemented to the different time windows of forty years previously defined. In Figure 11.1 it is shown a diagrammatic representation of the hierarchical model for each time window; each layer is fully described in the next paragraphs.

11.2.1 Data level

At data level, series of $M = 149$ annual maximum ground snow loads, obtained implementing the snow load algorithm on climate projections provided by each RCM r (where $r = 1, 2, .., 6$), are available for each cell i in the study region. In order to evaluate the evolution in time of the extreme value process, data are divided, as discussed in the previous chapters, in subsequent time windows of 40 years shifted by ten years, thus obtaining eleven time window t (1951-1990, 1961-2000,..., 2041-2080 and 2051-2090).
Then, for each time window t, N=40 yearly maxima snow load are given at each cell i in the study region. Assuming an extreme value distribution Type I (EVI) as marginal distribution for annual maxima ground snow loads at each location i as in [126], the random variable $Y_{i,t,r}$ is described by the cumulative distribution function $F(y)$

$$F(Y_{i,t,r} < y) = \exp\{-\exp[-\frac{y - \mu_{i,t,r}}{\sigma_{i,t,r}}]\} \tag{11.1}$$

and probability density function $f(y)$

$$f(Y_{i,t,r} < y) = \frac{1}{\sigma_{i,t,r}} \exp\{-[\frac{y - \mu_{i,t,r}}{\sigma_{i,t,r}} + \exp(-\frac{y - \mu_{i,t,r}}{\sigma_{i,t,r}})]\} \tag{11.2}$$

where $\mu_{i,t,r}$ and $\sigma_{i,t,r}$ are the location and scale parameter for cell i, time window t and RCM r. The first level of the hierarchical model structure for each climate model r will be described by

$$\mathrm{Y}_t(s)|\Theta_t \sim \mathrm{EVI}(\mu_t(s,\omega), \exp(\log(\sigma_t(s,\omega)))) \tag{11.3}$$

with

$Y_t(s)$ are the annual maxima snow load at the location s in the study region for the time window t

Θ_t are the parameter of the model in the time window t

$\mu_t(s,\omega)$ is a random field describing the spatial variation of location parameter of EVI distribution in the time window t, where $\omega \in \Omega$ express the random event [89]

$\log(\sigma_t)(s,\omega)$ is a random field describing the spatial variation of log-scale parameter of EVI distribution in the time window t, where $\omega \in \Omega$ express the random event [89]

If $Y_{i,t}$ is a vector of the annual maxima snow load in the investigated time window t for the cell i in the region and $Y_t = (Y_{1,t}^T, ..., Y_{D,t}^T)$ contains all the maxima for the D cells in the region, then assuming the conditional independence of Y_i for all location, common assumption in hierarchical modelling [5], starting from eq. 11.2 the likelihood function becomes

$$p(Y_t|\Theta_t) = \prod_{i=1}^{D}\prod_{k=1}^{40}\frac{1}{\sigma_i}\exp\{-[\frac{y_{ik}-\mu_i}{\sigma_i} + \exp(-\frac{y_{ik}-\mu_i}{\sigma_i})]\} \tag{11.4}$$

11.2.2 Process level

In the hierarchical model, at the process level, the latent spatial process is formulated by constructing a structure that relates the parameter of the data level to the characteristics of the region. In particular, a Gaussian random field has been defined to model spatial variation of location and log-scale parameters according the following formulas

$$\mu_t(s,\omega) \sim N(X\beta_{\mu,t} + W_{\mu,t}(s,\omega), \tau_\mu^2) \tag{11.5}$$

$$\log(\sigma_t)(s,\omega) \sim N(X\beta_{\sigma,t} + W_{\sigma,t}(s,\omega), \tau_\sigma^2) \tag{11.6}$$

with

$W_{\mu,t}$ is a spatial random effect described by a zero mean Gaussian random field $N(0, \Sigma_\mu(l_{\mu,t}, s_{\mu,t}))$ with covariance matrix Σ_μ defined by an exponential model with parameter correlation length $l_{\mu,t}$ and sill $s_{\mu,t}$;

$W_{\sigma,t}$ is a spatial random effect described by a zero mean Gaussian random field $N(0, \Sigma_\sigma(l_{\sigma,t}, s_{\sigma,t}))$ with covariance matrix Σ_σ defined by an exponential model with parameter correlation length $l_{\sigma,t}$ and sill $s_{\sigma,t}$;

X is a matrix of covariate information

$\beta_{\mu,t}$ is a vector of regression coefficients for μ given X

$\beta_{\sigma,t}$ is a vector of regression coefficients for σ given X

$\tau^2_{\mu,t}$ is a precision term for the location field

$\tau^2_{\sigma,t}$ is a precision term for the log-scale field

Among possible covariate information, altitude shows most significant influence on extreme snow loads, it has been then considered as the only covariate and a quadratic model has been chosen as defined by the ESLRP [126] and adopted in the Eurocode EN1991-1-3 [14]:

$$X = \begin{bmatrix} 1 & alt_1 & alt_1^2 \\ . & . & . \\ . & . & . \\ 1 & alt_D & alt_D^2 \end{bmatrix} \tag{11.7}$$

$$\beta_{\mu,t} = \begin{bmatrix} \beta_{\mu,0,t} \\ \beta_{\mu,1,t} \\ \beta_{\mu,2,t} \end{bmatrix} \tag{11.8}$$

$$\beta_{\sigma,t} = \begin{bmatrix} \beta_{\sigma,0,t} \\ \beta_{\sigma,1,t} \\ \beta_{\sigma,2,t} \end{bmatrix} \tag{11.9}$$

The precision terms, τ^2_μ and τ^2_σ in eq. 11.5 and 11.6, can be viewed as a noise associated with replication of measurement at location s [5], and in this case represents the variability of the data related to internal climate model uncertainty. As discussed in the previous sections, internal variability of climate models is one of the three main source of uncertainty in climate projections, however the availability of only one realization of climate model run due to the enormous computational demand doesn't allow a direct assessment of this source of uncertainty. Then, an *ad hoc* weather generator has been developed and illustrated in chapter 7 to generate climate projections directly from RCM ouput. The analysis of the generated series allows an evaluation of the uncertainty related to the RCM internal variability and has lead to the definition of the constant precision terms $(\tau^2_\mu)_{i,t}$ and $(\tau^2_\sigma)_{i,t}$ associated at each investigated climate model r, depending on the cell i and the time window t.

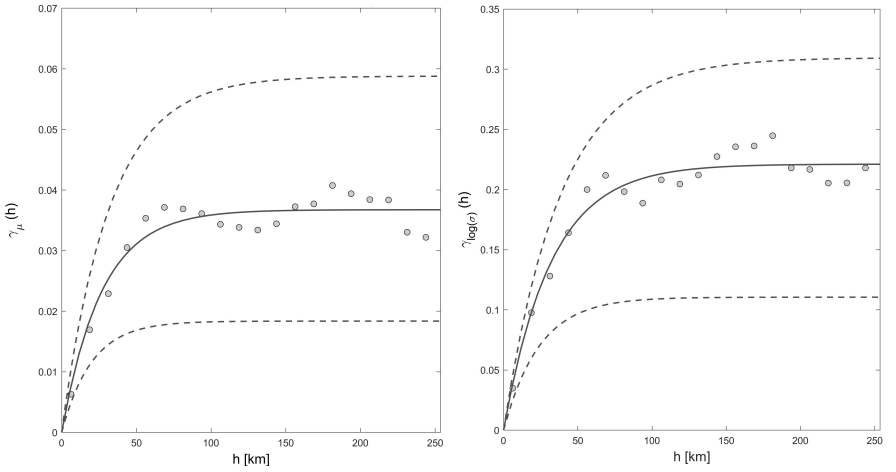

(a) Semi-variogram $\gamma_\mu(h)$ **(b)** Semi-variogram $\gamma_{\log(\sigma)}(h)$

Figure 11.2: Empirical semi-variograms for μ and $\log(\sigma)$ (solid black lines) with the envelope of possible semi-variograms (dashed black lines).

11.2.3 Prior level

Prior distribution are finally assigned to the hyperparameters of the model at each time window $\Theta_t = (\beta_{\mu,t}, \beta_{\sigma,t}, l_{\mu,t}, s_{\mu,t}, l_{\sigma,t}, s_{\sigma,t})$. Where possible, uninformative priors are assigned to these parameters and conjugate priors are used to facilitate the use of Gibbs sampling in the model implementation.
For the intercept term of the regression coefficients ($\beta_{\mu,0,t}$, $\beta_{\sigma,0,t}$) a normal distribution is assigned with mean set to the mean of the point estimated values in the region for each parameter ($\mu_{t,i}$ and $\log(\sigma_{t,i})$) at the investigated time window and large variance. For the other regression coefficient normal distributions with mean zero and large variance have been assigned.
In order to define a proper prior for the sill ($s_{\mu,t}$, $s_{\sigma,t}$) and correlation length (l_μ, l_σ) parameters a preliminary analysis has been carried out defining the experimental semi-variogram [24] for μ and σ starting from the estimated values at each location. The results are reported in Figure 11.2 for the first time window ($t = 1$). Then, the prior distribution for the parameters have been chosen defining a wide envelope around the estimated semi-variogram (dashed line in Figure 11.2) as proposed in [22] for extreme precipitations.

11.2.4 Implementation of the model

In order to update each parameter Θ of the described model a Metropolis–Hastings algorithm within a Gibbs sampler has been implemented. This hybrid MCMC algorithm [121] consists of a Gibbs sampler where a Metropolis step is used in order to sample from conditional distributions which are not known. Parameters of the model, which will be implemented for each time window t, are collected at each step i of the algorithm in the vector $\Theta^{(i)} = (\mu^{(i)}, \log(\sigma)^{(i)}, \beta_\mu^{(i)}, \beta_\sigma^{(i)}, l_\mu^{(i)}, s_\mu^{(i)}, l_\sigma^{(i)}, s_\sigma^{(i)}$. Then, applying the Gibbs sampler, we partition the sampling for location μ and log-scale $\log(\sigma)$ parameters and the next point in the chain $i+1$ is generated in the following way:

1. **Step 1**: *Updating correlation length parameter*
   Correlation Length $l_\mu^{(i+1)}$ is sampled according a random walk where the acceptance probability is computed as

$$\alpha(l_\mu^{(i)}, l_\mu^{(i+1)}) = \min\{1, \frac{f(\mu^{(i)}|\beta_\mu^{(i)}, l_\mu^{(i+1)}, s_\mu^i)p(l_\mu^{(i+1)})}{f(\mu^{(i)}|\beta_\mu^{(i)}, l_\mu^{(i)}, s_\mu^{(i)})p(l_\mu^{(i)})}\} \tag{11.10}$$

   that is, a ratio of multivariate Normal likelihoods $f(\mu)$ times a ratio of prior probability $p(l_\mu)$.

2. **Step 2**: *Updating sill parameter*
   Sill s_μ^{i+1} is sampled according a random walk where the acceptance probability is computed as

$$\alpha(s_\mu^{(i)}, s_\mu^{(i+1)}) = \min\{1, \frac{f(\mu^{(i)}|\beta_\mu^{(i)}, l_\mu^{(i+1)}, s_\mu^{i+1})p(s_\mu^{(i+1)})}{f(\mu^{(i)}|\beta_\mu^{(i)}, l_\mu^{(i+1)}, s_\mu^{(i)})p(s_\mu^{(i)})}\} \tag{11.11}$$

   that is again a ratio of multivariate Normal likelihoods $f(\mu)$ times a ratio of prior probability $p(s_\mu)$.

3. **Step 3**: *Updating regression parameters*
   Regression parameters $\beta_\mu^{(i+1)}$ is sampled according a random walk where the acceptance probability is computed as

$$\alpha(\beta_\mu^{(i)}, \beta_\mu^{(i+1)}) = \min\{1, \frac{f(\mu^{(i)}|\beta_\mu^{i+1}, l_\mu^{i+1}, s_\mu^{i+1})p(\beta_\mu^{(i+1)})}{f(\mu^{(i)}|\beta_\mu^{(i)}, l_\mu^{(i+1)}, s_\mu^{(i+1)})p(\beta_\mu^{(i)})}\} \tag{11.12}$$

that is again a ratio of multivariate Normal likelihoods $f(\mu)$ times a ratio of prior probability $p(\beta_\mu)$.

4. **Step 4**: *Updating the EVI parameters at each site k*
Each component k of $\mu^i = (\mu_1^{(i)}, \mu_2^{(i)}, \ldots, \mu_D^{(i)})$ is updated singly according the following transition density defined in [12]

$$q(\mu_k^{(i)}|\mu_k^{(i+1)}) = f(\mu_k^{i+1}|\mu_{-k}^{(i)}, \beta_\mu^{(i+1)}, l_\mu^{(i+1)}, s_\mu^{(i+1)}) \tag{11.13}$$

In this way each new component $\mu_k^{(i+1)}$ is sampled from the univariate conditional distribution of one component of a D-dimensional Multivariate Normal, MVN$(\mu_\mu^{(i)}, \Sigma_\mu^{(i)})$, that in accordance with multivariate normal theory can be computed as

$$\mu_k^{(i+1)}|\mu_{-k}^{(i)} \sim N(\bar{\mu}, \bar{\Sigma_\mu}) \tag{11.14}$$

with

$$\bar{\mu} = \mu_{\mu,k}^{(i)} + \Sigma_{\mu,k}^{(i)} \Sigma_{\mu,-k}^{-1(i)} (\mu_{-k}^{i} - \mu_{\mu,-k}) \tag{11.15}$$

$$\bar{\Sigma_\mu} = \Sigma_{\mu,kk}^{(i)} - \Sigma_{\mu,k}^{(i)} \Sigma_{\mu,-k}^{-1(i)} \Sigma_{\mu,k}^{T(i)} \tag{11.16}$$

where $\mu_{\mu,k}^{(i)}$ and $\Sigma_{\mu,kk}^{(i)}$ are the mean and the variance of μ for location k at the step i, $\mu_{\mu,-k}$ is the vector containing the mean values of μ at the other $D-1$ locations, $\Sigma_{\mu,-k}$ is the covariance matrix obtained excluding the row associated to location k ($\Sigma_{\mu,k}$). Once sampled $\mu_k^{(i+1)}$ the acceptance probability is simply computed by means of a ratio of EVI-PDF (eq. 11.2)

$$\alpha(\mu_k^i, \mu_k^{i+1}) = \min\{1, \frac{f(Y_k|\mu_k^{i+1}, \sigma_k^{(i)})}{f(Y_k|\mu_k^{(i)}, \sigma_k^{(i)})}\} \tag{11.17}$$

5. **Step 5**: *Step from 1 to 4 are repeated for log-scale parameter.*

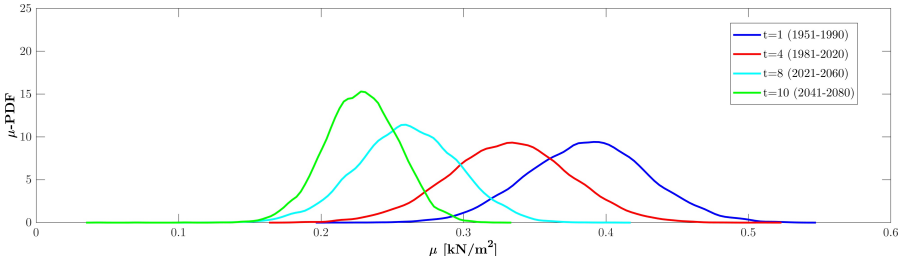

(a) Location μ

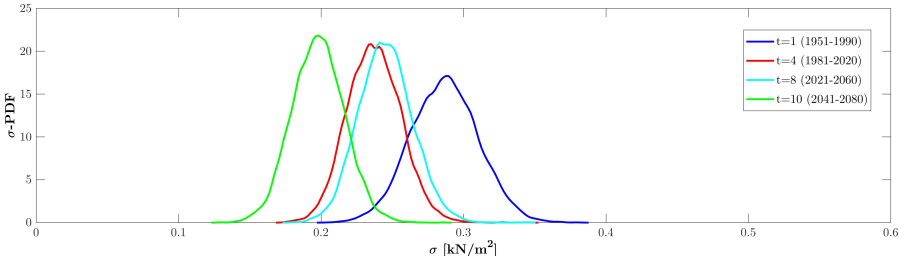

(b) Scale σ

Figure 11.3: Posterior PDFs of μ and σ for different time windows at cell 160, Climate Model 1 in Table 7.1.

The described hybrid MCMC algorithm has been then iterated 40000, for each time window, obtaining in these way posterior samples of the parameters $\Theta_t^{(i)}$. As an example, in Figure 11.3, the results in terms of posterior densities of location μ and scale σ EVI parameters are presented for one cell in the study region in different time windows ($t = 1, 4, 8, 10$) according to one of the investigated climate model.

We can observe how the hierarchical model combined with the Bayesian approach enables a direct assessment of the uncertainties affecting the extreme value process using the posterior distribution of parameters. Moreover, the implementation of the model in subsequent time window allows a direct estimation of the effect of climate change on extreme ground snow loads by means of the analysis of changes in posterior densities of EVI parameters.
In design context, we are interested in return level estimates rather than in the parameters of extreme value distribution. Then, return level ensembles are produced combining the MCMC results in terms of posterior samples for μ_t^i and σ_t^i at each time windows t. In particular, characteristic values $q_{k,t}$ are computed according the definition given in Eurocode EN1990 [13], as the value having a probability of 2% to be exceeded in one year, i.e. the value

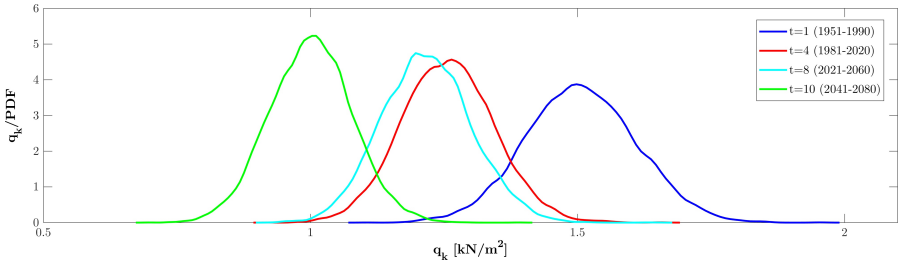

Figure 11.4: Posterior PDFs of q_k for different time windows at cell 160, Climate Model 1 in Table 7.1.

characterized by a return period of around 50 years

$$q^i_{k,t} = \mu^i_t + \sigma^i_t\{-\log[-\log(1-0.02)]\} \tag{11.18}$$

In Figure 11.4, the results in terms of posterior PDFs for q_k in different time windows ($t = 1, 4, 8, 10$) are reported for the same cell and climate model shown in Figure 11.3.

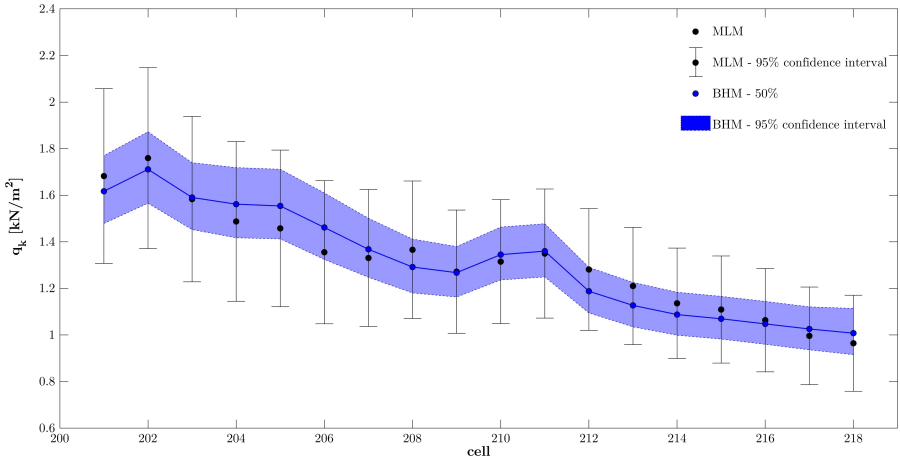

Figure 11.5: q_k estimates by maximum likelihood method (MLM) and bayesian hierarchical model(BHM) with 95% confidence intervals.

As mentioned before, the Bayesian hierarchical model allows a direct estimation of the uncertainty in the prediction of extreme value parameters and return levels. Moreover, the spatial pooling of the data presents an added value in comparison with classical approach based on maximum likelihood estimates at

point level leading to more precise and less variable estimates [12].
The reduced uncertainty in the estimation is shown in Figure 11.5 where q_k estimates obtained by the presented spatial model are compared with the classical site by site analysis according the maximum likelihood method, for some cells at increasing distance in the study region. The results in terms of 95% confidence interval clearly show the reduced uncertainty for the illustrated spatial model confirming the advantages of spatial pooling for tail estimation.

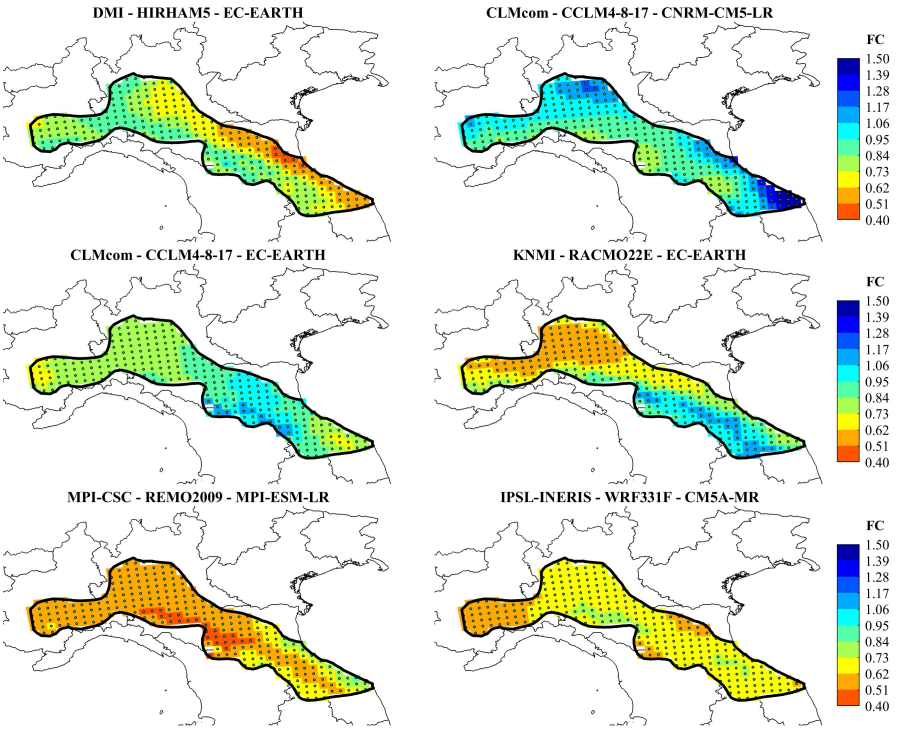

Figure 11.6: Posterior mean of q_k factors of change for 2021-2060 w.r.t. 1951.1990 according to the climate models in Table7.1, Scenario RCP4.5.

11.3 Return level maps

Return level maps can also be drawn from the posterior samples of q_k obtained according the investigated climate models and scenarios. As discussed in the previous sections, factors of change maps represent a good solution for the

estimation and the visualization of future trends in climatic actions and then mean FC are defined from the posterior mean of q_k

$$FC(q_{k,t}) = \frac{\overline{q_{k,t}}}{\overline{q_{k,1}}} \tag{11.19}$$

In Figure 11.6 and Figure 11.8, factors of change maps of q_k are shown for t=8 (2021-2060) with respect to t=1 (1951-1990) according to the six investigated climate models and the RCP4.5 and RCP8.5 scenario respectively.

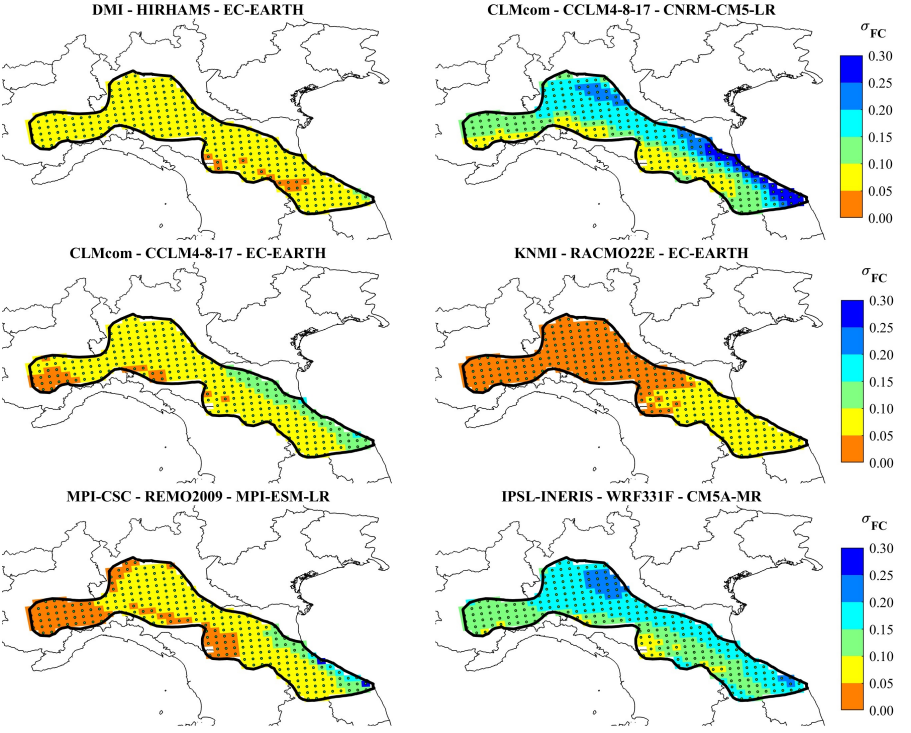

Figure 11.7: Standard deviation of q_k factors of change for 2021-2060 w.r.t. 1951.1990 according to the climate models in Table7.1, Scenario RCP4.5.

From the posterior draws of the return level distributions standard deviation for FC can be directly obtained and used to evaluate the uncertainty in the definition of factors of change.

$$\sigma_{FC(q_{k,t})} = \frac{\sigma_{q_{k,t}}}{\overline{q_{k,1}}} \tag{11.20}$$

In Figure 11.7 and Figure 11.9 the standard deviations derived for FC in the same time window at which posterior means are given in Figure 11.6 and Figure 11.8.

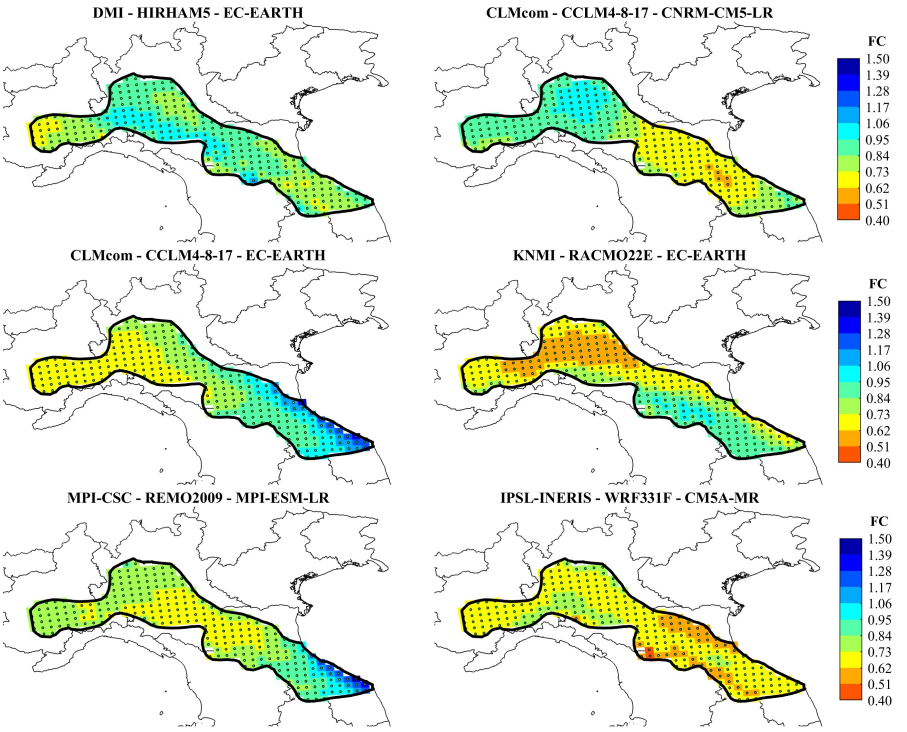

Figure 11.8: Posterior mean of q_k factors of change for 2021-2060 w.r.t. 1951.1990 according to the climate models in Table7.1, Scenario RCP8.5.

It is important to notice that each RCM can tell a slightly different story about changes in extreme snow loads, as already observed for extreme precipitations in [128], but a general decrease is expected for the region in the period 2021-2060 except for Model 2 (RCP4.5 scenario) and for the southern part of the study region in Model 3 and 5 (RCP8.5).

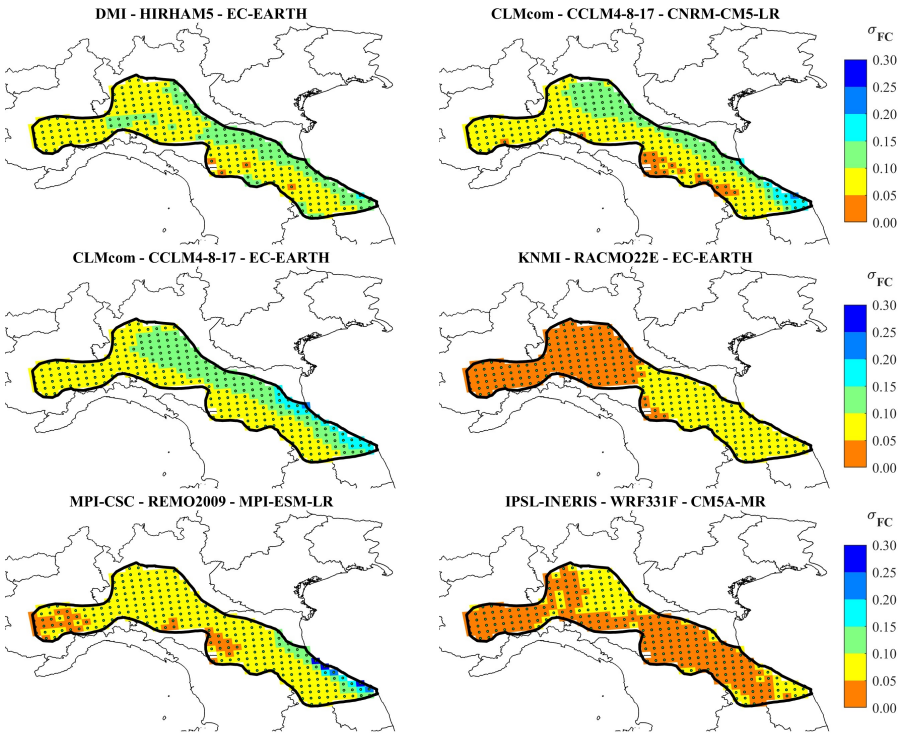

Figure 11.9: Standard deviation of q_k factors of change for 2021-2060 w.r.t. 1951.1990 according to the climate models in Table7.1, Scenario RCP8.5.

The results presented for the different climate models can be finally combined considering each climate model of the ensemble as an equally likely representation of future climate. In this way, a complete description of future changes in characteristic loads is obtained providing guidance for potential amendments of the current version of climatic load maps in structural Codes.
In Figure 11.10 and 11.11, the results in terms of factors of change maps for characteristic ground snow load (q_k) are presented in three time windows (1991-2030, 2011-2050, and 2031-2080), according the RCP4.5 and RCP8.5 scenario respectively. In the same Figures, on the top row left, the current snow load map for the study region, obtained implementing the load-altitude relationship given in the Annex C of EN1991-1-3 [14], is also reported.

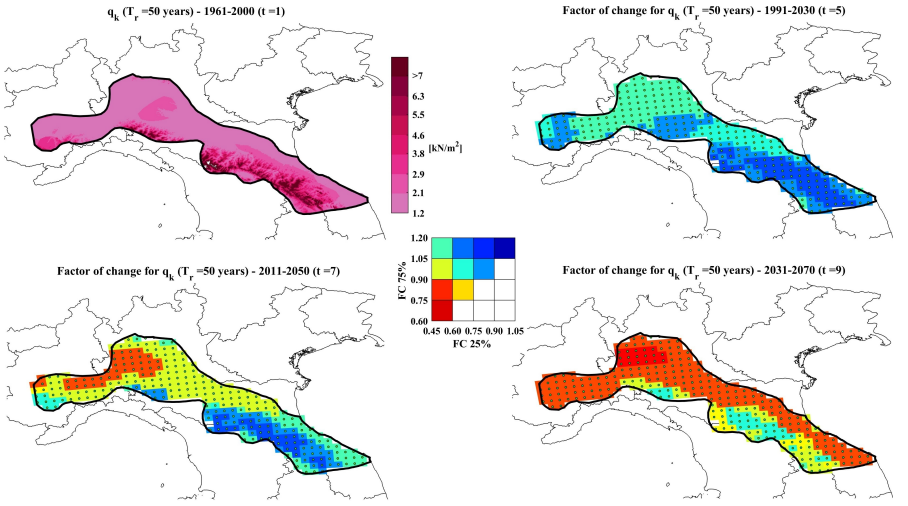

Figure 11.10: Factors of Change for q_k - Confidence interval [25-75%] Map (Scenario RCP4.5).

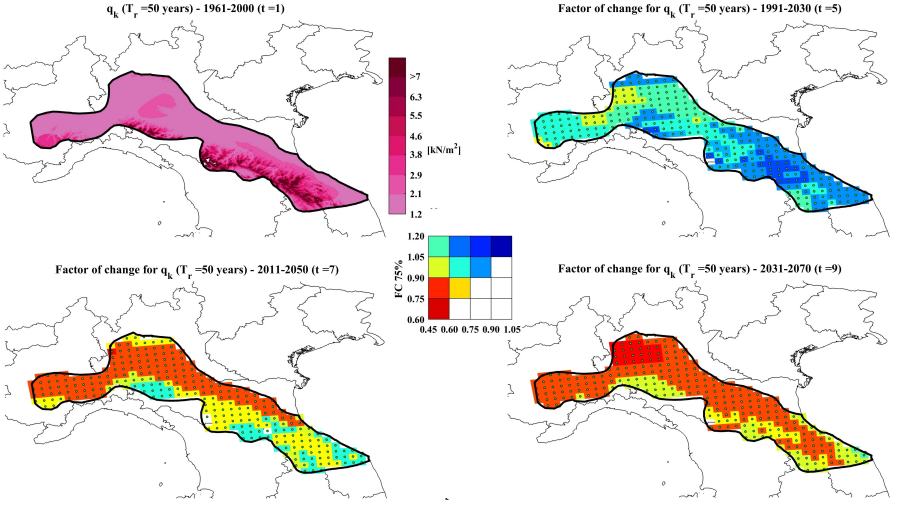

Figure 11.11: Factors of Change for q_k - Confidence interval [25-75%] Map (Scenario RCP8.5).

In conclusion, snow load maps in structural Codes can be so updated having considered in the estimation of future trends of characteristic ground snow loads: the influence of inherent uncertainty of the outcomes of climate models,

the spatial variation of the extreme value process and the dependence on future emission scenarios.

Chapter 12

Conclusion and outlook

In this chapter the conclusions about the work are drawn. The main goals achieved are summarised and suggestions for the future steps of the research are given.

Contents

12.1 Conclusion

This thesis aimed to evaluate the impact of climate change on structural design with a focus on snow load on structures. The main goals achieved during the development of this thesis can be summarised in the following way:

- a procedure for the assessment of future trends of climatic actions, starting from regional climate model output, has been developed. The procedure combine the analysis of an ensemble of high resolution Regional Climate Models with the use of an *ad hoc* weather generator developed to investigate the internal variability of climate models. The results presented in terms of factors of change for extreme statistics derived together with their uncertainty range, allow a direct evaluation of the impact of climate change providing guidance for potential amendments of climatic load maps in technical standards.

- in order to evaluate future trends of ground snow loads from available climate models outputs, a general algorithm for the simulation of snow load formation process from the analysis of daily data of maximum and minimum temperature and water precipitation, has been set-up. The algorithm is implemented by means of the Monte Carlo method where daily climate data are supplemented by local information of snowfall and snow melting conditions, which are expressed in terms of conditional probability functions of snowfall in the presence of precipitation and snow melting in the presence of snow cover defined as function of daily temperatures. Ground snow load maxima are thus estimated and from them the characteristic value of the load is derived via extreme value analysis.

- concerning the local assessment of future trends in climatic action, an alternative approach to that based on the definition of factors of change from the analysis of weather generated series according an ensemble of climate models, has been developed. In particular a stochastic technique for bias correction and downscaling of climate projections has been set-up. The methodology has been presented together with an application for the local assessment of future trends of snow loads. The results show the ability of the methodology to reproduce recorded past climate extremes underlining its suitability for a probabilistic assessment of impacts of

climate change on climatic actions also preserving the climate change signal simulated by the uncorrected climate models.

- following the Bayesian approach, a technique for snow load map refinement has been proposed to optimally combine gridded climate data, like those provided by climate models, with point measurements. The theoretical development based on the definition of a prior random field from the analysis of gridded data and a consequent Bayesian updating carried out incorporating available point measurements, has been presented together with an application for ground snow loads. The proposed Bayesian technique allows a sequential, continuous and dynamical updating process and the results demonstrate that the method is very promising as it is capable to lead to a more refined snow map, avoiding the underestimation of the extremes, which is typical of the area averaged data maps.
- a Bayesian hierarchical model for extreme snow loads has been set-up in order to evaluate the variation of the extreme value process over an homogeneous climatic region. The Bayesian framework enables a direct assessment of the uncertainties affecting the prediction of the extreme value parameters and return levels. Moreover, the spatial pooling of the data leads to more precise and less variable estimates. The hierarchical model has been presented for extreme snow loads but can be easily extended to different climate variables, and its implementation in different time windows according to an ensemble of regional climate models provide a complete overview on the variation of the extreme value process in general, and return levels in particular, taking into account the major sources of uncertainty.

12.2 Outlook

During the writing and the development of this thesis several problems and questions came out. Some of these would need further investigation:

- methods and procedures for the assessment of future trends of climatic actions has been presented mainly focusing on ground snow loads as declared in the objectives of the thesis. However they are general and can be easily extended for the evaluation of the impact of climate

change on other environmental loads such as thermal actions, rainfall precipitation extremes, wind and ice loads. A proper evaluation of future climate extremes is the basis for a risk assessment of the impact of climate change on engineering systems of various nature. The proposed methodology, which allow a probabilistic description of future changes, can be thus integrated in a more general procedure for the probabilistic safety assessment of critical structures and infrastructures [148].

- the definition of climatic load maps in structural Codes based on the assumption of stationary climate is becoming debatable. The factor of change approach based on the analysis of regional climate model output presented in this work, can provide guidance for potential amendment of current load values. In the author's opinion, since a new structure shall withstand loads acting during its life, the variations of characteristic values of climatic actions over time should be duly taken into account in design by means of a suitable envelope, where the maximum characteristic load value estimated for the future time windows should be assumed as new design load. However, the way to implement these potential changes should be further discussed having in mind the uncertainty in the predictions, and considering also policy measures to mitigate greenhouse gas emissions and then to slow the rate of future climate change.

- the estimated changes in climatic loads have been illustrated in terms of characteristic load variations that derive from changes in extreme value distribution's parameters. Since they are commonly due to variation in both location and scale parameter it would be interesting to evaluate also the impact on design loads and in the achievement of target reliability levels. In this context, the influence of climate change on long-term structural reliability of new and existing structures under non stationary loads should be also further investigated. A possible solution would be to evaluate the time-dependent reliability starting from the estimated changes in the extreme value distribution's parameters and comparing the resulting trends in failure probabilities with the target reliability levels defined in structural Codes.

List of Figures

List of Tables

Bibliography

[1] American Society of Civil Engineers. *Minimum design loads for buildings and other structures (ASCE 7-10).* 2010.

[2] Asociación Española de Normalización. *UNE EN 1991-1-3/NA, Eurocode 1 – Actions on structures – Part 1-3: General actions – Snow loads –National Annex (in Spanish).*

[3] Association Française de Normalisation. *NF EN 1991-1-3/NA, Eurocode 1 – Actions on structures – Part 1-3: General actions – Snow loads –National Annex (in French).*

[4] Austrian Standards Institute. *ÖNORM EN 1991-1-3/NA, Eurocode 1 – Actions on structures – Part 1-3: General actions – Snow loads –National specifications concerning ÖNORM EN 1991-1-3, national comments and national supplements (in Austrian).*

[5] Banerjee, S., Carlin, B. P., and Gelfand, A. E. *Hierarchical modeling and analysis for spatial data.* CRC Press LLC, 2004.

[6] Biegus, A., and Rykaluk, K. Collapse of Katowice Fair Building. *Engineering Failure Analysis 16* (2009), 1643–1654.

[7] Brekke, L. D., and Barsugli, J. J. Uncertainties in Projections of Future Changes in Extremes. In *Extremes in a Changing Climate*, A. AghaKouchak, D. Easterling, K. Hsu, Sorooshian, S. Schubert, and S. Sorooshian, Eds. Springer, 2013, pp. 309–346.

[8] British Standards Institution. *BS EN 1991-1-3/NA, Eurocode 1 – Actions on structures – Part 1-3: General actions – Snow loads –National Annex.*

[9] Bulgarian Institute of Standardization. *BDS EN 1991-1-3/NA, Eurocode 1 – Actions on structures – Part 1-3: General actions – Snow loads –National Annex.*

[10] Bureau de Normalisation. *NBN EN 1991-1-3/NA, Eurocode 1 – Actions on structures – Part 1-3: General actions – Snow loads –National Annex (in French).*

[11] Cario, M. C., and Nelson, B. L. Modeling and generating random vectors with arbitrary marginal distributions and correlation matrix. Tech. rep., Department of Industrial Engineering and Managment Sciences Northwestern University, 1997.

[12] Casson, E., and Coles, S. Spatial Regression Models for Extremes. *Extremes 1*, 4 (1999), 449–468.

[13] CEN. *Eurocode - Basis of structural design.* 2002.

[14] CEN. *EN 1991-1-3:2003 - Eurocode 1: Actions on structures - Part 1-3: General actions - Snow loads.* 2003.

[15] CEN. *EN 1991-1-5:2003 – Eurocode 1: Actions on structures – Part 1-5: General Actions – Thermal Loads.* 2003.

[16] CEN. *EN 1991-1-4:2005 – Eurocode 1: Actions on structures – Part 1-4: General Actions – Wind Loads.* 2005.

[17] CEN/TC250. *Response to Mandate M / 515 "Towards a second generation of EN Eurocodes".* 2013.

[18] Cheng, L., AghaKouchak, A., Gilleland, E., and Katz, R. W. Non-stationary extreme value analysis in a changing climate. *Climatic Change 127*, 2 (2014), 353–369.

[19] Coles, S. *An introduction to statistical modeling of extreme values.* Springer-Verlag London, 2001.

[20] Collins, M., Chandler, R. E., Cox, P. M., Huthnance, J. M., Rougier, J., and Stephenson, D. B. Quantifying future climate change. *Nature Climate Change 2*, 6 (2012), 403–409.

[21] Cooley, D. Return Periods and Return Levels Under Climate Change. In *Extremes in a Changing Climate*, A. AghaKouchak, D. Easterling, K. Hsu, Sorooshian, S. Schubert, and S. Sorooshian, Eds. Springer, 2013.

[22] Cooley, D., Nychka, D., and Naveau, P. Bayesian Spatial Modeling of Extreme Precipitation Return Levels. *Journal of the American Statistical Association 102*, 479 (2007), 824–840.

[23] Cooley, D., and Sain, S. R. Spatial hierarchical modeling of precipitation extremes from a regional climate model. *Journal of Agricultural, Biological, and Environmental Statistics 15*, 3 (2010), 381–402.

[24] Cressie, N. A. C. *Statistics for Spatial Data, Revised Edition.* John Wiley & Sons, 1994.

[25] Croatian Standards Institute. *HRN EN 1991-1-3/NA, Eurocode 1 – Actions on structures – Part 1-3: General actions – Snow loads –National Annex.*

[26] Croce, P., Formichi, P., Friedman, N., Landi, F., and Marsili, F. Snow load on structures under changing climate conditions. In *Safety, Reliability, Risk, Resilience and Sustainability of Structures and Infrastructure* (2017), pp. 3504–3513.

[27] Croce, P., Formichi, P., and Landi, F. Effect of Climate Change on Snow Load on Ground : Bayesian Approach for Snow Map Definition. In *Proc. of the 15th International Probabilistic Workshop* (2017), pp. 231–244.

[28] Croce, P., Formichi, P., Landi, F., and Marsili, F. A novel probabilistic methodology for the local assessment of future trends of climatic actions. *Beton- und Stahlbetonbau 113* (2018), 110–115.

[29] Croce, P., Formichi, P., Landi, F., and Marsili, F. Climate change: Impact on snow loads on structures. *Cold Regions Science and Technology 150*, October 2016 (2018), 35–50.

[30] Croce, P., Formichi, P., Landi, F., and Marsili, F. Evaluating the effect of climate change on thermal actions on structures. In *Life-Cycle Analysis and Assessment in Civil Engineering: Towards an Integrated Vision* (2019), pp. 1751–1758.

[31] Croce, P., Formichi, P., Landi, F., Marsili, F., and Friedman, N. Effect of Climate Change on Snow Load on Ground: Bayesian Approach for Snow Map Refinement. In *14th International Probabilistic Workshop*, R. Caspeele, L. Taerwe, and D. Proske, Eds. Springer, Cham, 2017, pp. 231–244.

[32] Croce, P., Formichi, P., Landi, F., Mercogliano, P., Bucchignani, E., Alessandro, D., and Dimova, D. Towards new European Snow Load Map: Support to policies and standards for sustainable construction. Tech. rep., Joint Research Centre (JRC), 2016.

[33] Croce, P., Formichi, P., Landi, F., Mercogliano, P., Bucchignani, E., Dosio, A., and Dimova, S. The snow load in Europe and the climate change. *Climate Risk Management 20*, October 2017 (2018), 138–154.

[34] Croce, P., Landi, F., Formichi, P., and Castelluccio, R. Use of weather generators to assess impact of climate change : thermal actions on structures. In *Proc. of the Fifth Intl. Conf. Advances in Civil, Structural and Mechanical Engineering - CSM 2017* (2017), pp. 32–36.

[35] Cyprus Organization for Standardisation. *CYS EN 1991-1-3/NA, Eurocode 1 – Actions on structures – Part 1-3: General actions – Snow loads –National Annex.*

[36] Czech office for Standards Metrology and Testing. *ČSN EN 1991-1-3/NA, Eurocode 1 – Actions on structures – Part 1-3: General actions – Snow loads –National Annex.*

[37] Dansk Standard. *DS EN 1991-1-3/NA, Eurocode 1 – Actions on structures – Part 1-3: General actions – Snow loads –National Annex.*

[38] de Normalisation, O. L. *ILNAS EN 1991-1-3/NA, Eurocode 1 – Actions on structures – Part 1-3: General actions – Snow loads –National Annex (in French).*

[39] Deutsches Institut für Normung. *DIN EN 1991-1-3/NA, Eurocode 1 – Actions on structures – Part 1-3: General actions – Snow loads –National Annex (in German).*

[40] Donat, M. G., Lowry, A. L., Alexander, L. V., O'Gorman, P. A., and Maher, N. More extreme precipitation in the world' s dry and wet regions. *Nature Climate Change 6*, 5 (2016), 508–513.

[41] Ente Nazionale Italiano di Unificazione. *UNI EN 1991-1-3/NA, Eurocode 1 – Actions on structures – Part 1-3: General actions – Snow loads –National Annex (in Italian).*

[42] Estonian Centre for Standardisation. *EVS EN 1991-1-3/NA, Eurocode 1 – Actions on structures – Part 1-3: General actions – Snow loads –National Annex.*

[43] European Commission. Mandate M/515 EN – Mandate for amending existing Eurocodes and extending the scope of Structural Eurocodes, 2012.

[44] European Commission. COM(2013) 216 - An EU Strategy on adaptation to climate change, 2013.

[45] European Commission. Mandate M/526 EN - Commission Implementing Decision of 28.5.2014 on deciding to make a standardisation request to the European standardisation organisations pursuant to Article 10 (1) of Regulation (EU) No 1025/2012 of the European Parliament and of the C, 2014.

[46] European Commission. SWD(2013) 137 - Adapting infrastructure to climate change, 2014.

[47] Fatichi, S., Ivanov, V. Y., and Caporali, E. Simulation of future climate scenarios with a weather generator. *Advances in Water Resources 34* (2011), 448–467.

[48] Feiccabrino, J., Gustafsson, D., and Lundberg, A. Surface-based precipitation phase determination methods in hydrological models. *Hydrology Research 44*, 1 (2013), 44–57.

[49] Fischer, E. M., and Knutti, R. Observed heavy precipitation increase confirms theory and early models. *Nature Climate Change 6* (2016), 986–991.

[50] Fowler, H. J., Blenkinsop, S., and Tebaldi, C. Linking climate change modelling to impacts studies: Recent advances in downscaling techniques for hydrological modelling. *International Journal of Climatology 27* (2007), 1547–1578.

[51] Frei, P., Kotlarski, S., Liniger, M. A., and Schär, C. Future snowfall in the Alps: Projections based on the EURO-CORDEX regional climate models. *The Cryosphere 12*, 1 (2018), 1–24.

[52] Frühwald, E., and Thelandersson, S. Design of safe timber structures - How can we learn from structural failures in concrete, steel and timber? Tech. rep., Lund Institute of Technology, Lund University, 2008.

[53] Geis, J., Strobel, K., and Liel, A. Snow-Induced Building Failures. *Journal of Performance of Constructed Facilities 26*, 4 (2012), 377–388.

[54] Goodison, B., Louie, P. Y. T., and Yang, D. WMO solid precipitation measurement intercomparison-Final report. Tech. rep., World Meteorological Organization (WMO), 1998.

[55] Hawkins, E., and Sutton, R. The potential to narrow uncertainty in regional climate predictions. *Bulletin of the American Meteorological Society 90*, 8 (2009), 1095–1107.

[56] Hawkins, E., and Sutton, R. The potential to narrow uncertainty in projections of regional precipitation change. *Climate Dynamics 37*, 1 (2011), 407–418.

[57] Haylock, M. R., Hofstra, N., Klein Tank, A. M. G., Klok, E. J., Jones, P. D., and New, M. A European daily high-resolution gridded data set of surface temperature and precipitation for 1950-2006. *Journal of Geophysical Research Atmospheres 113* (2008), 1–12.

[58] Ho, C. K., Stephenson, D. B., Collins, M., Ferro, C. A. T., and Brown, S. J. Calibration strategies a source of additional uncertainty in climate change projections. *Bulletin of the American Meteorological Society 93*, 1 (2012), 21–26.

[59] Holický, M. Safety design of lightweight roofs exposed to snow load. *WIT Transactions on Engineering Sciences 58* (2007), 51–57.

[60] Holicky, M., and Sykora, M. Failures of Roofs under Snow Load: Causes and Reliability Analysis. In *Fifth Forensic Engineering Congress* (2009).

[61] Hosaka, M., Nohara, D., and Kitoh, A. Changes in Snow Cover and Snow Water Equivalent Due to Global Warming Simulated by a 20km-mesh Global Atmospheric Model. *Science Online Letters on the Atmosphere 1* (2005), 93–96.

[62] Hungarian Standards Institution. *MSZT EN 1991-1-3/NA, Eurocode 1 – Actions on structures – Part 1-3: General actions – Snow loads –National Annex.*

[63] Icelandic Standards. *IST EN 1991-1-3/NA, Eurocode 1 – Actions on structures – Part 1-3: General actions – Snow loads –National Annex.*

[64] Institute, S. S. *SIS EN 1991-1-3/NA, Eurocode 1 – Actions on structures – Part 1-3: General actions – Snow loads –National Annex.*

[65] Instituto Português da Qualidade. *NP EN 1991-1-3/NA, Eurocode 1 – Actions on structures – Part 1-3: General actions – Snow loads –National Annex (in Portuguese).*

[66] IPCC. Emission Scenarios. A Special Report of Working Group III of the Intergovernmental Panel on Climate Change. Tech. rep., 2000.

[67] IPCC. Climate Change 2013 - The Physical Science Basis, 2013.

[68] Isaacs, E. H., and Srivastava, M. *An Introduction to Applied Geostatistics.* Oxford University Press, New York, 1989.

[69] ISO. *ISO 4354:2009 Wind actions on structures.* 2009.

[70] ISO. *ISO 4355:2013 Bases for design of structures - Determination of snow loads on roofs.* 2013.

[71] ISO. *ISO 12494:2017 Atmospheric icing of structures.* 2017.

[72] Isyumov, N., and Davenport, A. A Probabilistic Approach to the Prediction of Snow Loads. *Canadian Journal Civil Engineering I* (1974), 28–49.

[73] Jacob, D., Petersen, J., Eggert, B., Alias, A., Christensen, O. B., Bouwer, L. M., Braun, A., Colette, A., Déqué, M., Georgievski, G., Georgopoulou, E., Gobiet, A., Menut, L., Nikulin, G., Haensler, A., Hempelmann, N., Jones, C., Keuler, K., Kovats, S., Kröner, N., Kotlarski, S., Kriegsmann, A., Martin, E., van Meijgaard, E., Moseley, C., Pfeifer, S., Preuschmann, S., Radermacher, C., Radtke, K., Rechid, D., Rounsevell, M., Samuelsson, P., Somot, S., Soussana, J. F., Teichmann, C., Valentini, R., Vautard, R., Weber, B., and Yiou, P. EURO-CORDEX: New high-resolution climate change projections for European impact research. *Regional Environmental Change 14*, 2 (2014), 563–578.

[74] Journel, A. G., and Huijbregts, C. J. *Mining geostatistics.* The Blackburn Press, New York, 2003.

[75] Karhunen, K. Zur Spektraltheorie stochastischer Prozesse. *Ann. Acad. Sci. Finnicae Ser. A* (1946).

[76] Karl, T. R., Meehl, G. a., Miller, C. D., Hassol, S. J., Waple, A., and Murray, W. *Weather and Climate Extremes in a Changing Climate Regions of Focus: North America, Hawaii, Caribbean, and U.S. Pacific Islands*, vol. 3.3. 2008.

[77] Katz, R. W. Statistical Methods for Non stationary Extremes in a Changing Climate. In *Extremes in a Changing Climate*, A. AghaKouchak, D. Easterling, K. Hsu, Sorooshian, S. Schubert, and S. Sorooshian, Eds. Springer, 2013.

[78] Katz, R. W., and Brown, B. G. Extreme events in a changing climate: Variability is more important than averages. *Climatic Change 21*, 3 (1992), 289–302.

[79] Katz, R. W., Parlange, M. B., and Naveau, P. Statistics of extremes in hydrology. *Advances in Water Resources 25* (2002), 1287–1304.

[80] Kendall, M. G. *Rank Correlation Methods.* Charles Griffin & Co., London, 1955.

[81] Kilsby, C. G., Jones, P. D., Burton, A., Ford, A. C., Fowler, H. J., Harpham, C., James, P., Smith, A., and Wilby, R. L. A daily weather generator for use in climate change studies. *Environmental Modelling and Software 22* (2007), 1705–1719.

[82] Klein Tank, A. M., Zwiers, F. W., and Zhang, X. Guidelines on Analysis of extremes in a changing climate in support of informed decisions for adaptation. Tech. Rep. WCDMP-No. 72, World Meteorological Organization, 2009.

[83] Knutti, R. Should we believe model predictions of future climate change? *Philosophical Transactions of the Royal Society A: Mathematical, Physical and Engineering Sciences 366* (2008), 4647–4664.

[84] Kotlarski, S., Keuler, K., Christensen, O. B., Colette, A., Déqué, M., Gobiet, A., Goergen, K., Jacob, D., Lüthi, D., Van Meijgaard, E., Nikulin, G., Schär, C., Teichmann, C., Vautard, R., Warrach-Sagi, K., and Wulfmeyer, V. Regional climate modeling on European scales: A joint standard evaluation of the EURO-CORDEX RCM ensemble. *Geoscientific Model Development 7*, 4 (2014), 1297–1333.

[85] Kottegoda, N. T., and Rosso, R. *Applied Statistics for Civil and Environmental Engineers.* Wiley-Blackwell, 2008.

[86] Krasting, J. P., Broccoli, A. J., Dixon, K. W., and Lanzante, J. R. Future changes in northern hemisphere snowfall. *Journal of Climate 26* (2013), 7813–7828.

[87] Kvande, T., Taje Tilley, H. T., and Hygen, H. O. Present and Future Snow Loads in Norway (in Norwegian). Tech. rep., Stiftelsen for industriell og teknisk forskning (SINTEF), 2013.

[88] Latvian Standard. *LVS EN 1991-1-3/NA, Eurocode 1 – Actions on structures – Part 1-3: General actions – Snow loads –National Annex (in Latvian).*

[89] Lemaire, M. *Structural reliability.* John Wiley and Sons, New Yoirk, 2009.

[90] Lemke, P., Ren, J., Alley, R. B., Allison, I., Carrasco, J., Flato, G., Fujii, Y., Kaser, G., Mote, P., Thomas, R. H., and Zhang, T. Observations: Changes in snow, ice and frozen ground. In *Climate Change 2007: The Physical Science Basis. Contribution of Working Group I to the Fourth Assessment Report of the Intergovernmental Panel on Climate Change.* 2007.

[91] Lendvai, A., Ranzi, R., Peretti, G., Barbenni, F., Praolini, A., and Urbani, S. Misura delle precipitazioni nevose mediante i pluviometri. Stima degli errori sistematici e correzione delle serie storiche. *AINEVA - Neve e Valanghe 84* (2015), 12–21.

[92] Lithuanian Standards Board. *LST EN 1991-1-3/NA, Eurocode 1 – Actions on structures – Part 1-3: General actions – Snow loads –National Annex (in Lithuanian).*

[93] Loeve, M. Fonction aléatoires de second ordre. *La Revue Scientifique* (1946).

[94] López-Moreno, J. I., Goyette, S., Vicente-Serrano, S. M., and Beniston, M. Effects of climate change on the intensity and frequency of heavy snowfall events in the Pyrenees. *Climatic Change 105*, 3-4 (2011), 489–508.

[95] Lorenz, E. N. Deterministic Nonperiodic Flow. *Journal of the Atmospheric Sciences 20* (1963), 130–141.

[96] Lorenz, E. N. The predictability of a flow which possesses many scales of motion. *Tellus XXI*, 3 (1969), 289–307.

[97] Lowery, M., and Nash, J. A comparison of methods of fitting the double exponential distribution. *Journal of Hydrology 10* (1970), 259–275.

[98] Makkonen, L. Plotting positions in extreme value analysis. *Journal of Applied Meteorology and Climatology 45* (2006), 334–340.

[99] Makkonen, L., Ruokolainen, L., Raisanen, J., and Tikanmaki, M. Regional Climate Model Estimates for Changes in Nordic Extreme Events. *Geophysica 43(1-2)* (2007), 25–48.

[100] Mann, H. B. Nonparametric Tests Against Trend. *Econometrica 13*, 3 (1945), 245–259.

[101] Mannshardt-Shamseldin, E. C., Smith, R. L., Sain, S. R., Mearns, L. O., and Cooley, D. Downscaling extremes: A comparison of extreme value distributions in point-source and gridded precipitation data. *Annals of Applied Statistics* (2012).

[102] Maraun, D. Bias Correction, Quantile Mapping, and Downscaling: Revisiting the Inflation Issue. *Journal of Climate 26* (2013), 2137–2143.

[103] Maraun, D. Bias Correcting Climate Change Simulations - a Critical Review. *Current Climate Change Reports 2*, 4 (2016), 211–220.

[104] Maraun, D., and Widmann, M. *Statistical Downscaling and Bias Correction for Climate Research*. Cambridge University Press, 2018.

[105] Matthies, H. G., Zander, E., Rosi, B. V., Litvinenko, A., and Pajonk, O. Inverse Problems in a Bayesian Setting. In *Computational Methods for Solids and Fluids*, A. Ibrahimbegovic, Ed. 2016.

[106] Mellor, M. Blowing Snow. *Cold Regions Science and Engineering* (1965).

[107] Meløysund, V., Lisø, K. R., Siem, J., and Apeland, K. Increased Snow Loads and Wind Actions on Existing Buildings: Reliability of the Norwegian Building Stock1. *Journal of Structural Engineering 132*, November (2006), 1813–1820.

[108] National Quality Infrastructure System. *ELOT EN 1991-1-3/NA, Eurocode 1 – Actions on structures – Part 1-3: General actions – Snow loads –National Annex (in Greek).*

[109] National Standards Authority of Ireland. *I.S. EN 1991-1-3/NA, Eurocode 1 – Actions on structures – Part 1-3: General actions – Snow loads –National Annex.*

[110] Nederlands Normalisatie Instituut. *NEN EN 1991-1-3/NA, Eurocode 1 – Actions on structures – Part 1-3: General actions – Snow loads –National Annex (in Dutch).*

[111] O'Gorman, P. A. Contrasting responses of mean and extreme snowfall to climate change. *Nature 515* (2014), 416–418.

[112] O'Gorman, P. A. Precipitation Extremes Under Climate Change. *Current Climate Change Reports 1*, 2 (2015), 49–59.

[113] O'Rourke, M., and Wikoff, J. *Snow-related roof collapse Winter of 2010–2011. Implications for Building Codes.* American Society of Civil Engineers, 2011.

[114] P. Formichi, L. Danciu, S. Akkar, O. Kale, N. Malakatas, P. Croce, D. Nikolov, A. Gocheva, P. Luechinger, M. Fardis, A. Yakut, R. Apostolska, M.L. Sousa, S. Dimova, A. P. Eurocodes: background and applications. Elaboration of maps for climatic and seismic actions for structural design with the Eurocodes. Tech. rep., Joint Research Centre (JRC), 2015.

[115] Piani, C., Haerter, J. O., and Coppola, E. Statistical bias correction for daily precipitation in regional climate models over Europe. *Theoretical and Applied Climatology 99* (2010), 187–192.

[116] Piani, C., Weedon, G. P., Best, M., Gomes, S. M., Viterbo, P., Hagemann, S., and Haerter, J. O. Statistical bias correction of global simulated daily precipitation and temperature for the application of hydrological models. *Journal of Hydrology 395* (2010), 199–215.

[117] Polish Committee for Standardization. *PN EN 1991-1-3/NA, Eurocode 1 – Actions on structures – Part 1-3: General actions – Snow loads –National Annex.*

[118] Räisänen, J. Warmer climate: Less or more snow? *Climate Dynamics 30*, 2-3 (2008), 307–319.

[119] Räisänen, J., and Eklund, J. 21st Century changes in snow climate in Northern Europe: A high-resolution view from ENSEMBLES regional climate models. *Climate Dynamics* (2012).

[120] Rasmussen, R., Baker, B., Kochendorfer, J., Meyers, T., Landolt, S., Fischer, A. P., Black, J., Thériault, J. M., Kucera, P., Gochis, D., Smith, C., Nitu, R., Hall, M., Ikeda, K., and Gutmann, E. How well are we measuring snow: The NOAA/FAA/NCAR winter precipitation test bed. *Bulletin of the American Meteorological Society 93*, 6 (2012), 811–829.

[121] Robert, C. P., and Casella, G. *Monte Carlo Statistical Methods*, vol. 95. Springer, New York., 2004.

[122] Romanian Standards Association. *SR EN 1991-1-3/NA, Eurocode 1 – Actions on structures – Part 1-3: General actions – Snow loads –National Annex.*

[123] Rosić, B. V., Kučerová, A., Sýkora, J., Pajonk, O., Litvinenko, A., and Matthies, H. G. Parameter identification in a probabilistic setting. *Engineering Structures 50* (2013), 179–196.

[124] Sain, S. R., Furrer, R., and Cressie, N. A spatial analysis of multivariate output from regional climate models. *Annals of Applied Statistics 5*, 1 (2011), 150–175.

[125] Sampaolesi, L. Phase 2 Final Report to the European Commission, Scientific Support Activity in the Field of Structural Stability of Civil Engineering Works: Snow Loads. Tech. rep., Department of Structural Engineering, University of Pisa, 1999.

[126] Sanpaolesi, L. Phase 1 Final Report to the European Commission, Scientific Support Activity in the Field of Structural Stability of Civil Engineering Works: Snow Loads. Tech. rep., Department of Structural Engineering, University of Pisa, 1998.

[127] Sanpaolesi, L., and Gulvanessian, H. EC1:Snow loads. In *IABSE reports* (1992).

[128] Schliep, E. M., Cooley, D., Sain, S. R., and Hoeting, J. A. A comparison study of extreme precipitation from six different regional climate models via spatial hierarchical modeling. *Extremes 13*, 2 (2010), 219–239.

[129] Schweizerische Normen-Vereinigung. *SN EN 1991-1-3/NA, Eurocode 1 – Actions on structures – Part 1-3: General actions – Snow loads –National Annex (in German).*

[130] Semenov, M. A., and Barrow, E. M. Use of a stochastic weather generator in the development of climate change scenarios. *Climatic Change 35* (1997), 397–414.

[131] Sevruk, B. Correction of measured precipitation in the Alps using the water equivalent of new snow. *Nordic Hydrology* (1983), 49–58.

[132] Sevruk, B. Conversion of Snowfall Depths to Water Equivalents in the Swiss Alps. *Zurcher Geographische Schriften 23* (1986), 13–23.

[133] Slovak Office of Standards Metrology and Testing. *STN EN 1991-1-3/NA, Eurocode 1 – Actions on structures – Part 1-3: General actions – Snow loads –National Annex (in Slovak).*

[134] Slovenian Institute for Standardization. *SIST EN 1991-1-3/NA, Eurocode 1 – Actions on structures – Part 1-3: General actions – Snow loads –National Annex (in Slovenian).*

[135] Standards Norway. *NS EN 1991-1-3/NA, Eurocode 1 – Actions on structures – Part 1-3: General actions – Snow loads –National Annex (in Norwegian).*

[136] Strasser, U. Snow loads in a changing climate: New risks? *Natural Hazards and Earth System Science 8* (2008), 1–8.

[137] Suomen Standardisoimisliitto r.y. *SFS EN 1991-1-3/NA, Eurocode 1 – Actions on structures – Part 1-3: General actions – Snow loads –National Annex.*

[138] Sýkora, M., Diamantidis, D., Retief, J. V., Viljoen, C., and Rózsás, b. Á. On Risk-Based Design of Structures Exposed to Changing Climatic Actions. In *Life-Cycle ofEngineering Systems: Emphasis on Sustainable Civil Infrastructure* (2016), J. Bakker, D. M. Frangopol, and K. van Breugel, Eds., pp. 1366–1373.

[139] Takahashi, T., and Ellingwood, B. R. Reliability-based assessment of roofs in Japan subjected to extreme snows: Incorporation of site-specific data. *Engineering Structures 27*, 1 (2005), 89–95.

[140] Tarantola, A. *Inverse Problem Theory and Methods for Model Parameter Estimation*. Society of Industrial and Applied Mathematics (SIAM), 2004.

[141] Taylor, K. E., Stouffer, R. J., and Meehl, G. A. An overview of CMIP5 and the experiment design. *Bulletin of the American Meteorological Society 93*, 4 (2012), 485–498.

[142] Tebaldi, C., and Knutti, R. The use of the multi-model ensemble in probabilistic climate projections. *Philosophical Transactions of the Royal Society A: Mathematical, Physical and Engineering Sciences 365*, 1857 (2007), 2053–2075.

[143] Teuling, A. J., Stöckli, R., and Seneviratne, S. I. Bivariate colour maps for visualizing climate data. *International Journal of Climatology 31*, 9 (2011), 1408–1412.

[144] Teutschbein, C., and Seibert, J. Bias correction of regional climate model simulations for hydrological climate-change impact studies: Review and evaluation of different methods. *Journal of Hydrology 456-457* (2012), 12–29.

[145] Thom, H. C. S. Distribution of Maximum Annual Water Equaivalent of Snow on the Ground. *Monthly Weather Review 94*, 4 (1966), 265–271.

[146] Tierney, L. Markov Chains for Exploring Posterior Distributions. *The Annals of Statistics 22*, 4 (1994), 1701–1762.

[147] U.S. National Water Service. Snow Measurement Guidelines for National Weather Service Surface Observing Programs. Tech. rep., U.S. Department of Commerce National Oceanic and Atmospheric Administration, 2013.

[148] Vagnoli, M., Maio, F. D., and Zio, E. Ensembles of climate change models for risk assessment of nuclear power plants. *Journal of Risk and Reliability* (2017), 1–16.

[149] Van Der Linden, P., and Mitchell, J. F. B., Eds. *ENSEMBLES: Climate Change and its Impacts: Summary of research and results from the ENSEMBLES project.* 2009.

[150] van Vuuren, D. P., Edmonds, J., Kainuma, M., Riahi, K., Thomson, A., Hibbard, K., Hurtt, G. C., Kram, T., Krey, V., Lamarque, J. F., Masui, T., Meinshausen, M., Nakicenovic, N., Smith, S. J., and Rose, S. K. The representative concentration pathways: An overview. *Climatic Change 109*, 1 (2011), 5–31.

[151] Vašek, M. Some problems of timber structures solved by forensic control. In *Proceedings of World Conference on Timber Engineering 2006* (2006).

[152] Von Storch, H. On the use of 'inflation' in statistical downscaling. *Journal of Climate 12*, 12 (1999), 3505–3506.

[153] Von Storch, H. Models of Global and Regional Climate. *Encyclopedia of Hydrological Sciences* (2006), 477–490.

[154] Weibull, W. A Statistical Theory of the Strength of Materials. *Royal Swedish Institute for Engineering Research 151* (1939).

[155] Westra, S., Alexander, L. V., and Zwiers, F. W. Global increasing trends in annual maximum daily precipitation. *Journal of Climate 26*, 11 (2013), 3904–3918.

[156] Wilks, D., and Wilby, R. The weather generation game: a review of stochastic weather models. *Progress in Physical Geography 23*, 3 (1999), 329–357.

[157] Wong, G., Maraun, D., Vrac, M., Widmann, M., Eden, J. M., and Kent, T. Stochastic model output statistics for bias correcting and downscaling precipitation including extremes. *Journal of Climate 27*, 18 (2014), 6940–6959.

[158] Xiu, D. *Numerical Methods for Stochastic Computations.* Princeton University Press, 2010.

[159] Yang, D., Goodison, B. E., Metcalfe, J. R., Golubev, V. S., Bates, R., Pangburn, T., and Hanson, C. L. Accuracy of NWS 8 standard nonrecording precipitation gauge: Results and application of WMO intercomparison. *Journal of Atmospheric and Oceanic Technology 15*, 1 (1998), 54–68.